RICE UNIVERSITY

Surface Modification and Self-Assembly of Gold Nanostructures

By

Pramit Manna

A THESIS SUBMITTED

IN PARTIAL FULFILMENT OF

THE REQUIREMENTS FOR THE DEGREE

Doctor of Philosophy

APPROVED, THESIS COMMITTEE

Eugene R. Zubarev, Chair

Associate Professor of Chemistry

Stephan Link

Assistant Professor of Chemistry

Jason H. Hafner

Associate Professor of Physics and Astronomy

HOUSTON, TX

JUNE 2011

Abstract

Surface Modification and Self-Assembly of Gold Nanostructures

By

Pramit Manna

This thesis describes self-assembly and surface modification of gold nanoparticles and nanorods. It begins with an efficient surface functionalization of gold nanoparticles with a liquid crystalline ligand that structurally resembles liquid crystal 5CB. Functionalized gold nanoparticles show increased solubility in liquid crystal compared to their alkanethiolated analogues. Surface modification technique was also applied to detoxify gold nanorods for biological applications. The process involves a ligand exchange step where cytotoxic CTAB bilayer of gold nanorods was replaced by thiolated CTAB. Covalent nature of gold-sulfur bond allows for the complete removal of CTAB via centrifugation. Functionalized gold nanorods are virtually non-toxic and they show efficient cellular uptake by cancer cells. This thesis also describes self-assembly of gold nanoparticles and nanorods into well organized colloidal crystals. Slow precipitation technique was implemented to prepare three dimensional colloidal crystals of alkanethiolated gold nanoparticles. Colloidal crystals of gold nanorods were prepared by evaporation induced self –assembly technique. Additionally, orientation of nanorods in a colloidal crystal can be altered from side-on to tip-on by controlling the hydrophobicity of the underlying substrate. Our investigation showed that the presence of excess surfactant (CTAB) strongly influences the crystallization process. The shape and size of self assembled structures were also controlled by creating patterned hydrophobic and hydrophilic areas on a substrate. A variety of self assembled structures can be prepared

by controlling the dimensions of the patterns. Finally, an efficient synthesis of hybrid cadmium sulfide-gold nanowires was described.

To my wife Saptaparni (Titir)

To my mother and father, Dipa and Anup K. Manna

Acknowledgements

I would like to express my deepest and sincere gratitude to my advisor Prof. Eugene R. Zubarev. He has been a great mentor giving continuous support, creative ideas, and constructive guidance. I am thankful to him for always believing in me and helping me out at my most difficult times. Without his support this work would not have been completed.

I take this opportunity to thank former and current group members of Zubarev group (Arshad S. Sayyad, Bishnu P. Khanal, Leonid Vigderman, Jacob D. Gibson, and Jeremy Lee). They have always been helpful in providing excellent ideas and I have learned a lot from each of them.

I would like to thank Prof. Stephan Link, Prof. Jeffrey Hartgerink, Prof. Ronald Parry, and Prof. Vicki Colvin for letting me use some of their valuable instruments.

A special thanks to Rice University Chemistry Department for giving me this wonderful opportunity. This has been truly a great experience. I would like to thank all staff members of Rice University Shared Equipment Authority for training me on various instruments.

Finally, I would like to thank my lovely wife Titir for being there at my side at all times. I thank my parents and my sister who have always been a great source of inspiration.

Table of Contents

List of Figures

Chapter V

List of Schemes

Chapter II

Chapter III

List of Abbreviations

Au	Gold
AuNPs	Gold Nanoparticles
AuNRs	Gold Nanorods
NRs	Nanorods
MRs	Microrods
NPs	Nanoparticles
AuMR	Gold microrods
CTAB	Cetyltrimethylammonium bromide
DDAB	Didoceyldimethylammonium bromide
SAM	Self-assembled monolayer
5CB	4 –cyano-4-pentylbiphenyl
SOPB	4-sulfanylphenyl-4-[4-(octyloxy)phenyl]benzoate
DT	1-decanethiol
HDT	1-hexadecanethiol
MHDA	16-mercaptohexadecanoic acid
PDMS	Polydimethylsiloxane
TCTAB	16-thiocetyltrimethylammonium bromide
AuNWs	Gold nanowires
CdS	Cadmium Sulfide
UV-Vis	Ultraviolet Visible
PL	Photoluminescence
NIR	Near Infra Red
TEM	Transmission electron microscopy
HRTEM	High resolution transmission electron microscopy
SEM	Scanning electron microscopy
HRSEM	High resolution scanning electron microscopy
NMR	Nuclear magnetic resonance
EISA	Evaporation induced self-assembly

TGA	Thermogravimetric analysis
SEC	Size exclusion chromatography
CH_2Cl_2	Methylene chloride
$CHCl_3$	Chloroform
THF	Tetrahydrofuran
DMF	N,N-dimethylformamide
DIPC	N,N'-diisopropylcarbodiimide
DPTS	4-(*N, N*-dimethylamino)pyridinium-4-toluenesulfonate
NBS	N-bromosuccinamide
DDA	Dodecylamine
TOPO	Triocylphoosphine oxide
TOP	Triocylphosphine
ODPA	Octadecylphosphonic acid
TDPA	Tetradecylphosphonic acid

Chapter I

Introduction and Literature Overview

1.1 Synthesis and Self-assembly of Nanostructures

Sub-micrometer or "nano-sized" objects are of special interest because their physicochemical properties are distinctly different from their bulk counterparts. For example, nanocrystalline quantum dots show an increase in the bandgap as a result of quantum confinement effect (QCE).[1-5] Noble metal nanoparticles and nanorods show size-dependent optical absorption due to the collective oscillation of conduction band electrons.[6-9] This phenomenon is known as surface plasmon resonance.[6-9] Interesting magnetic and electrical properties are also observed for nanometer-sized objects.[10-14] Properties of nanostructures are known to be dependent on their chemical composition as well as on their morphology.[1-14] For that reason, significant advances have been made in the "top-down" and "bottom-up" syntheses of well-defined metallic nanostructures,[15-22] bimetallic nanostructures,[14,17,23-26] metal oxide,[27-29] semiconductor nanocrystals,[1-5, 27] carbon nanomaterials,[30-34] and polymeric particles.[35,36] In the "top-down" synthesis, monodisperse nanostructures are prepared by vapor phase deposition of bulk components on top of a patterned substrate designed by optical lithography. Although this process produces highly monodisperse structures, it is limiting in terms of high volume materials production. Additionally, nanostructures produced by this method are often polycrystalline in nature. "Bottom-up" or wet chemical synthesis of nanostructures is an excellent alternative to the "top-down" approach as it offers the production of high quality nanocrystals in a cost effective and scalable way. However, rational synthetic

modifications are often required to control structural monodipsersity of the nanocrystals prepared by this method.

In addition to synthesis, formation of well-defined aggregates of these nanocrystals is an important task because macroscopic properties of nanostructured materials depend on the extent of order among their individual building blocks.[37-50] In this respect, self-assembly is extremely useful as it allows for the preparation of ordered 2D and 3D aggregates without the influence of external forces.[37-50] This is achieved by rational structural manipulations that tailor noncovalent interactions such as electrostatic attraction/repulsion, hydrophobic interactions, van der Waals forces, and π-π stacking. Essentially, self-assembly is a "bottom-up" technique for arranging the nanoobjects into periodic arrays. Additionally, "top-down" and "bottom-up" strategies can be used as complementary techniques for device fabrication where the device is first fabricated by lithography followed by the integration of nanostructures by self-assembly.[50-59]

1.2 Colloidal Crystallization of Nanostructures

Self-assembled periodic arrays of nanostructures are known as colloidal supercrystals. These structures often show unique photonic properties which are useful for preparing optical filters, switches, and photonic bandgap materials.[60-67] Opal is an example of naturally occurring colloidal crystal made of close-packed silica spheres. Due to the presence of structural periodicity, it displays beautiful colors, also known as opalescence. Structural monodipsersity of nanostructures is the most important factor for the preparation of colloidal crystals with large domain size and fewer defects (Figure 1.1). Most of the literature reports describe crystallization of *isotropic spherical particles* as their size monodipsersity is easier to attain compared to anisotropic nanostructures.[37-

[50, 60-66] In addition, surface charge of the particles and surfactants present in the reaction media influence the colloidal crystallization by balancing electrostatic repulsion and attractive depletion, thus preventing random aggregation of nanoparticles.[50,68]

Crystallization via solvent evaporation is used to prepare a variety of colloidal crystals of spherical particles.[43,50,63] For example, Colvin and co-workers reported a "lost-wax" method for the crystallization of silica spheres.[63] In this case, a solid substrate was first vertically immersed into a solution of silica spheres and then dried very slowly to produce high quality colloidal crystals. These crystals generally have face centered cubic (FCC) or hexagonal close-packed (HCP) order among individual particles, whereas strong van der Waals forces between interdigitated layers of capping agents provide structural and mechanical robustness.

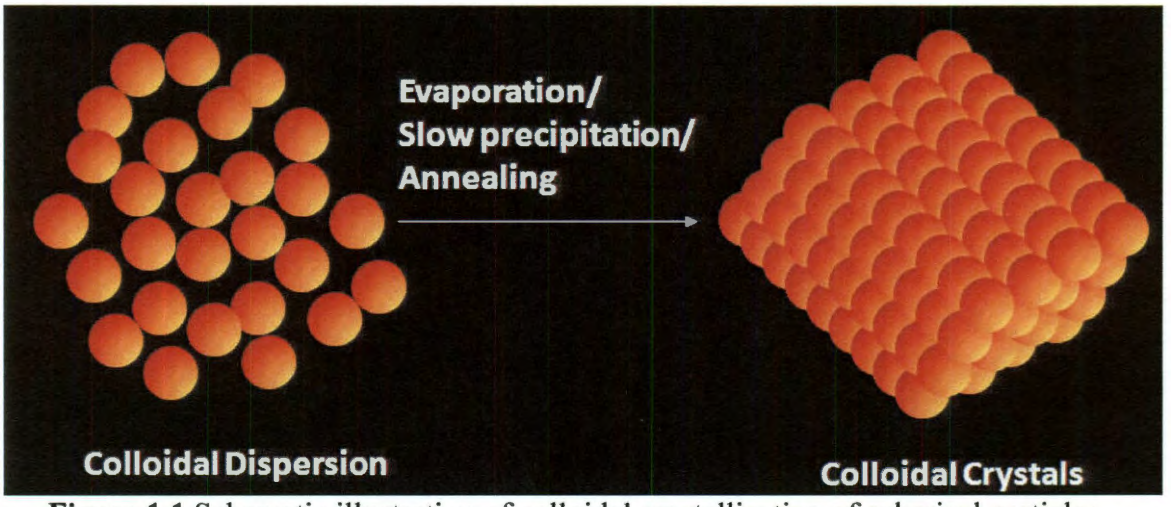

Figure 1.1 Schematic illustration of colloidal crystallization of spherical particles.

In addition, electrostatic forces of attraction between oppositely charged nanoparticles have been exploited to prepare colloidal crystals.[50] This is achieved by modifying the surface charge of particles, which enables their favorable interactions with the oppositely charged nanostructures. However, a delicate balance of forces must be

maintained in order to avoid random aggregation.[69] Grzybowski and co-workers were able to prepare diamond-like binary superlattices of positively charged gold and negatively charged silver nanocrystals using electrostatic self-assembly technique.[70] Other examples of colloidal crystallization include the use of Langmuir-Blodgett assembly,[71] surfactant assisted assembly,[72] and liquid crystal mediated assembly of nanostructures.[73] Unlike spherical particles, there are only few literature reports describing colloidal crystallization of anisometric particles.[74] This is mainly due to the difficulties associated with the synthesis of monodisperse non-spherical structures. The nature of the packing and assembly will depend on the shape and overall size of the particles, which allows for creating many unusual superlattices.

1.3 Assembly on Patterned Substrates

Slow sedimentation of colloidal particles on lithographically patterned substrates, also known as "colloidal epitaxy" can be utilized to prepare macroscopic colloidal crystals with controlled orientation and lattice parameters.[50-59,75] When a solution containing colloidal nanoparticles is placed on a patterned substrate, de-wetting, capillary forces, and gravitational sedimentation direct the assembly of the particles inside the lithographically etched patterns. [50-58, 76-78] This assembly process depends not only on the dimension of the colloids, but also on the shape and size of the pattern. Therefore, various superlattices can be produced by controlling the particle and pattern size. Other methods of controlled assembly include the examples of mechanical rubbing, electrostatic interaction, and hydrophobic-hydrophilic interactions.[50,59,79-83] Although many literature reports describe the patterned assembly of spherical nanoparticles, controlled assembly of anisotropic nanostructures remains to be a formidable challenge.

1.4 Gold Nanoparticles

The history of gold nanoparticles or "colloidal gold" goes back to the 5th century when they were used as colorants for staining the glass. [84] In the Middle Ages, colloidal gold was also used as a panacea medicine. However, modern research related to gold particles did not start until Michael Faraday reported the synthesis of gold nanoparticles by chemical reduction of chloroaurate ions.[85] Another breakthrough for the synthesis of gold particles was the development of citrate reduction method.[86] In the last few decades, the emergence of nanoscience resulted in significant advances in the field of gold nanostructures as researchers were able to find their unique applications in biotechnology and medicine. For that reason, various research groups have implemented different synthetic strategies to control the shape and size of gold nanoparticles. Additionally, gold has strong chemical affinity to sulfur, which allows for the functionalization of gold nanoparticles by various thiols. The exact nature of gold-sulfur bond has been a subject of debate until Kornberg *et al.* demonstrated its covalent nature by solving the X-ray crystal structures of thiol-coated gold nanoclusters.[87]

In 1994, Brust and co-workers developed a two-phase synthesis of stable, monodisperse gold nanoparticles (~2 nm) stabilized by akanethiols.[88] They have also reported a one phase synthesis of 4-mercaptophenol-coated gold nanoparticles.[89] These gold nanoparticles have free hydroxyl groups on their surface which provide active sites for further chemical modification. Zubarev *et al.* reported covalent coupling of diblock amphiphilic polymers to mercaptophenol-coated gold nanoparticles using an esterification reaction.[90] The resulting amphiphilic gold nanoparticles undergo spontaneous self-assembly in water to form well-defined spherical and cylindrical

micelles.[91] Klabunde and co-workers reported "digestive ripening" of alkanethiolated gold particles to produce near-monodisperse gold colloids.[92] There are numerous reports in the literature describing covalent stabilization of gold structures using thiolated polymers, dendrimers, and organometallic compounds.[15] Biomolecules, such as peptides, DNA, and lipids were also used to functionalize and assemble gold nanoparticles.[15] Mirkin *et al.* reported switchable self-assembly of gold nanoparticles coated with DNA.[9394]

1.5 Gold Nanorods

In addition to spherical gold particles, gold nanorods have gained much interest because of their unique plasmonic properties arising from their inherent structural anisotropy.[8-9] Gold nanorods have two distinct plasmon peaks. The low intensity transverse plasmon peak corresponds to the oscillation of electrons along the short axis of the nanorods, whereas the high intensity longitudinal plasmon corresponds to the oscillation along their principal axis (Figure 1.2). Both theoretical and experimental results suggest that the longitudinal plasmon band can be controlled over a broad range of wavelengths by controlling the aspect ratio of nanorods.[95]

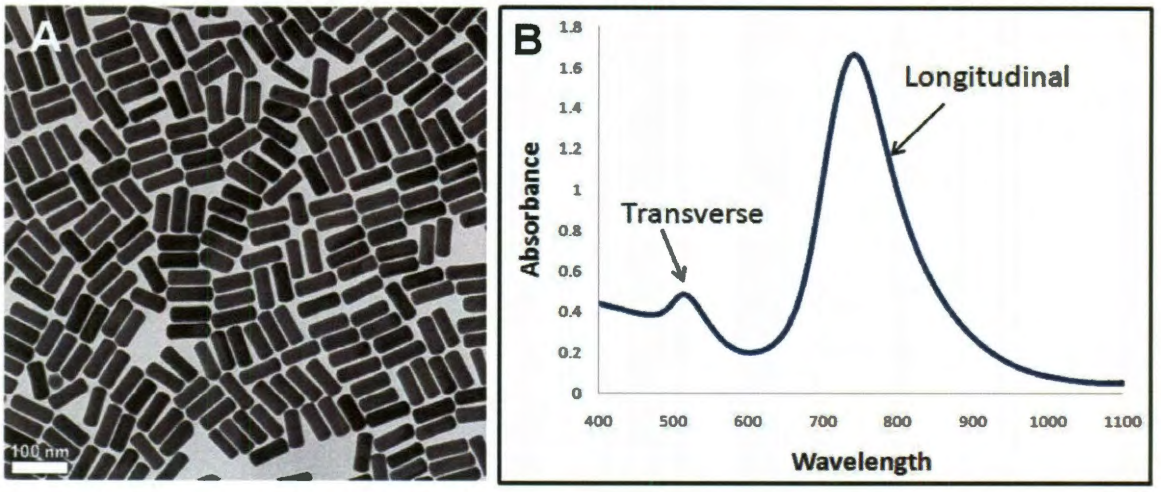

Figure 1.2 TEM image of gold nanorods (A) and their UV-vis spectrum (B).

In most cases the longitudinal plasmon peak appears in the near infrared region making these nanorods suitable for biomedical imaging.[21] In addition, when a laser light of appropriate wavelength is shone upon gold nanorods, they instantly heat up to cause rapid increase in local temperature. This property can be successfully applied for photothermal therapy of cancer.[21,96-98] For that purpose gold nanorods are selectively delivered to tumor cells, which are then destroyed by exposing them to a laser irradiation. Selective delivery of gold nanorods can be achieved by functionalizing them with targeting molecules and antibodies.[96] Even without any surface modification, gold nanorods have strong propensity to accumulate in the cancer cells because of the leaky vasculature of tumors, i.e. enhanced permeability and retention effect (EPR).[99]

1.6 Synthesis of Gold Nanorods

During the past decade several research groups have explored "top-down" and "bottom-up" approaches for the synthesis of anisotropic gold nanorods. The "top-down" method generally utilizes electron beam lithography (EBL).[21,95,100] For that purpose, a substrate is first coated with an electron sensitive material such as PMMA and then

exposed to an electron beam. The exposed areas are subsequently etched to form nanometer-sized patterns on top of the coated substrate. Nanorods are obtained by depositing metallic gold followed by the removal of unexposed resist and the gold film deposited on top of it. Although this technique produces monodisperse nanorods with precision, it is limiting in terms of large scale production. Additionally, template based synthesis of gold nanorods has also been reported in the literature by Martin *et al.* In this case, nanorods are synthesized by electrochemical deposition of metallic gold inside a porous alumina or polycarbonate template.[101] The diameter of nanorods can be controlled by changing the pore size of the template. Once the deposition is complete, the template can be dissolved to prepare an ordered array of gold nanorods.

In contrast to "top-down" approach, the "bottom-up" chemical synthesis of nanorods is cost-effective and scalable. Wang *et al.* described electrochemical synthesis of gold nanorods in an aqueous solution that contained a mixture of cationic surfactants.[102] The most important breakthrough in the field of gold nanorods is the development of seed-mediated growth method where smaller gold nanoparticles are used as seeds to grow nanorods in aqueous solution. This method also offers the flexibility to control the particle size by manipulating synthetic conditions. Murphy *et al.* reported the synthesis of pentahedrally twinned gold nanorods using citrate-capped gold nanoparticles as seeds. The seed particles were prepared by sodium borohydride reduction of gold chloride in the presence of sodium citrate as capping agent.[103-105] These seed particles were introduced to gold (I) growth solution prepared by reduction of gold (III) ions with ascorbic acid in the presence of cetyltrimethylammonium bromide (CTAB). Continuous one dimensional growth of the seed particles results in the formation of gold nanorods

with aspect ratio ca. 12. However, this process also produces other shapes such as cubes, platelets, and spherical particles mixed with nanorods. The authors reported that the ratio between nanorods vs. other shapes can be increased by introducing a small amount of silver nitrate in the growth solution. Although spherical particles are easy to remove from this reaction mixture, separation of platelets and nanorods is very difficult. In 2003, El-sayed *et al.* reported an improved synthesis gold nanorods by using CTAB-capped seed and silver nitrate.[106] Growth of CTAB-capped seeds produces single crystalline gold nanorods with an aspect ratio ca. 4. Other methods for the preparation of gold nanorods include solvothermal synthesis, photochemical reduction, X-ray irradiation, and microwave assisted reduction.[21]

Gold nanorods often show anisotropic chemical reactivity due to the different crystal facets on their tips and sides.[95] For example, when treated with gold(III)/CTAB complex, gold nanorods undergo tip-selective oxidative dissolution.[107] Selective dissolution process decreases the aspect ratio of gold nanorods resulting in a blue-shift in the absorption spectrum. In addition, high aspect ratio nanorods can be anisotropically grown by slow addition of gold (I) ions into the growth solution. Tip-selective growth increases the aspect ratio which results in a red shift. Therefore, gold nanowires measuring up to several microns can be synthesized by using the continuous anisotropic growth process.[11] Anisotropic growth of gold nanorods can also be controlled by changing the pH of the growth solution. Decrease in the pH of the growth solution slows the rate of reaction and leads to the formation of ultra long gold nanowires.[108] Recently, syntheses of ultra long gold nanowires in organic media were reported.[109,110]

1.7 Self-Assembly of Gold Nanorods

CTAB capped gold nanorods have strong propensity to form ordered assemblies upon solvent evaporation. El-Sayed and co-workers fist reported evaporation-induced self assembly of gold nanorods into two- and three-dimensional structures.[114] Murphy *et al.* also observed liquid crystalline assemblies of pentahendrally-twinned gold nanorods. [115] Further investigations by Jana proved that the assembly process also depends on the shape and the size of nanocrystals.[116] Recent reports in surfactant mediated self-assembly of gold nanorods describe the preparation of smectic-like arrays of gold nanorods via droplet evaporation,[117] and self-assembly of gold nanorods into vertically standing superlattices.[118]

Systematic surface modification allows one to tailor the noncovalent forces that direct self-assembly.[74] The tips of gold nanorods can be easily functionalized with thiolated ligands because of the preferential binding of CTAB to the sides of the nanorods. Kumacheva *et al.* reported tip-selective functionalization of gold nanorods with hydrophobic polymers.[119] Resulting nanorods are amphiphilic in nature because their sides are still coated with hydrophilic CTAB. These amphiphilic nanorods self assemble into spherical and ring like aggregates due to the hydrophobic effect. In addition, gold nanorods can be functionalized with functional thiols that are capable of forming hydrogen bonding. Kamat and co-workers reported preferential end-to-end assembly of gold nanorods by modifying their surface with carboxyl-terminated thiols.[120] Electrostatic self-assembly of gold nanorods was also observed when they are functionalized with zwitterionic molecules.[121] Other reports of end-to-end assemblies of nanorods utilize functionalization with PVP,[122] alkanedithiols,[123,124] olegonucleotides,[125]

organometallic compounds,[126] biotin-streptavidin,[127] aptamers,[128] and antibodies.[129] DNA-functionalized gold nanorods assemble into three dimensional structures via hybridization of complementary strands.[130] Side-by-side and vertical assembly was observed for lipid functionalized gold nanorods.[131] Unusual "ring like" assemblies of polystyrene functionalized hydrophobic gold nanorods were reported by Zubarev *et al.*[107] When a methylene chloride solution of polystyrene functionalized gold nanorods was dried on a TEM grid, they readily assemble into ring like structures. The assembly process is templated by water droplets that form due to evaporative cooling of methylene chloride.

Both experimental and theoretical studies indicate that long-range periodic assemblies of anisotropic nanostructures may possess *vectorial* optical and electrical properties.[132,133] Plasmonic properties of gold nanorods can be tuned by controlling the orientation of nanorods. For example, red shift in plasmon resonance is observed for end-to-end assembly of gold nanorods, whereas a blue shift occurs when nanorods are oriented in a side-by-side fashion.[120] Additionally, self-assembly of gold nanorods into ordered arrays can significantly increase the local electromagnetic field at the nanorods junctions, thus forming a periodic arrays of "hot spots". These "hot spots" can be utilized to detect bioorganic compounds at very low concentration.[134] Self-assembled structures of gold nanorods can also be used to prepare metamaterials, negative refractive index materials, and data encoding devices.[135-137]

1.8 Outline of the Thesis

Although, there were significant advances in the field of surface modification of gold nanostructures, the characterization of such hybrid materials by conventional analytical techniques still remains as an elusive goal. In this thesis, we have addressed some of the challenges involved in surface modification and self-assembly of gold nanostructures. We report various ways of functionalizing gold nanoparticles and nanorods with functional ligands that render them soluble in various solvents. Additionally, small size of these functional ligands allows for the characterization by conventional analytical techniques and exact amount of organic residue can be determined. Another goal of this thesis is to find reproducible techniques for the controlled self-organization of monodisperse gold nanorods into near macroscopic structures which is a long standing problem in the field of self-assembly of gold nanorods. We have also combined optical lithography with self-assembly to control the shape and size of the self-assembled structures on various substrates. These materials should be ideal for studying optical and electronic properties of periodic arrays of self-assembled structures and may enable us to fabricate devices for various applications.

Chapter II describes the synthesis of liquid crystal functionalized gold nanoparticles. As synthesized alkanethiolated gold particles show poor solubility in liquid crystals owing to the structural dissimilarity between the liquid crystal and alkanethiol. For that reason, we exchanged alkanethiol with functional SOPB ligand that structurally resembles liquid crystal 5CB. Functionalized gold nanoparticles show increased solubility in liquid crystal solvent and they were effectively used to prepare gold nanoparticle- liquid crystal composite material.

Chapter III presents an efficient way to reduce the cytotoxicity of gold nanorods by exchanging CTAB with its thiolated analogue TCTAB. Covalent nature of gold-sulfur bond allows for the complete removal of CTAB by multiple rounds of centrifugations. We were also able to show complete exchange of CTAB by ^{1}HNMR and TGA. In stark contrast to polyethylene glycol coated rods, TCTAB functionalized structures are efficiently internalized in cells while maintaining their low cytotoxicity.

Colloidal crystallization of gold nanoparticles and nanorods is described in chapter IV. Slow precipitation technique was applied to prepare faceted 3D colloidal crystals of monodisperse 6 nm gold nanoparticles. Additionally, colloidal crystallization of gold nanorods was investigated in detail. Colloidal single crystals measuring up to 1000 square microns were prepared by evaporative self-assembly technique. These are by far the largest colloidal single crystals made of anisotropic building blocks. In these colloidal crystals nanorods are hexagonally closed packed and oriented parallel to the substrate. The orientation of nanorods in a colloidal crystal can be altered from side-on to tip-on by making the substrate slightly hydrophobic.

In chapter V, a complementary use of "top-down" and "bottom-up" techniques for controlling the shape and size of self-assembled structures is described. It is demonstrated that the nanorods have strong preference for hydrophilic silicon surface and avoid regions coated with the hydrophobic photoresist S1813. When an aqueous solution of nanorods was slowly dried on top of the substrate having photolithographic pattern, all the nanorods selectively fill up the hydrophilic areas forming parallelly packed or vertically standing arrays. This is the first example of forming periodic arrays of self-assembled superstructures composed of anisotropic building blocks. The assembly on

gold nanorods was also controlled by drying them on a gold surface with alternating hydrophobic and hydrophilic monolayers (SAM) of thiols. Additionally, periodic arrays of gold nanowires were formed on silicon substrate by template-assisted evaporative self assembly. When an aqueous solution of gold nanowires was placed between a TEM grid (template) and a solid surface and allowed to dry very slowly, all the nanowires self-assembled into 2-D network. Conductivity measurements proved that the network was highly conductive.

Finally, the synthesis of hybrid gold on cadmium sulfide nanowires is discussed in chapter VI. Cadmium sulfide nanowires measuring several microns in length were prepared by solvothermal process. These nanowires maintained wurtzite crystal structure during their one dimensional growth. In addition, selective deposition of gold clusters on top of pre-synthesized nanowires is also described.

References

(1) Murray, C. B.; Norris, D. J.; Bawendi, M. G. *J. Am. Chem. Soc.* **1993**, *115*, 8706.

(2) Peng, X. G.; Manna, L.; Yang, W. D.; Wickham, J.; Scher, E.; Kadavanich, A.; Alivisatos, A. P. *Nature* **2000**, *404,* 59.

(3) Peng, Z. A.; Peng, X. *J. Am. Chem. Soc.* **2001**, *123*, 183

(4) Ghezelbash, A.; Koo, B.; Korgel, B. A. *Nano Lett.* **2006**, 6, 1832.

(5) Talapin, D. V.; Shevchenko, E. V.; Murray, C. B.; Kornowski, A.; Forster, S.; Weller, H. *J. Am. Chem. Soc.* **2004**, *126*, 12984.

(6) Kreibig, U.; Vollmer, M. *Optical Properties of Metal Clusters*; Springer: Berlin, **1995**.

(7) Heath, J. R. *Phys. Rev. B* **1989**, *40*, 9982

(8) Link, S.; Wang, Z. L.; El-Sayed, M. A. *J. Phys. Chem. B* **1999**, *103*, 3529.

(9) Link, S.; El-Sayed, M. A. *J. Phys. Chem. B* **1999**, *103*, 4212.

(10) Sun, S.; Murray, C. B. *J. App. Phys.* **1999**, *85*, 4324.

(11) Critchley, K.; Khanal, B. P.; Gorzny, M. L.; Vigderman, L.; Evans, S. D.; Zubarev, E. R.; Kotov, N. A. *Adv. Mater.* **2010**, *22*, 2338.

(12) Schmid, G.; Simon, U. *Chem. Commun.* **2005**, 697.

(13) Goya, G. F.; Berquo, T. S.; Fonseca, F. C.; Morales, M. P. *J. App. Phys.* **2003**, *94*, 3250.

(14) Lu, A.-H.; Salabas, E. L.; Schüth, F. *Angew. Chem. Int. Ed.* **2007**, *46*, 1222.

(15) Daniel, M.-C.; Astruc, D. *Chem. Rev.* **2003**, *104*, 293.

(16) Wang, Y.; Xia, Y. *Nano Lett.* **2004**, *4*, 2047.

(17) Cushing, B. L.; Kolesnichenko, V. L.; O'Connor, C. J. *Chem. Rev.* **2004**, *104*, 3893.

(18) Murphy, C. J.; Sau, T. K.; Gole, A. M.; Orendorff, C. J.; Gao, J.; Gou, L.; Hunyadi, S. E.; Li, T. *J. Phys. Chem. B* **2005**, *109*, 13857.

(19) Henglein, A.; Giersig, M. *J. Phys. Chem. B* **1999**, *103*, 9533.

(20) Sun, Y.; Xia, Y. *Science* **2002**, *298*, 2176.

(21) Huang, X. H.; Neretina, S.; El-Sayed, M. A. *Adv. Mater.* **2009**, *21*, 4880.

(22) Sun, Y.; Gates, B.; Mayers, B.; Xia, Y. *Nano Lett.* **2002**, *2*, 165.

(23) Mizukoshi, Y.; Okitsu, K.; Maeda, Y.; Yamamoto, T. A.; Oshima, R.; Nagata, Y. *J. Phys. Chem. B* **1997**, *101*, 7033.

(24) Lim, B.; Jiang, M.; Camargo, P. H. C.; Cho, E. C.; Tao, J.; Lu, X.; Zhu, Y.; Xia, Y. *Science* **2009**, *324*, 1302.

(25) Khanal, B. P.; Zubarev, E. R. *Angew. Chem. Int. Ed.* **2009**, *48*, 6888.

(26) Xiang, Y.; Wu, X.; Liu, D.; Jiang, X.; Chu, W.; Li, Z.; Ma, Y.; Zhou, W.; Xie, S. *Nano Lett.* **2006**, *6*, 2290.

(27) Jun, Y.-W.; Choi, J.–S.; Cheon, J. *Angew. Chem. Int. Ed.* **2006**, *45*, 3414.

(28) Park, J.; An, K.; Hwang, Y.; Park, J.-G.; Noh, H.-J.; Kim, J.-Y.; Park, J.-H.; Hwang, N.-M.; Hyeon, T. *Nat. Mater.* **2004**, *3*, 891.

(29) Yavuz, C. T.; Mayo, J. T.; Yu, W. W.; Prakash, A.; Falkner, J. C.; Yean, S.; Cong, L.; Shipley, H. J.; Kan, A.; Tomson, M.; Natelson, D.; Colvin, V. L. *Science* **2006**, *314*, 964.

(30) Iijima, S. *Nature* **1991**, *354*, 56.

(31) Kroto, H. W.; Heath, J. R.; O'Brien, S. C.; Curl, R. F.; Smalley, R. E. *Nature* **1985**, *318*, 162.

(32) Novoselov, K. S.; Geim, A. K.; Morozov, S. V.; Jiang, D.; Zhang, Y.; Dubonos, S. V.; Grigorieva, I. V.; Firsov, A. A. *Science* **2004**, *306*, 666.

(33) Baughman, R. H.; Zakhidov, A. A.; de Heer, W. A. *Science* **2002**, *297*, 787.

(34) Dai, H. *Acc. Chem. Res.* **2002**, *35*, 1035.

(35) Dendukuri, D.; Pregibon, D. C.; Collins, J.; Hatton, T. A.; Doyle, P. S. *Nat. Mater.* **2006**, *5*, 365.

(36) Pekarek, K. J.; Jacob, J. S.; Mathiowitz, E. *Nature* **1994**, *367*, 258.

(37) Peschel, S.; Schmid, G. *Angew. Chem., Int. Ed. Engl.* **1995**, *34*, 1442.

(38) Collier, C. P.; Saykally, R. J.; Shiang, J. J.; Henrichs, S. E.; Heath, J. R. *Science* **1997**, *277*, 1978.

(39) Fendler, J. H. *Chem. Mater.* **1996**, *8,* 1616.

(40) Mirkin, C. A. *Inorg. Chem.* **2000**, *39*, 2258.

(41) Lopes, W. A.; Jaeger, H. M. *Nature* **2001**, *414*, 735.

(42) Boal, A. K.; Ilhan, F.; DeRouchey, J. E.; Thurn-Albrecht, T.; Russell, T. P.; Rotello, V. M. *Nature* **2000**, *404*, 746.

(43) Murray, C. B.; Kagan, C. R.; Bawendi, M. G. *Science* **1995**, *270,* 1335.

(44) Andres, R. P.; Bielefeld, J. D.; Henderson, J. I.; Janes, D. B.; Kolagunta, V. R.; Kubiak, C. P.; Mahoney, W. J.; Osifchin, R. G. *Science* **1996**, *273,* 1690.

(45) Motte, L.; Billoudet, F.; Lacaze, E.; Pileni, M. P. *Adv. Mater.* **1996**, *8*, 1018.

(46) Shenton, W.; Pum, D.; Sleytr, U. B.; Mann, S. *Nature* **1997**, *389*, 585.

(47) Schmitt, J.; Decher, G.; Dressick, W. J.; Brandow, S. L.; Geer, R. E.; Shashidar, R.; Calvert, J. M. *Adv. Mater.* **1997**, *9*, 61.

(48) Heath, J. R.; Knobler, C. M.; Leff, D. V. *J. Phys. Chem. B* **1997**, *101*, 189.

(49) Li, M.; Schnablegger, H.; Mann, S. *Nature* **1999**, *402*, 393.

(50) Li, F.; Josephson, D. P.; Stein, A. *Angew. Chem. Int. Ed.* **2011**, *50*, 360.

(51) Yin, Y.; Lu, Yu.; Gates, B.; Xia, Y. *J. Am. Chem. Soc.* **2001**, *123,* 8718.

(52) Nagle, L.; Fitzmaurice, D. *Adv. Mater.* **2003**, *15*, 933.

(53) Wang, D.; Mohwald, H. *J. Mater. Chem.* **2004**, *14*, 459.

(54) Wang, D.; Salgueirino-Maceria, V, Liz-Marzan, L. M.; Caruso, F. *Adv. Mater.* **2002**, *14*, 908.

(55) Zheng, H.; Rubner, M. F.; Hammond, P.T. *Langmuir* **2002**, *18*, 4505.

(56) Hwang, H.; Park, Y.-H. Park, J.-K. *Langmuir* **2009**, *25*, 6010.

(57) Schaak, R. E.; Cable, R. E.; Leonard, B. M.; Norris, B. C. *Langmuir* **2004**, *20*, 7293.

(58) Rycenga, M, Camargo, P. H. C.; Xia, Y. *Soft Mater.* **2009**, *5*, 1129.

(59) Khanh, N. N.; Yoon, K. B. *J. Am. Chem. Soc.* **2009,** *131,* 14228.

(60) Vlasov, Y. A.; Bo, X. Z.; Sturm, J. C.; Norris, D. J. *Nature* **2001**, *414*, 289.

(61) Jiang, P.; Ostojic, G. N.; Narat, R.; Mittleman, D. M.; Colvin, V. L. *Adv. Mater.* **2001**, *13,* 389.

(62) García-Santamaría, F.; Ibisate, M; Rodríguez, I.; Meseguer, F.; and López, C. *Adv. Mater.* **2003,** *15,* 788.

(63) Jiang, P.; Bertone, J. F.; Colvin, V. L. *Science* **2001**, 291, 453-457.

(64) Noda, S.; Chutinan, A., Imada, M. *Nature* **2000**, *407*, 608.

(65) Nelson, E. C.; García-Santamaría, F.; Braun, P. V. *Adv. Funct. Mater.* **2008**, *18*, 1983.

(66) Rinne, S. A.; García-Santamaría, F.; Braun, P. V. *Nature Photonics* ***2008***, *2*, 52.

(67) Potyrailo, R.A.; Ding, Z.; Butts, M. D.; Genovese, S. E.; Deng, T.; *IEEE Sensors Journal* **2008**, *8*, 815.

(68) Shevchenko, E. V.; Talapin, D. V.; Murray, C. B.; O'Brien, S. *J. Am. Chem. Soc.* **2006**, *128*, 3620.

(69) Leunissen, M. E.; Christova, C. G.; Hynninen, A.-P.; Royall, C. P.; Campbell, A. I.; Imhof, A.; Dijkstra, M.; van Roij, R.; van Blaaderen, A. *Nature* **2005**, *437*, 235.

(70) Kalsin, A.; Fialkowski, M.; Paszewski, M.; Smoukov, S. K.; Bishop, K. J. M.; Grzybowski, B. A. *Science* **2006**, *312*, 420

(71) Tao, A. R.; Huang, J.; Yang, P. *Acc. Chem. Res.* **2008**, *41*, 1662.

(72) Fukao, M.; Sugawara, A.; Shimojima, A.; Fan, W.; Arunagirinathan, M. A.; Tsapatsis, M.; Okubo, T. *J. Am. Chem. Soc.* **2009**, *131*, 16344.

(73) Muševič, I.; Škarabot, M.; Tkalec, U.; Ravnik, M.; Žumer, S. *Science* **2006**, *313*, 954.

(74) Liu, K.; Zhao, N.; Kumacheva, E. *Chem. Soc. Rev.* **2011**, *40*, 656.

(75) van Blaaderen, A.; Ruel, R.; Wiltzius, P. *Nature* **1997**, *385*, 321.

(76) Zhang, X.; Imae, T. *J. Phys. Chem. C* **2009,** *113,* 5947.

(77) Kuemin, C.; Tutz, R.; Spencer, N. D.; Wolf, H. *Langmuir* **2011**, *27*, 6305.

(78) Zareie, M. H.; Xu, X.; Cortie, M. B. *Small* **2007**, *3*, 139.

(79) Xia, Y.; Whitesides, G. M. *Angew. Chem. Int. Ed. Engl.* **1998**, *37*, 550-575.

(80) Santhanam, V.; Andres, R. P. *Nano Lett.* **2004**, 4, 41.

(81) Kinge, S.; Crego-Calama, M.; Reinhoudt, D. N. *ChemPhysChem.* **2008**, *9*, 20.

(82) Zhang, Li, Si, H. –Y, Zhang, H. –L. *J. Mater Chem.* **2008**, *18*, 2660.

(83) Lu, G.; Li, W.; Yao, J.; Zhang, G.; Yang, B.; Shen, J. *Adv. Mater.* **2002**, *14*, 1049.

(84) Pollard, A. M.; Heron, C. *Archaeological Chemistry*, Royal Society of Chemistry, Cambridge, **1996**

(85) Faraday, M. *Philos. Trans.* **1857**, *147*, 145.

(86) Brown, D. H.; Smith, W. E. *Chem. Soc. Rev.* **1980**, *9*, 217.

(87) Jadzinsky, P. D.; Calero, G.; Ackerson, C. J.; Bushnell, D. A.; Kornberg, R. D. *Science* **2007**, *318*, 430.

(88) Brust, M.; Walker, M.; Bethell, M.; Schiffrin, D. J.; Whyman, R., *J. Chem. Soc., Chem. Commun.* 1994, 801.

(89) Brust, M.; Fink, J.; Bethell, D.; Schiffrin, D. J.; Kiely, C. *J. Chem. Soc., Chem. Commun.* **1995**, 1655.

(90) Zubarev, E. R.; Xu, J.; Sayyad, A.; Gibson, J. D. *J. Am. Chem. Soc.* **2006**, *128*, 4958.

(91) Zubarev, E. R.; Xu, J.; Sayyad, A.; Gibson, J. D. *J. Am. Chem. Soc.* **2006**, *128*, 15098.

(92) Prasad, B. L. V.; Stoeva, S. I.; Sorensen, C. M.; Klabunde, K. J. *Chem. Mater.* **2003**, *15*, 935.

(93) Mirkin, C. A.; Letsinger, R. L.; Mucic, R. C.; Storhoff, J. J. *Nature* **1996**, *382,* 607.

(94) Boisselier, E.; Astruc, D. *Chem. Soc. Rev.* **2009**, *38*, 1759.

(95) Pérez-Juste, J.; Pastoriza-Santos, I.; Liz-Marzán, L. M.; Mulvaney, P. *Coord. Chem. Rev.* **2005**, *249*, 1870.

(96) Huang, X.; El-Sayed, I. H.; Qian, W.; El-Sayed, M. A. *J. Am. Chem. Soc.* **2006**, *128*, 2115.

(97) Oyelere, A. K.; Chen, P. C.; Huang, X; El-Sayed, I. H; El-Sayed, M. A. *Bioconjugate Chem.* **2007,** *18*, 1490.

(98) Huff, T. B.; Tong, L.; Zhao, Y.; Hansen, M. H.; Cheng, J.-X.; Wei, A. *Nanomedicine* **2007**, *2*, 125.

(99) Chanda, N.; Shukla, R.; Katti, K. V.; Kannan, R. *Nano Lett.* **2009**, *9*, 1798.

(100) Billot, L.; Lamy de la Chapelle, M.; Grimault, A. S.; Vial, A.; Barchiesi, D.; Bijeon, J. L.; Adam, P. M.; Royer, P. *Chem. Phys. Lett.* **2006**, *422*, 303.

(101) Foss, C. A.; Hornyak, G. L.; Stockert, J. A.; Martin, C. R. *J. Phys. Chem.* **1992**, *96*, 7497.

(102) Yu; Chang, S.-S.; Lee, C.-L.; Wang, C. R. C. *J. Phys. Chem. B* **1997**, *101*, 6661.

(103) Jana, N. R.; Gearheart, L.; Murphy, C. J. *J. Phys. Chem. B* **2001**, *105*, 4065.

(104) Jana, N. R.; Gearheart, L.; Murphy, C. J. *Adv. Mater.* **2001**, *13*, 1389.

(105) Jana, N. R.; Gearheart, L.; Murphy, C. J. *Chem. Mater.* **2001**, *13*, 2313.

(106) Nikoobakht, B.; El-Sayed, M. A. *Chem. Mater.* **2003**, *15*, 1957.

(107) Khanal, B. P.; Zubarev, E. R. *J. Am. Chem. Soc.* **2008**, *130*, 12634.

(108) Kim, F.; Sohn, K.; Wu, J.; Huang, J. *J. Am. Chem. Soc.* **2008**, *130*, 14442.

(109) Lu, X.; Yavuz, M. S.; Tuan, H.-Y.; Korgel, B. A.; Younan Xia, Y. N. *J. Am. Chem. Soc.* **2008**, *130*, 8900.

(110) Pazos-Perez, N.; Baranov, D.; Irsen, S.; Hilgendorff, M.; Liz-Marzan, L. M.; Giersig, M. *Langmuir* **2008**, *24*, 9855.

(111) Rostro-Kohanloo, B. C.; Bickford, L. R.; Payne, C. M.; Day, E. S.; Anderson, L. J.; Zhong, M.; Lee, S.; Mayer, K. M.; Zal, T.; Adam, L.; Dinney, C. P. N.; Drezek, R. A.; Westand, J. L.; Hafner, J. H. *Nanotechnology* **2009**, *20*, 434005.

(112) Khanal, B. P.; Zubarev, E. R. *Angew. Chem. Int. Ed.* **2007**, *46*, 2195.

(113) Mitamura, K.; Imae, T.; Saito, N.; Takai, O. *J. Phys. Chem. B* **2007**, *111*, 8891.

(114) Nikoobakht, B.; Wang, Z. L.; El-Sayed, M. A. *J. Phys. Chem. B* **2000**, *104*, 8635.

(115) Jana, N.R.; Gearheart, L. A.; Obare, S. O.; Johnson, C. J.; Edler, K. J.; Mann, S.; Murphy, C. J. *J. Mater. Chem.* **2002**, *12*, 2909.

(116) Jana, N. R. *Angew. Chem.* **2004**, *116*, 1562.

(117) Ming, T.; Kou, X.S.; Chen, H. J.; Wang, T.; Tam, H.L.; Cheah, K.W.; Chen, J. Y.; Wang, J. F. *Angew. Chem. Int. Ed.* **2008**, *47*, 9685.

(118) Guerrero-Martínez, A.; Pérez-Juste, J.; Carbó-Argibay, E.; Tardajos, G.; Liz-Marzán, L.M. *Angew. Chem. Int. Ed.* **2009**, *48*, 9484

(119) Nie, Z.; Fava, D.; Kumacheva, E.; Zou, S.; Walker, G. C.; Rubinstein, M. *Nat. Mater.* **2007**, *6*, 609.

(120) Thomas, K. G.; Barazzouk, S.; Ipe, B. I.; Joseph, S. T. S.; Kamat, P. V. *J. Phys. Chem. B* **2004**, *108*, 13066.

(121) Sudeep, P. K.; Joseph, S. T. S.; Thomas, K. G. *J. Am. Chem. Soc.* **2005**, *127*, 6516.

(122) Correa-Duarte, M. A.; Pérez-Juste, J.; Sánchez-Iglesias, A.; Giersig, M.; Liz-Marzán, L. M. *Angew. Chem. Int. Ed.* **2005**, *44*, 4375.

(123) Pramod, P.; Thomas, K. G. *Adv. Mater.* **2008**, *20*, 4300.

(124) Shibu Joseph, S. T.; Ipe, B. I.; Pramod, P.; Thomas, K. G. *J. Phys. Chem. B* **2005**, *110*, 150.

(125) Wang, Y.; Li, Y. F.; Wang, J.; Sang, Y.; Huang, C. Z. *Chem. Commun.* **2010**, *46*, 1332.

(126) Chan, Y. T.; Li, S.N.; Moorefield, C. N.; Wang, P. S.; Shreiner, C. D.; Newkome, G. R. *Chem. Eur. J.* **2010**, *16*, 4164.

(127) Caswell, K. K.; Wilson, J. N.; Bunz, U. H. F.; Murphy, C. J. *J. Am. Chem. Soc.* **2003**, *125*, 13914.

(128) Zhen, S. J.; Huang, C. Z.; Wang, J.; Li, Y. F. *J. Phys. Chem. C* **2009**, *113*, 21543.

(129) Chang, J.-Y.; Wu, H.; Chen, H.; Ling, Y.-C.; Tan, W. *Chem. Commun.* **2005**, 1092.

(130) Dujardin, E.; Hsin, L.-B.; Wang, C. R. C.; Mann, S. *Chem. Commun.* **2001**, 1264.

(131) Nakashima, H.; Furukawa, K.; Kashimura, Y.; Torimitsu, K. *Langmuir* **2008**, *24*, 5654.

(132) Talapin, D. V.; Shevchenko, E. V.; Murray, C. B.; Kornowski, A.; Forster, S.; Weller, H. *J. Am. Chem. Soc.* **2004**, *126*, 12984.

(133) Titov, A. V.; Kral, P. *Nano Lett.* **2008**, *8*, 3605.

(134) Alvarez-Puebla, R. A.; Agarwal, A.; Manna, P.; Khanal, B. P.; Aldeanueva-Potel, P.; Carbo-Argibay, E.; Pazos-Perez, N.; Vigderman, L.; Zubarev, E. R.; Kotov, N. A.; Liz-Marzan, L. M. *Proc. Natl. Acad. Sci. U.S.A.* **2011**, *108*, 8157.

(135) Shalaev, V. M.; Cai,W. S.; Chettiar, U. K.; Yuan, H. K.; Sarychev, A. K.; Drachev, V. P.; Kildishev, A. V. *Optics Lett.* **2005**, *30*, 3356.

(136) Agarwal, A.; Lilly, G.D.; Govorov, A. O.; Kotov, N. A *J. Phys. Chem. C* **2008**, *112*, 18314.

(137) Zijlstra, P.; Chon, J. W. M.; Gu, M. *Nature* **2009**, *459*, 410.

Chapter II

Covalent Functionalization of Gold Nanoparticles with Liquid Crystalline Ligands

2.1 Introduction

Over the past few decades, noble metal nanoparticles have gained much attention because of their characteristic optical absorption and scattering generated by collective oscillation of conduction band electrons, also known as surface plasmon resonance.[1,2] The plasmon resonance depends not only on the morphology of the nanoparticles,[3-8] but also on the relative permittivity of the surrounding media.[9-11] Therefore, it is possible to tune the optical properties of nanoparticles by dispersing them in various matrices with different dielectric constants. Liquid crystalline materials are interesting in this respect because their inherent structural anisotropy is suitable for electric field induced switching of plasmon resonance.[12-18] Also, the local orientation of liquid crystal can be determined by monitoring the shift of the optical absorption of the nanoparticles.[19,20] This is generally achieved by immobilizing the nanoparticles on a solid substrate followed by coating them with a thin layer of liquid crystal.[12-20] However, there are no example describing uniform dispersion of large plasmonic nanoparticles in bulk liquid crystal matrix. Preparation of these composite materials is very important to study optical and electronic properties of plasmonic nanoparticles solubilized in a liquid crystal. Proper surface modification of nanoparticles is required to produce such composites. There are several reports in the literature highlighting the preparation of organic-inorganic hybrid material by modifying nanoparticle surface with functional organic compounds and these materials show

enhanced solubility and stability in various solvents.[21-30] Similar strategy can be applied to functionalize the particles with ligands that contain mesogenic units resembling the chemical structure of the liquid crystal solvent.[31-36] Gold nanoparticles of 2-3 nm show only a very weak and broad surface plasmon resonance because the strength of the plasmon oscillation strongly depends on the total number of electrons.[1,33] However, larger gold nanopatricles show strong plasmon resonance because of the presence of larger number of surface electrons.[1,33] For that purpose it is important to develop synthetic methodologies to dissolve larger gold nanoparticles in liquid crystals.

In this chapter, we describe the preparation of plasmonic gold nanoparticles (~6 nm) soluble in nematic liquid crystal 4-cyano-4-*n*-pentylbiphenyl (5CB). This is achieved by chemically modifying the surface of gold nanoparticles with 4-sulfanylphenyl-4-[4-(octyloxy)phenyl]benzoate (SOPB) which structurally resembles 5CB (Figure 2.1). We used a two step synthetic methodology where alkanethiols on gold nanoparticle surface were first exchanged with a hydroxyl-terminated thiol. Thhe hydroxyl group was chemically attached to 4′-octyloxybiphenyl-4-carboxylic acid by esterification reaction. The final product was quantitatively characterized by standard spectroscopic and analytical techniques. The surface modified gold nanoparticles showed enhanced solubility and stability in the liquid crystal media.

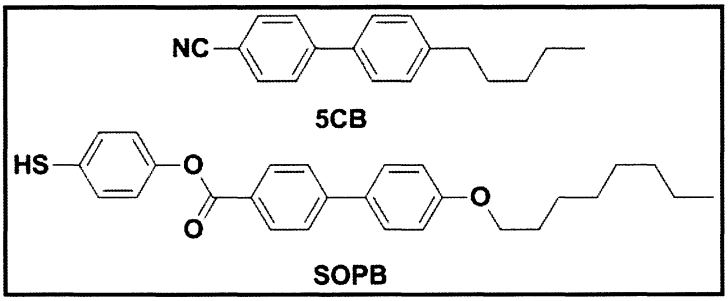

Figure 2.1 Structure of 5CB and SOPB

2.2 Result and Discussion

To study the plasmonic properties of liquid crystal-gold nanoparticle composites, we focused on the preparation of relatively large and near-monodisperse nanoparticles (6 nm) that exhibit a significantly larger and narrower absorption in the visible range when compared with their smaller polydisperse analogues (1-3 nm).[3] Although the synthesis of alkanethiol-capped monodisperse gold nanoparticles is known,[38] there are no examples of monodisperse gold particles coated with functional organic molecules. We developed a two-step synthetic route that enabled us to transform decanethiol-coated gold nanoparticles into their functional analogues carrying alkyloxybiphenyl thiols that resemble the structure of the nematic liquid crystal 5CB.

2.2.1 Ligand exchange of 6 nm gold nanoparticles

In the first step, outlined in Scheme 2.1, monodisperse decanethiol-coated gold nanoparticles synthesized by a literature procedure[38] were treated with a concentrated isopropyl alcohol solution of a low molar mass functional thiol 4-mercaptophenol (Scheme 2.1). We found that under these conditions, nearly 70 % of the decanethiol ligands were exchanged for mercaptophenol molecules, as determined by ^{1}H NMR of the organic residue (Figure 2.2) that formed after complete dissolution of the gold cores in the presence of iodine. The integration value of the aromatic proton peak (α) is 4.35 whereas the methyl group of 1-decanethiol (β) integrates as 3.01. In case of 1:1 mixture the α/β ratio should be 2:3. Therefore, the amount of 4-mercaptophenol present on AuNP surface is 2.2 times greater than the amount of 1-decanethiol which corresponds to a 70% exchange. The resulting nanoparticles became poorly soluble in organic solvents, but retained their narrow size distribution, which was similar to that of the starting material

as determined by TEM (Figure 2.3). The use of the low molecular mass thiol, as opposed to polymeric thiols, is critically important to increase the degree of exchange. Additionally, the choice of organic solvent for the exchange is also very important. Our repeated attempts to perform the ligand exchange in chloroform or THF was not successful as decanethiolated AuNPs crashed out of solution right after the addition of functional thiol. High polarity of isopropanol stabilized the AuNPs in solution for a longer period of time and hence better surface coverage was obtained.

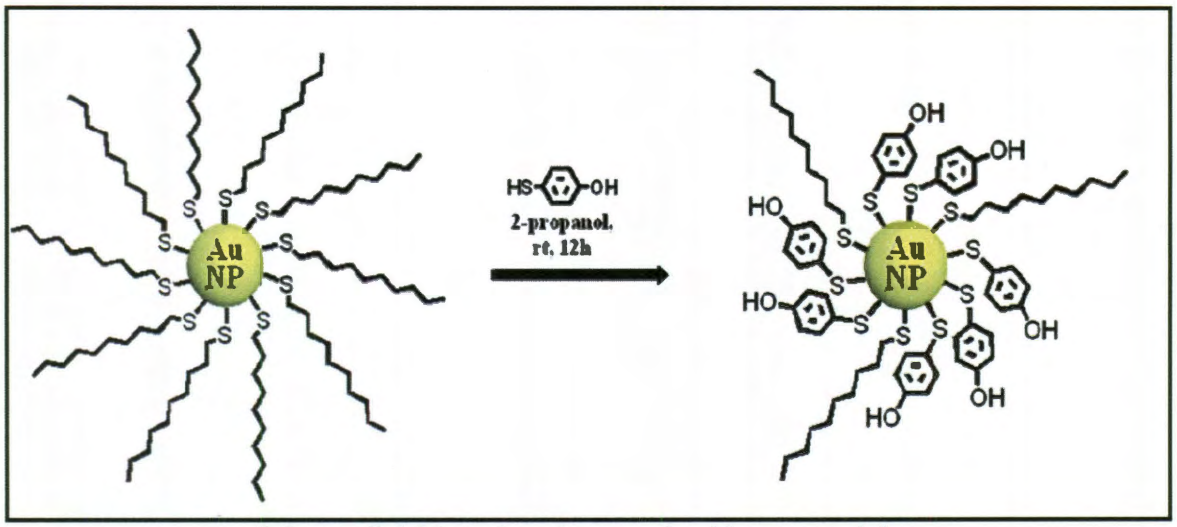

Scheme 2.1 Ligand exchange of gold nanoparticles

It is important to detach surface bound thiols to quantify the ligand exchange. Otherwise, their NMR spectra will suffer from excessive peak broadening and the integration values will not be accurate. A mixture of iodine and potassium iodide can quickly oxidize and dissolve metallic gold, which releases the surface thiol ligands into solution phase. Additionally, the presence of iodine does not interfere with the ^{1}H NMR signals of organic compounds. On the other hand, this dissolution process completely destroys the nanoparticles and they cannot be used for further chemical modifications.

Also, large amount (~100 mg) of AuNP has to be used for this purpose as the mass of thiols present on gold surface is very small.

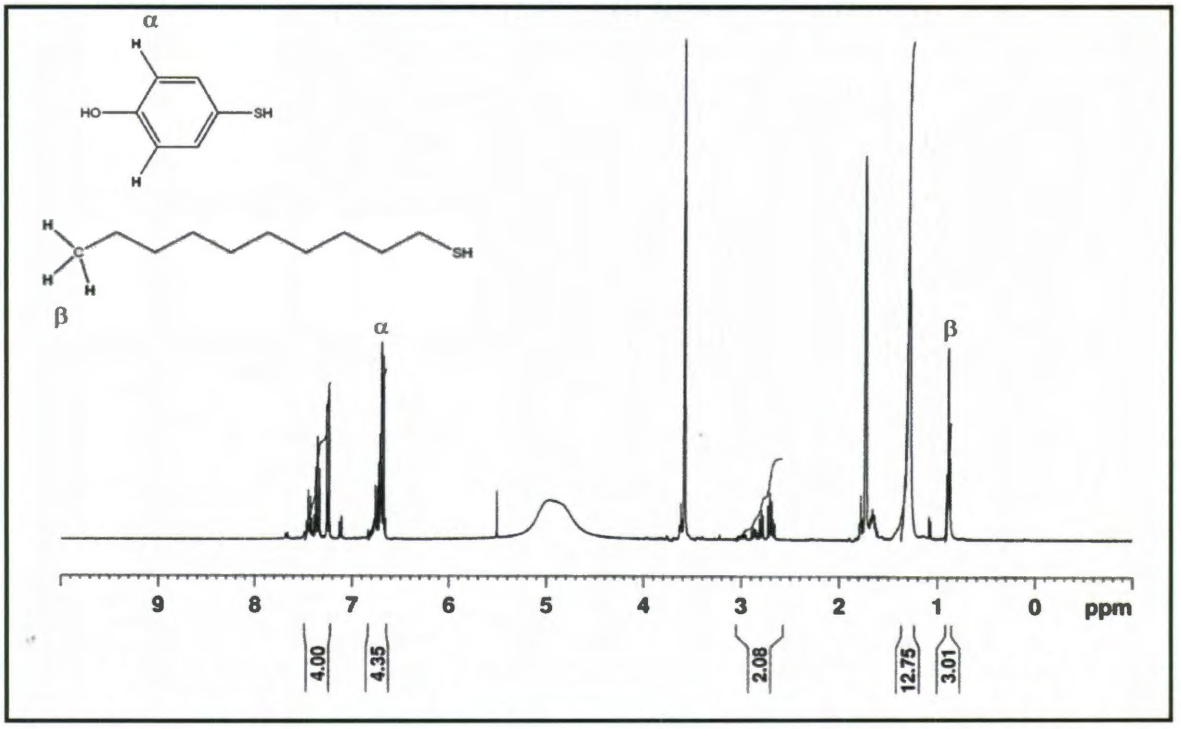

Figure 2.2 ^{1}H NMR spectrum of the free ligands obtained after the dissolution of the gold core of nanoparticles isolated after the ligand exchange between the decanethiol and mercaptophenol. The integration values show that 70 % of decanethiol ligands have been replaced by mercaptophenol ligands on the surface of gold nanoparticles.

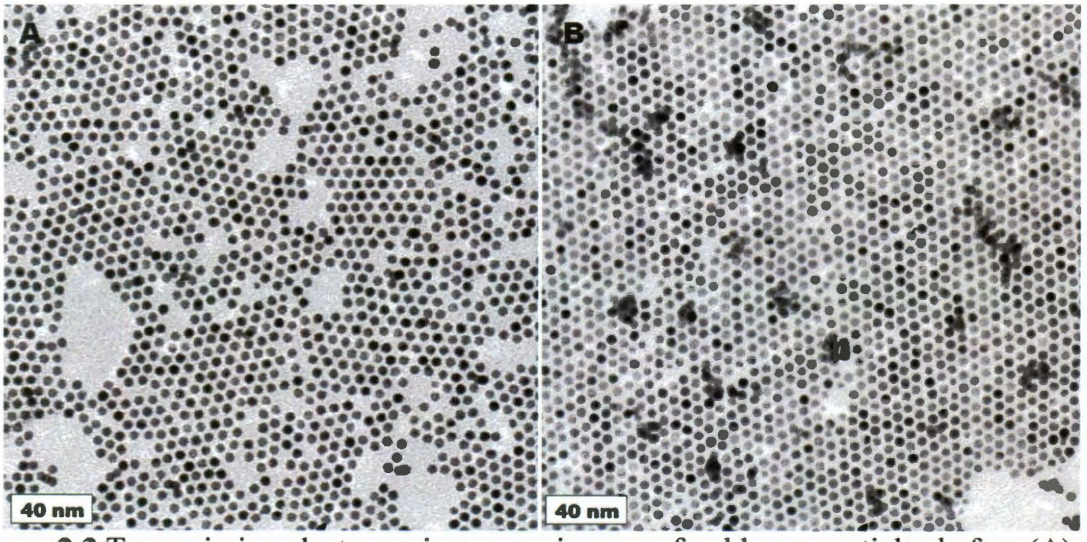

Figure 2.3 Transmission electron microscopy images of gold nanoparticles before (A) and after (B) the ligand exchange.

2.2.2 Synthesis of 4-sulfanylphenyl-4-[4-(octyloxy)phenyl]benzoate (SOPB) functionalized gold nanorparticles

In the second step (Scheme 2.2), the mercaptophenol-coated gold nanoparticles were reacted with 4′-octyloxybiphenyl-4-carboxylic acid under mild esterification conditions using DIPC and DPTS as coupling agents. During the coupling reaction, the nanoparticles gradually dissolved and formed a stable, homogeneous solution in methylene chloride, which was indicative of successful covalent attachment of the liquid-crystal-like 4′-octyloxybiphenyl-4-carboxylic acid ligands. The reaction can be easily monitored by TLC where the mercaptophenol-functionalized nanoparticles with a retention factor of R_f= 0 gradually moves to R_f= 0.75 in 10 % THF in CH_2Cl_2 (Figure 2.4). The reaction mixture was purified according to standard procedures published elsewhere,[21] and the 6 nm nanoparticles functionalized with SOPB ligands were isolated in the form of a dark red powder with an 80 % yield. The purity of the product was confirmed by a TLC (Figure 2.4) and size exclusion chromatography (SEC).[21,23] Unlike smaller particles,[21,23] functionalized 6 nm gold particles did not pass though the SEC column. However, the absence of free organic material was confirmed as no low molecular mass peak was observed in SEC. Figure 2.5 shows a molecular graphics representation of a polyhedral gold nanoparticle functionalized by SOPB ligands and, for comparison, a molecule of 5CB.

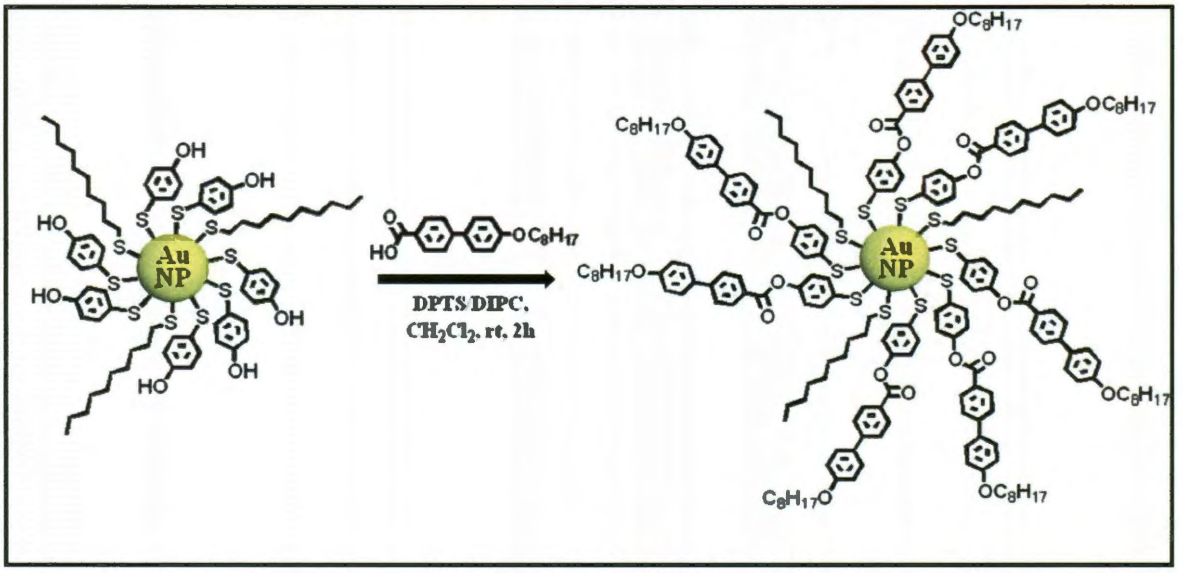

Scheme 2.2 Synthesis of SOBP-Functionalized Gold Nanoparticles

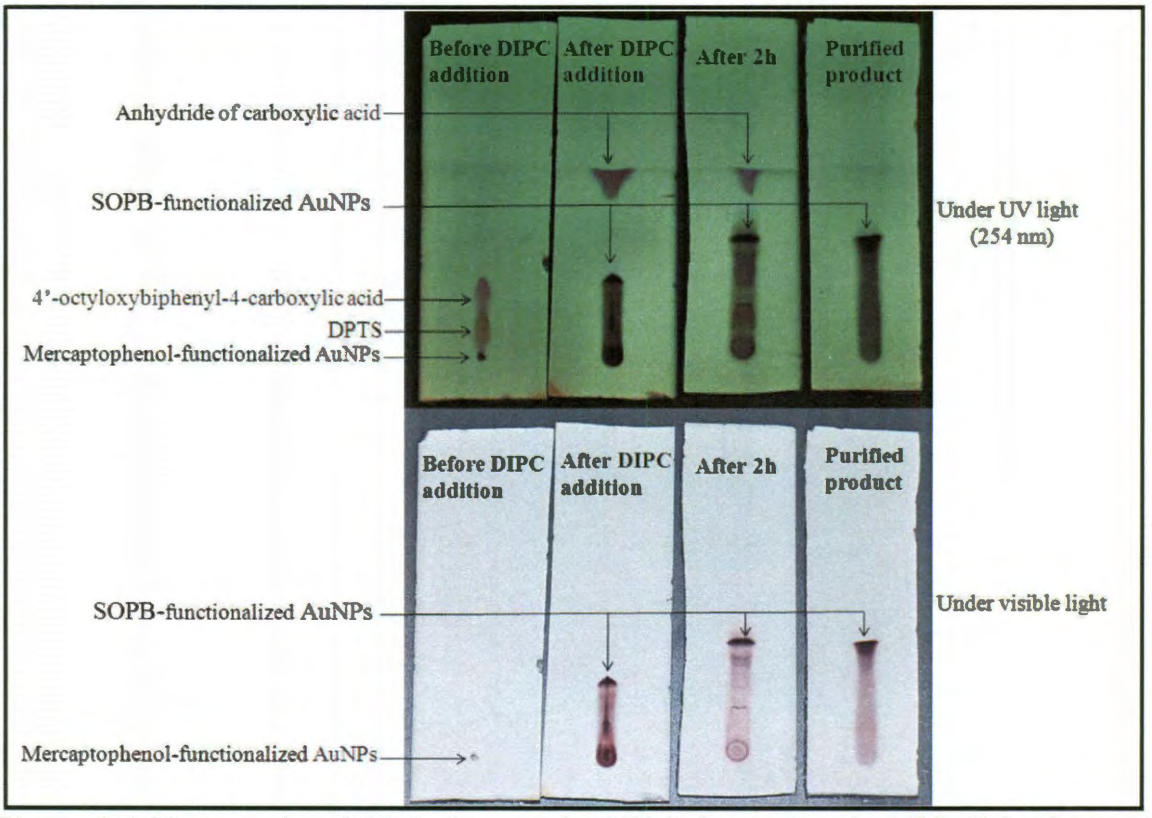

Figure 2.4 Photographs of TLC plates under UV light (top) and visible light (bottom) showing the progress of the esterification reaction between mercaptophenol-functionalized gold particles (AuNPs) and 4'-octyloxybiphenyl-4-carboxylic acid. Note the purity of the final product (SOPB-functionalized AuNPs) and the large increase in retention factor (R_f) from the starting material (mercaptophenol-capped Au NPs, R_f=0) to the final product (SOPB-capped Au NPs, R_f=0.75).

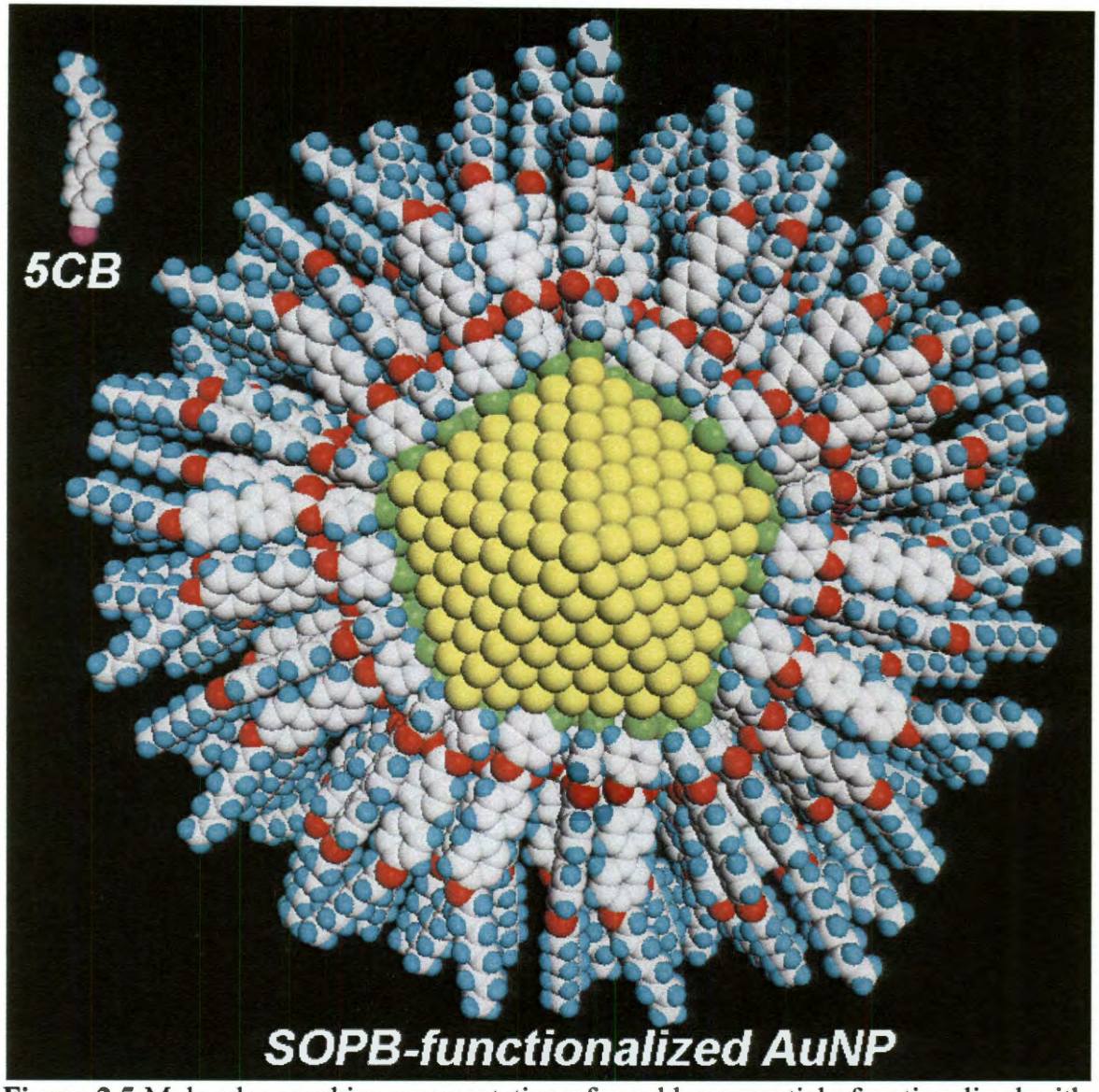

Figure 2.5 Molecular graphics representation of a gold nanoparticle functionalized with SOPB thiols. A 5CB molecule is shown for comparison in the upper left corner.

^{1}HNMR spectra of the purified SOPB functionalized nanoparticles (Figure 2.6) were obtained and compared to the ^{1}HNMR of pure SOPB ligand (Figure 2.7) synthesized by reacting 4-mercaptophenol and 4'-octyloxybiphenyl-4-carboxylic acid under standard esterification condition (Scheme 2.3). The presence of aromatic and aliphatic signals was confirmed. The integration values were consistent with the estimations based on the oxidative dissolution of the gold core (Figure. 2.2) and the TGA

data (Figure 2.8) for the starting material and the final product (70 % SOPB and 30 % residual decanethiol ligands). However, we observed significant broadening of NMR signals in case of SOPB functionalized gold particles indicating the covalent attachment of SOPB molecule to the gold surface. When an organic molecule attaches to gold surface, its rotational mobility is reduced and signal broadening is observed. NMR also confirmed that there are no free SOPB molecules in the mixture as no sharp aromatic signal were present in the spectrum.

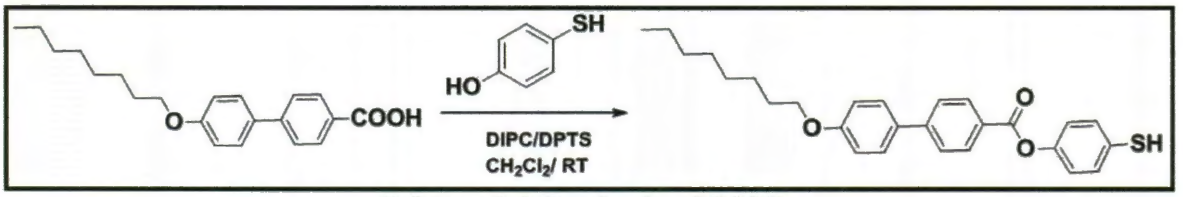

Scheme 2.3 Synthesis of SOPB

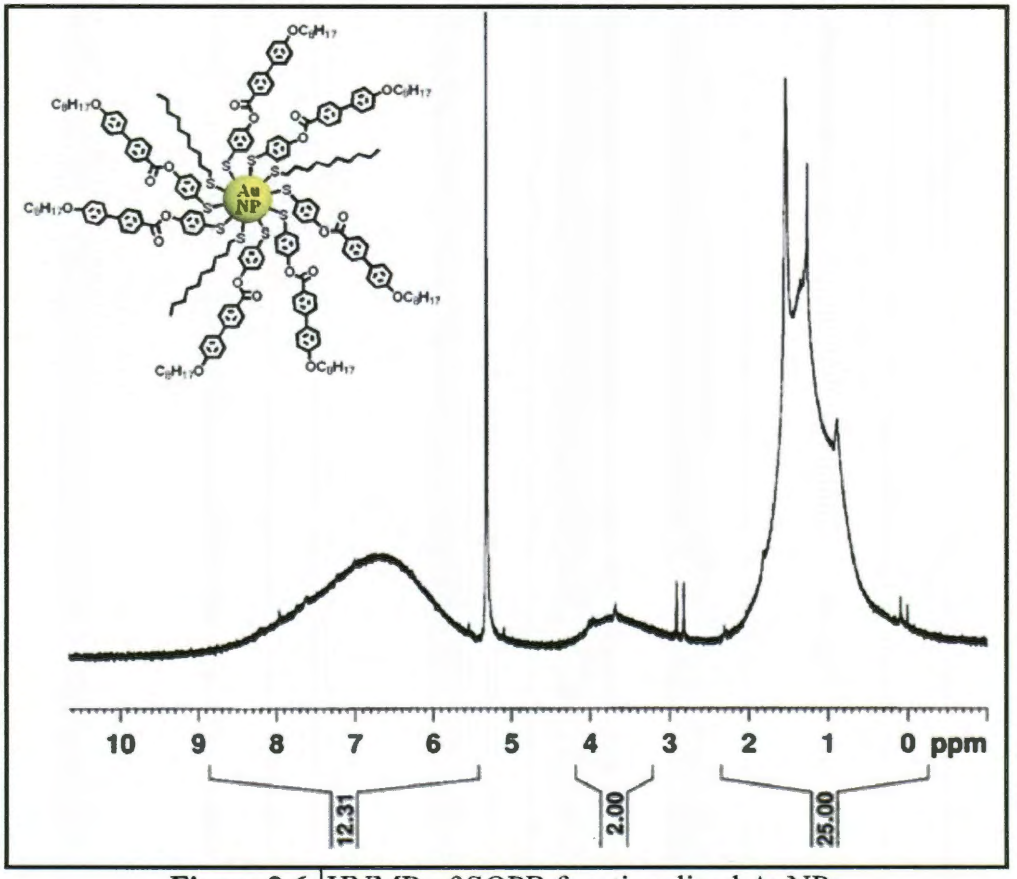

Figure 2.6 ^{1}HNMR of SOPB functionalized AuNPs

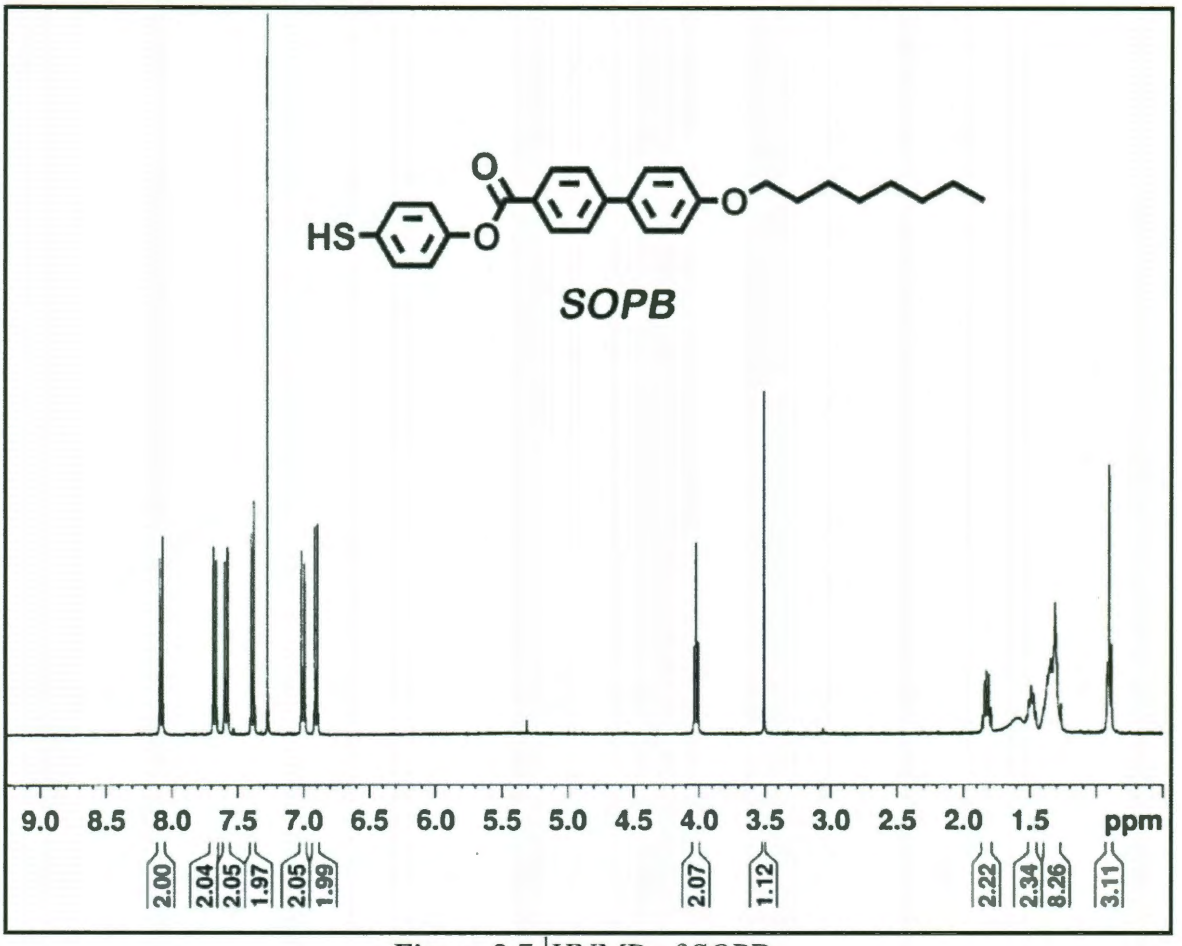

Figure 2.7 ^{1}HNMR of SOPB

Thermo gravimetric analysis (TGA) was also performed to quantify the amount of organic material present on the surface of gold nanoparticles (Figure 2.8). From the TGA data we obtained 5% increase in the weight of the organic residue attached to the gold surface. The increase in weight is due to the covalent attachment of higher molecular weight organic compound. Additionally, we also calculated that the number of decanethiol molecule per gold particle is 630. Therefore, after the ligand exchange the number of 4-mercaptophenol molecules per AuNP would be 441 (70 %). The weight loss of the final product should be 17 % if all the 4-mercaptophenol moieties react with carboxylic acid. However, our TGA result shows 12 % weight loss which is due to the incomplete consumption of 4-mercatophenol during the esterification reaction. TGA data

also showed the higher thermal stability of SOPB-capped gold nanoparticles compared to its decathiolated analogue. In the case of decanethiolated gold particles the weight reduction started at 145° C whereas in case of SOPB-coated particles, the weight reduction began around 210° C (Figure 2.8). This is expected because larger surface coating provides higher stability to the nanoparticles. The TGA curve for SOPB-AuNP is much broader compared to TGA curve of Decanethiol-AuNP. This is due to the presence of mixture of compounds (1-decanethiol, 4-mercaptophenol, and SOPB) on NP surface.

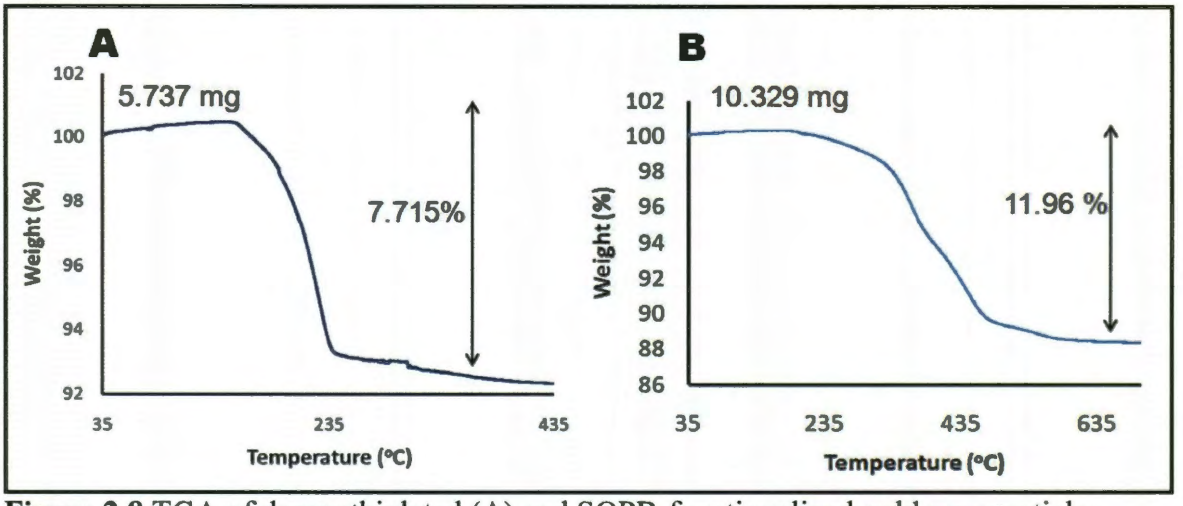

Figure 2.8 TGA of decanethiolated (A) and SOPB-functionalized gold nanoparticles

In order to confirm the presence of larger organic shell on the surface of nanoparticles, we also performed TEM experiments (Figure 2.9). High magnification TEM image of mercaptophenol coated particles showed an interparticle distance of ~1 nm which is consistent with the previous studies.[39] However, for SOPB functionalized gold particles the interparticle distance increased to ~3 nm, which is due to the presence of larger organic shell. The interparticle distance (~3 nm) value is close to the size of SOPB in its fully extended conformation. This is expected because the biphenyl moiety of SOPB makes it structurally rigid and its extended conformation is favored.

Importantly, TEM image also showed that Ostwald ripening did not occur during the chemical modification process as the shape and size of the particles did not change. That also means that their optical properties remain unaltered throughout the ligand exchange process.

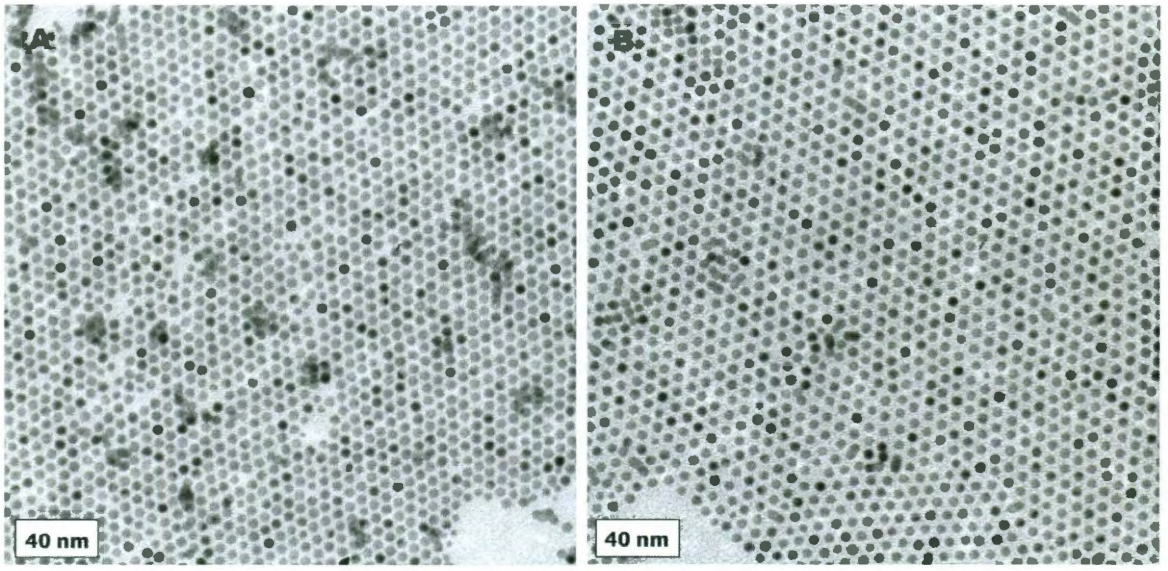

Figure 2.9 TEM image of mercaptophenol-functionalized (A) and SOPB-functionalized gold nanoparticles.

2.2.3 Synthesis SOPB-AuNP and liquid crystal (5CB) composite material

We found that the solubility of decanethiolated AuNPs was very poor in the liquid crystal 5CB. When methylene chloride solution of nanoparticles was mixed with 5CB, a homogeneous solution was formed. However, after removing methylene chloride, the nanoparticles were irreversibly agglomerated and they precipitated out of the solution. Optical studies also showed that there was no distinct plasmon peak at 531 nm corresponding to the particles (Figure 2.10 inset).[40] On the other hand, the solubility of the SOPB-functionalized particles was much better and we were able to dissolve 0.2-wt. % of nanoparticles in 5CB without any aggregation. Remarkably, the solvation does not require the addition of a common solvent like methylene chloride or THF as solid NPs

can be directly dissolved in 5CB upon mild heating. The increase in solubility can be attributed to the structural similarity between SOBP and 5CB. In addition, we also observed 8 nm red shift in plasmon resonance compared to the spectra taken in pure CH_2Cl_2 (Figure 2.10). This is due to an increase in the dielectric constant of the media. This spectral shift is not due to the particle agglomeration as the width of the peak did not broaden and no distinct shoulder was observed on the red side of the spectrum.[41, 42] Moreover, the optical densities remained unchanged even after several temperature cycling between the nematic and the isotropic phase. [40]

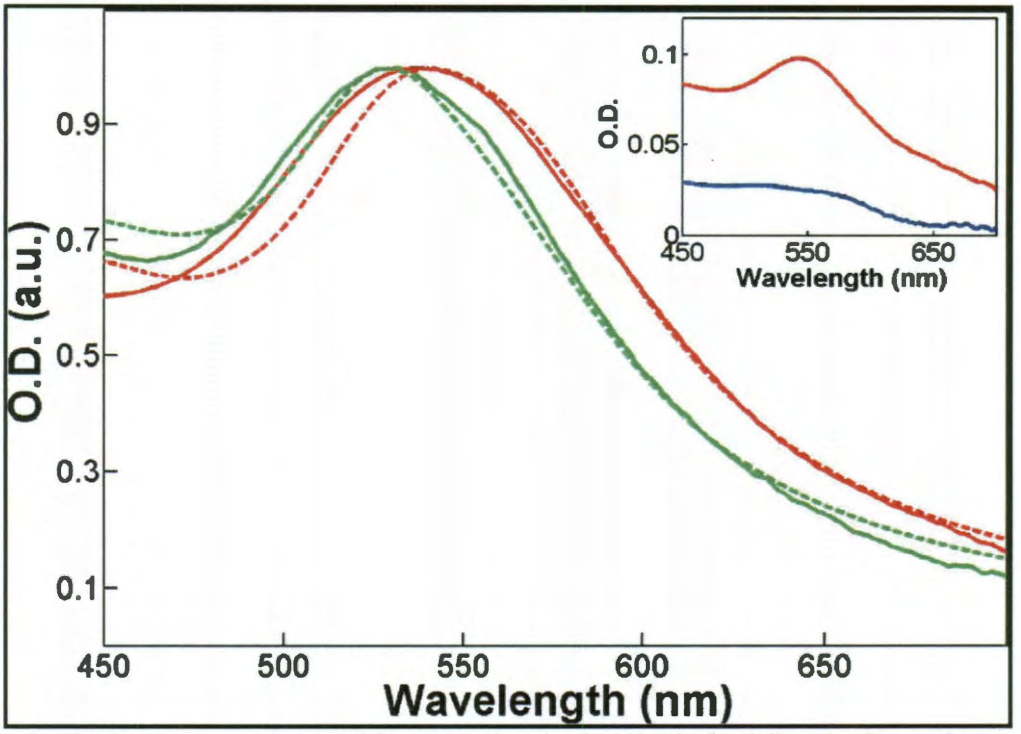

Figure 2.10 Experimental (solid lines) and calculated (dashed lines) absorption spectra of SOPB-functionalized gold nanoparticles in methylene chloride (green lines, λ_{max}) 531 nm) and in 5CB (red lines, λ_{max} 539 nm). The spectra were normalized at the corresponding absorption maxima. The inset compares the absorption spectra of decanethiol- and SOPB-functionalized gold nanoparticles in 5CB (blue and red, respectively).[40]

2.3 Conclusion

In summary, we have reported a two-step synthetic replacement of decanethiol with SOPB functional ligands which renders 6 nm gold nanoparticles soluble in the nematic phase of 5CB. The enhanced solubility was explained by the chemical similarity between the surface capping material and the liquid crystal solvent. This synthetic methodology can be further applied to anisotropic nanostructures in liquid crystals.

2.4 Experimental Section

Gold(III) chloride ($HAuCl_4 \cdot 3H_2O$), 1-decanethiol, sodium borohydride, *N*,*N*-diisopropylcarbodiimide (DIPC) were purchased from Aldrich Chemical Co. 4-Mercaptophenol and 4′-octyloxybiphenyl-4-carboxylic acid were purchased from TCI America and Alfa-Aesar, respectively. 4-(*N*,*N*-Dimethylamino) pyridinium-4-toluenesulfonate (DPTS) was prepared by mixing saturated tetrahydrofuran (THF) solutions of 4-(*N*,*N*dimethylamino) pyridine and *p*-toluenesulfonic acid at room temperature. Unless otherwise stated, all chemicals were used without any further purification. ^{1}HNMR spectra were recorded on solution of CD_2Cl_2 or $CDCl_3$ on a Bruker 400 MHz spectrometer. TEM imaging was done using JEOL 1230 high contrast microscope operating at 100 KV accelerating voltage. TEM samples were prepared by dipping a carbon coated copper TEM grid into the THF or $CHCl_3$ solution of nanoparticles. TGA data was obtained by Q-600 simultaneous TGA/DSC instrument. The digital picture was taken by a Nikon D60 digital camera.

2.4.1 Synthesis of 1-Decanethiol-Capped Gold Nanoparticles

Decanethiol-functionalized gold nanoparticles (~2 nm in diameter) were prepared by two-phase synthesis described by Brust and co-workers.[37] In a typical synthesis, 120 mg of gold(III) chloride was dissolved in 10 mL of DI water. In a separate vial, 730 mg of tetraoctylammonium bromide was dissolved in 27 mL of toluene. These two solutions were mixed and stirred vigorously until the gold chloride was completely transferred into the organic layer. To this organic layer, 65 mg of 1-decanethiol was added, and then a freshly prepared aqueous solution of sodium borohydride (123 mg in 8.5 mL water) was added slowly into the mixture. The organic layer turned dark brown during the reduction. After 5 min of stirring, an excess of methanol was added, and the gold nanoparticles were centrifuged at 1200 rpm for 5 min. Purified particles were dissolved in THF and kept as a stock solution.

2.4.2 Synthesis of Monodisperse 6 nm Gold Nanoparticles

Ten milligrams of decanethiol-capped, 2 nm gold particles were dissolved in 3 g of neat 1-decanethiol. The solution was transferred into an 8 mL vial and capped with a Teflon-coated cap. The vial was heated to 175 $^{\circ}$C and kept at that temperature for 1 h. During this annealing process, the solution became dark red, indicating the overall increase in the size of the gold nanoparticles. The solution was then treated with excess methanol, and the particles were centrifuged at 1200 rpm for 5 min. The precipitate containing decanethiol-capped 6 nm gold nanoparticles was dissolved in THF.

2.4.3 Ligand Exchange of 6 nm Gold Nanoparticles

A concentrated solution was prepared by dissolving 1 g of 4-mercaptophenol in 2 mL of isopropyl alcohol. Gold nanoparticles (10 mg) dissolved in 2 mL of THF were

added dropwise with vigorous stirring. The mixture was stirred for 12 h, followed by addition of excess hexane and centrifugation at 1200 rpm for 5 min. The precipitate was washed several times with methylene chloride to remove the residual organic ligands. The resulting material was treated with iodine in deuterated THF, and the supernatant was analyzed by NMR to determine the ratio of mercaptophenol and residual decanethiol ligands. According to the integration of NMR signals, the nanoparticles contained 70% mercaptophenol ligands in the organic shell.

2.4.4 Covalent Attachment of 4′-*n*-Octyloxybiphenyl-4-carboxylic Acid to Mercaptophenol-Functionalized 6 nm Gold Nanoparticles

4′-*n*-Octyloxybiphenyl-4-carboxylic acid (20 mg) was dissolved in 3 mL of methylene chloride, followed by addition of 10 mg DPTS and 10 drops of DIPC. After 5 min of stirring at room temperature, the mixture became clear, and a concentrated dimethylformamide (DMF) solution of nanoparticles (15 mg in 0.3 mL of DMF) was added to the reaction mixture. The color of the reaction mixture turned dark red, indicating the covalent coupling of nanoparticles with the carboxylic acid. After 2 h, DPTS and DMF were removed by multiple extractions with DI water. Methylene chloride was evaporated under reduced pressure, and the residue was rinsed several times with DMF (poor solvent for the resulting nanoparticles). The particles were dissolved in methylene chloride, and the residual DMF was extracted with DI water. Then the methylene chloride was evaporated, and the product was dissolved in dry THF.

2.4.5 Synthesis of 4-Sulfanylphenyl-4-[4-(octyloxy)phenyl]benzoate (SOPB) Thiol

4′-*n*-Octyloxybiphenyl-4-carboxylic acid (200 mg) and 387 mg of 4-mercaptophenol (5 equiv) were dissolved in 5 mL of methylene chloride. To this mixture,

200 mg of DPTS was added, followed by a dropwise addition of 0.5 mL of DIPC. The reaction was monitored by TLC (10 vol % THF in methylene chloride) in which the strongly UV active spot of the carboxylic acid anhydride (*Rf*) 1) disappeared gradually, and the product spot appeared (*Rf*) 0.6). After the completion of the reaction, the mixture was diluted three times with methylene chloride, and DPTS was removed by extracting with DI water. The methylene chloride was evaporated under reduced pressure, and the residue was treated with excess methanol. The precipitated product was isolated by centrifugation and rinsed several times with methanol. The product was dried under vacuum to yield 220 mg of a light brown powder (80% isolated yield). ^{1}H NMR (400 MHz, $CDCl_3$): δ 0.9 (t,3H), 1.30-1.35 (m, 11H), 1.80 (m, 2H), 3.5 (s, 1H), 4.02 (t,2H), 6.90 (d, 2H), 7.01 (d, 2H), 7.39 (d, 2H), 7.58 (d, 2H),7.68 (d, 2H), 8.08 (d, 2H).

2.4.6 Estimation of the number of ligands per nanoparticles

According to TEM images (Figure 2.3), the average diameter of the nanoparticles is 6 nm. Assuming the spherical shape for the nanoparticles, the volume of each particle is (4/3) π $(d/2)^3$ = 1.13.10-19cm3. Hence, the mass of each particle ($\mathbf{M_{Au}}$) is (19.3 x10^{-3}) x (1.13. 10^{-19}) mg = 2.18.10^{-15} mg. From the TGA analysis of decanethiol-capped gold particles (Fig. S6) the amount of gold core is 5.2944 mg. So the number of gold particles ($\mathbf{N_{DT}}$) is (5.2944/2.18)x10^{15}= 2.43.10^{15}. Also, from the TGA data (Figure 2.8), the amount of decanethiol (MW 173.35) present is 0.4426 mg. Therefore, the number of decanethiol molecules ($\mathbf{N_{DT}}$) is (0.4426x10^{-3}) x (6.023.10^{23})/173.35 = 1.53.10^{18}, and the number of decanethiol molecules per one gold particle is $\mathbf{N_{DT}}$/ $\mathbf{N_{Au}}$= 630. Based on the NMR data obtained by dissolving the gold core after ligand exchange (Figure 2.2), it is observed that 70 percent of decanethiol ligands were replaced by mercaptophenol

ligands. Assuming that all mercaptophenol ligands coupled with 4'-octyloxybiphenyl-4-carboxylic acid to give SOPB, the number of SOPB (MW=433 g/mol) ligands would be 441 per one nanoparticles, whereas the number of decanethiol ligands would be 189. The mass of 441 molecules of SOPB attached to the gold surface ($\mathbf{M_{SOPB}}$) is ($441 \times 433 \times 10^{-3}$)/$6.023.10^{23}$= $3.1703.10^{-16}$ mg. The mass of 189 molecules of decanethiol attached to the gold surface ($\mathbf{M_{DT}}$) is ($189 \times 174.35 \times 10^{-3}$)/$6.023.10^{23}$=$5.428.10^{-17}$mg. Therefore, the percentage of organic shell in SOPB-coated gold particles is $\mathbf{(M_{SOPB}+M_{DT})*100/\ (M_{Au}+M_{SOPB}+M_{DT})}$ = 16.74 %. The percentage weight loss observed experimentally form the TGA of SOPB-functionalized nanoparticles was 11.96 % (Fig. S7), which is close to this value. The difference may be explained by incomplete consumption of hydroxyl groups during esterification.

References

(1) Kreibig, U.; Vollmer, M. *Optical Properties of Metal Clusters*; Springer: Berlin, **1995.**

(2) Heath, J. R. *Phys. Rev. B* **1989**, *40*, 9982.

(3) Jana, N. R.; Gearheart, L.; Murphy, C. J. *Adv. Mater.* **2001**, *13*, 1389.

(4) Nikoobakht, B.; El-Sayed, M. A. *Chem. Mater.* **2003**, *15*, 1957.

(5) Lu, X.; Rycenga, M.; Skrabalak, S. E.; Wiley, B.; Xia, Y. *Annu. Rev. Phys. Chem.* **2009**, *60*, 167.

(6) Wang, H.; Brandl, D. W.; Nordlander, P.; Halas, N. J. *Acc. Chem. Res.* **2007**, *40*, 53.

(7) Link, S.; Wang, Z. L.; El-Sayed, M. A. *J. Phys. Chem. B* **1999**, *103*, 3529.

(8) Link, S.; El-Sayed, M. A. *J. Phys. Chem. B* **1999**, *103*, 4212.

(9) Ghosh , S. K.; Nath, S.; Kundu, S.; Esumi, K.; Pal, T. *J. Phys. Chem. B* **2004**, *108*, 13963.

(10) Templeton, A. C.; Pietron, J. J.; Murray, R. W.; Mulvaney, P. *J.Phys. Chem. B* **2000**, *104*, 564.

(11) Underwood, S.; Mulvaney, P. *Langmuir* **1994**, *10*, 3427.

(12) Wang, Y. *Appl. Phys. Lett.* **1995**, *67*, 2759.

(13) Wang, Y.; Russell, S. D.; Shimabukuro, R. L. *J. Appl. Phys.* **2005**, *97*, 023708.

(14) Kossyrev, P. A.; Yin, A.; Cloutier, S. G.; Cardimona, D. A.; Huang, D.; Alsing, P. M.; Xu, J. M. *Nano Lett.* **2005**, *5*, 1978.

(15) Dickson, W.; Wurtz, G. A.; Evans, P. R.; Pollard, R. J.; Zayats, A. V. *Nano Lett.* **2008**, *8*, 281.

(16) Chu, K. C.; Chao, C. Y.; Chen, Y. F.; Wu, Y. C.; Chen, C. C. *Appl. Phys. Lett.* **2006**, *89*, 103107.

(17) Evans, P. R.; Wurtz, G. A.; Hendren, W. R.; Atkinson, R.; Dickson, W.; Zayats, A. V.; Pollard, R. J. *Appl. Phys. Lett.* **2007**, *91*, 043101.

(18) Mueller, J.; Soennichsen, C.; von Poschinger, H.; von Plessen, G.; Klar, T. A.; Feldmann, J. *Appl. Phys. Lett.* **2002**, *81*, 171.

(19) Evans, S. D.; Allinson, H.; Boden, N.; Flynn, T. M.; Henderson, J. R. *J. Phys. Chem. B* **1997**, *101*, 2143.

(20) Koenig, G. M., Jr.; Meli, M.-V.; Park, J.-S.; de Pablo, J. J.; Abbott, N. L. *Chem. Mater.* **2007**, *19*, 1053.

(21) Zubarev, E. R.; Xu, J.; Sayyad, A.; Gibson, J. D. *J. Am. Chem. Soc.* **2006**, *128*, 4958.

(22) Khanal, B. P.; Zubarev, E. R. *Angew. Chem. Int. Ed.* **2007**, 46, 2195.

(23) Gibson, J. D.; Khanal, B. P.; Zubarev, E. R. *J. Am. Chem. Soc.* **2007**, *129,* 11653.

(24) Watson, K. J.; Zhu, J.; Nguyen, S. T.; Mirkin, C. A. *J. Am. Chem. Soc.* **1999**, *121*, 462.

(25) Templeton, A. C.; Wuelfing, W. P.; Murray, R. W. *Acc. Chem. Res.* **2000**, *33*, 27.

(26) El-Sayed, M. A. *Acc. Chem. Res.* **2001**, *34*, 257.

(27) Daniel, M.-C.; Astruc, D. *Chem. Rev.* **2004**, *104*, 293.

(28) Mirkin, C. A.; Letsinger, R. L.; Mucic, R. C.; Storhoff, J. J. *Nature* **1996**, *382*, 607.

(29) Wuelfing, W. P.; Gross, S. M.; Miles, D. T.; Murray, R. W. *J. Am. Chem. Soc.* **1998**, *120*, 12696.

(30) Chiu, J. J.; Kim, B. J.; Kramer, E. J.; Pine, D. J. *J. Am. Chem. Soc.* **2005**, *127*, 5036.

(31) Qi, H.; Kinkead, B.; Marx, V.; Zhangi, H.; Hegmann, T. *ChemPhysChem* **2009**, *10*, 1211.

(32) Kumar, S.; Pal, S. K.; Kumar, P. S.; Lakshminarayanan, V. *Soft Matter* **2007**, *3*, 896.

(33) Marx, V. M.; Girgis, H.; Heiney, P. A.; Hegmann, T. *J. Mater. Chem.* **2008**, *18*, 2983.

(34) Frein, S.; Boudon, J.; Vonlanthen, M.; Scharf, T.; Barbera, J.; Suss-Fink, G.; Burgi, T.; Deschenaux, R. *Helv. Chim. Acta* **2008**, *91*, 2321.

(35) In, I.; Jun, Y.-W.; Kim, Y. J.; Kim, S. Y. *Chem. Commun.* **2005**, 800.

(36) Zeng, X.; Liu, F.; Fowler, A. G.; Ungar, G.; Cseh, L.; Mehl, G. H.; Macdonald, E. J. *Adv. Mater.* **2009**, *21*, 1746.

(37) Brust, M.; Fink, J.; Bethell, D.; Schiffrin, D. J.; Kiely, C. *J. Chem. Soc., Chem. Commun.* **1995**, 1655.

(38) Lin, X. M.; Wang, G. M.; Sorensen, C. M.; Klabunde, K. J. *J.Phys. Chem. B* **1999**, *103*, 5488.

(39) Terrill, R. H.; Postlethwaite, T. A.; Chen, C. –H.; Poon, C.-D.; Terzis, A.; Chen, A.; Hutchison, J. E.; Clark, M. R.; Wignall, G.; Londono, J. D.; Superfine, R.; Favo, M.; Johnson, C. S.; Samulski, E. T.; Murray, R. W. *J. Am. Chem. Soc.* **1995**, *117*, 12537.

(40) Khatua, S.; Manna, P.; Chang, W.-S.; Tcherniak, A.; Friedlander, E.; Zubarev, E. R.; Link, S. *J. Phys. Chem. C.* **2010**, 114, 7251.

(41) Storhoff, J. J.; Mirkin, C. A. *Chem. Rev.* **1999**, *99*, 1849.

(42) Moskovits, M.; Vlckova, B. *J. Phys. Chem. B* ***2005, 109,*** 14*755*.

Chapter III

Covalent Functionalization of Gold Nanorods: Enhanced Stability and Biocompatibility

3.1 Introduction

Highly stable and biocompatible gold nanostructures are suitable for various application in biological systems.[1] Gold nanorods are particularly interesting in this respect because of their strong absorption and scattering in near infrared (NIR) region, also known as surface plasmon resonance.[2,3] It is also possible to tune surface plasmon resonance peak by changing the shape, size, and aspect ratio of gold nanorods.[3-15] For that reason gold nanorods have been extensively used for bio-medical imaging because their position inside the cells can be precisely located using a safe laser light.[16-22] In addition, when a laser light of appropriate wavelength is shone upon gold nanorods, they instantly heat up to cause rapid increase in local temperature.[23-28] This property can be successfully applied for photothermal cancer therapy.[23-28] For that purpose gold nanorods are selectively delivered to tumor cells, which are then destroyed by exposing them to a laser light. However, proper surface modification of gold nanorods is required to realize such targeted delivery. Gold nanorods synthesized by seed mediated growth method are stabilized by a cationic surfactant cetyltrimethylammonium bromide (CTAB).[4,5] CTAB not only acts as a template for one dimensional growth, but also stabilizes the AuNRs in aqueous solution by forming a dynamic bilayer on NR surface.[29] However, CTAB is a highly cytotoxic cationic surfactant and its complete removal is essential for any biological applications. Unfortunately, removal of excess CTAB from NR solution results

in the destruction of the dynamic bilayer leading to irreversible agglomeration of NRs. It was also demonstrated in the literature that the cytotoxicity of gold nanorods is due to the presence of free CTAB in the media, not due to the surface bound CTAB bilayer.[30]

To reduce the cytotoxicity of CTAB-coated rods, various research groups used layer by layer deposition of ionic polyelectrolytes on top of the CTAB coating of gold nanorods.[30-35] Although polyelectrolyte-CTAB interaction is quite strong, the attachment of CTAB first layer to gold surface is fairly weak due to its noncovalent nature. For that reason polyelectrolyte-CTAB is easily detached from NR surface and this complex is found to be even more cytotoxic than free CTAB.[33] In order to solve this problem a CTAB-like ligand must be covalently anchored to gold nanorods and then it can be used as robust platform for layer-by-layer deposition. Surface modification with water soluble thiolated polyethylene glycols (PEG-SH) is also used to detoxify gold nanorods for their application in biological systems.[36-43] However, the presence of large polymer shell around gold nanorods makes it hard to characterize the hybrid material by conventional analytical techniques. Additionally, PEG-NRs are neutral in nature and they are hardly taken by the cells.[44] Plasma membrane of cancer cells is known to be negatively charged and NRs should have positive charge for effective internalization. Synthesis of a positively charged functional thiol that can stabilize gold nanorods in aqueous solution is required for reduced cytotoxicity and high cellular uptake.

In this chapter, we described the synthesis of thiolated analogue of CTAB molecule thiocetyltrimethylammonium bromide (TCTAB) (Figure 3.1) which can stabilize gold nanorods in aqueous solution by forming a covalent bond via pendant thiol groups. The positive charge at the end of the alkyl tail provides necessary water

solubility. Unlike PEGylated NRs, TCTAB-functionalized nanorods are positively charged and they are readily internalized by cancer cells. Additionally, small size of these ligand molecules also allows one to characterize the hybrid material by conventional analytical techniques.

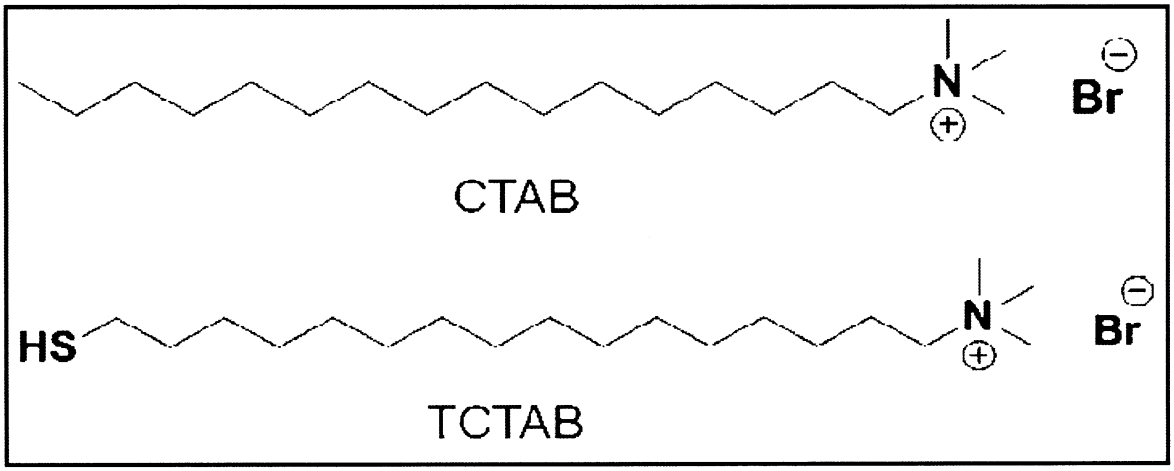

Figure 3.1 Structure of CTAB and TCTAB ligands.

3.2 Results and Discussions

The concentration of CTAB in the aqueous solution of gold nanorods must be maintained above certain value to avoid the irreversible aggregation of nanorods. As the attachment of CTAB is noncovalent in nature, there is a constant dynamic exchange between the free CTAB in the solution and the CTAB present in the bilayer that encapsulates the rods. Therefore, a continuous removal of CTAB by centrifugation eventually depletes the bilayer and NRs precipitate out of the solution. To replace the CTAB without disturbing the solubility of the nanorods, we decided to choose a functional organic ligand that structurally resembles CTAB, but is capable of binding strongly to the gold surface by forming gold-sulfur covalent bond.

3.2.1 Synthesis of thiocetyltrimethylammonium bromide (TCTAB)

The synthetic strategy of TCTAB (Scheme 3.1) begins with the bromination of commercially available hexadecane-1,16-diol **1** to produce 1,16-dibromohexadecane **2** in 70 % isolated yield. Compound **2** was reacted with stoichiometric amount of thiolacetic acid under basic condition to give 16-bromo-1-hexadecanethioacatate **3** in 50 % yield. Deprotection of thioacetate group gave the desired bromothiol **4** which was then converted to TCTAB **5** by exhaustive methylation.[45]

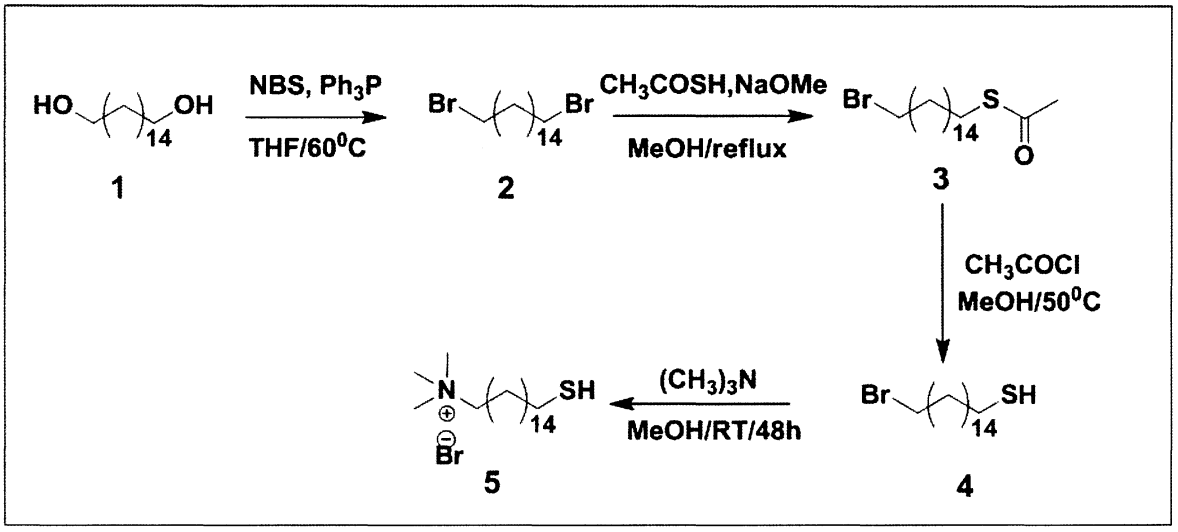

Scheme 3.1 Synthesis of TCTAB cationic thiol.

The only structural difference between TCTAB and CTAB is the presence of thiol group at the end of the alkyl tail, which can stabilize gold nanorods by forming a strong gold-sulfur bond. In addition, small size of TCTAB is ideal for carrying out an efficient exchange of CTAB. It is also expected that TCTAB will form a close-packed monolayer on the surface of gold nanorods which is similar to the self-assembled monolayer formation of thiols on macroscopically flat gold surfaces.[45] Essentially, this process will replace a non-covalent bilayer with covalent monolayer of cationic thiols.

3.2.2 Ligand exchange of gold nanorods with TCTAB

Unlike spherical gold nanoparticles, direct synthesis of thiol-functionalized gold nanorods is not possible because the presence of CTAB is essential for one dimensional growth of gold clusters. In a typical growth solution of gold nanorods the concentration of CTAB is very high (36.5 mg/mL). Hence, the chance of exchanging CTAB with its thiolated analogue in the presence of such a high concentration of CTAB is quite difficult unless a huge amount of expensive thiol is used. To solve this problem, the nanorods solution was centrifuged once and the precipitate was re-dispersed in pure water. This centrifugation process reduced the concentration of CTAB approximately 40 times without altering the solubility of AuNRs. However, additional rounds of centrifugation must be avoided to prevent the irreversible agglomeration of gold nanorods. The solution of nanorods was subsequently treated with appropriate amount of cationic thiol TCTAB solution (Scheme 3.2). In stark contrast to the conventional nanorods, TCTAB-functionalized structures can be centrifuged numerous times without losing any solubility. This was proven by collecting UV-vis spectra of the nanorods solution prepared after each round of centrifugation (Figure 3.2). Additionally, we did not observe any red shift or broadening of the plasmon peak of TCTAB-capped gold nanorods. This observation proves that the ligand exchange was successful and the nanorods were covalently functionalized with a water soluble compound. This ligand exchange essentially changes the surface coating from CTAB bilayer to a tightly packed monolayer of TCTAB thiol. Due to the presence of positively charged quaternary ammonium group at the terminus of this monolayer, the stability of nanorods in pure water is extremely high. To quantify the extent of exchange the ^{1}H NMR spectra were recorded by

dissolving the gold cores of TCTAB-coated nanorods. Dissolution of the gold core is essential to avoid excessive peak broadening. Comparing the spectra of these free ligands, it is evident that the isolated signal from the long-chain methyl group of CTAB at 0.93 ppm is not present in the TCTAB spectrum (Figure 3.3). This NMR data clearly proves that the ligand exchange is complete and there is no residual CTAB on nanorod surface. Thermogravimetric analysis (TGA) was also used to quantify the amount of TCTAB ligands. TCTAB coated AuNRs were first lyophilized to form a low density powder sample. These thiol coated nanorods were perfectly stable in the solid state and could be re-dissolved in water without any signs of aggregation. A weight loss of 5.3% was observed by TGA, which corresponds to a grafting density of 0.26 nm^2/molecule. This value is consistent with the values obtained for alkanethiolcapped flat gold substrates.[46]

We also observed that the ligand exchange procedure does not depend on the shape and size of the nanorods. Larger gold nanostructures (gold microrods, gold nanowires) can also be indefinitely stabilized in water by modifying their surface with positively charged thiols. This is important for stabilizing high aspect ratio gold nanostructures which readily agglomerate from their aqueous solution by forming bundles. The propensity of the nanowires to form bundles can be reduced by modifying their surface with TCTAB. Moreover, TCTAB nanorods can also be stored as powder because of the covalent nature of surface coating.

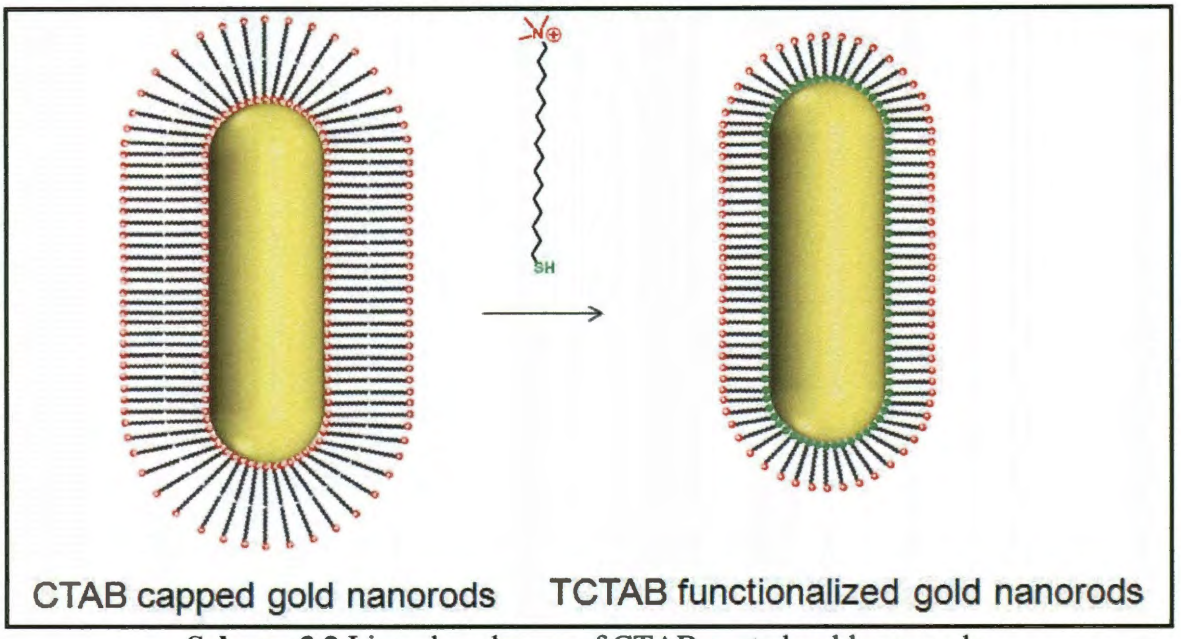

Scheme 3.2 Ligand exchange of CTAB coated gold nanorods

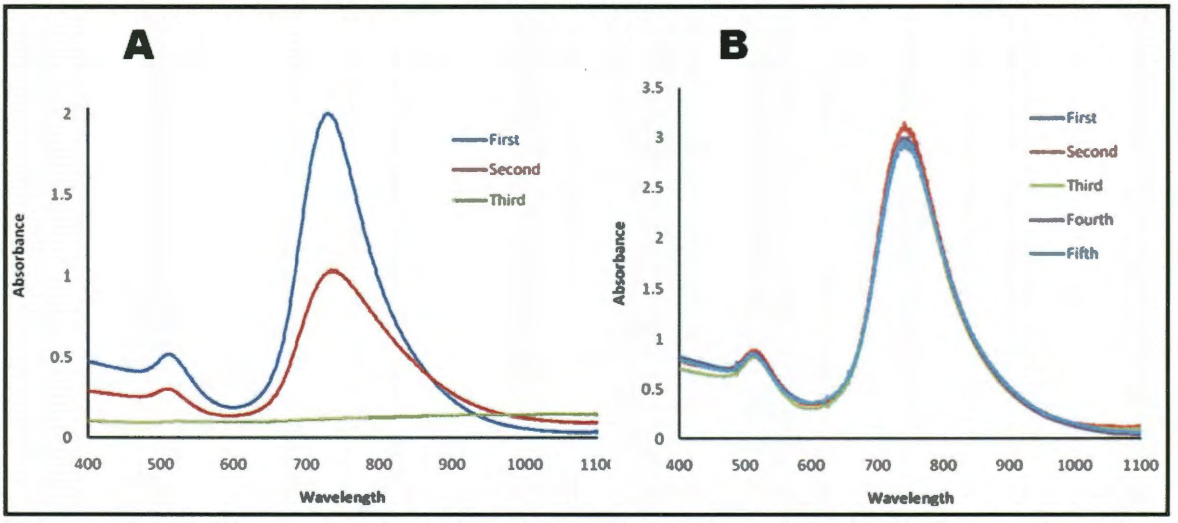

Figure 3.2 UV-Vis spectra of (A) CTAB-coated AuNRs and (B) TCTAB-coated AuNRs. The absorbance is recorded from samples prepared after each round of centrifugation. Note that the solubility of TCTAB-coated NRs remained unaltered after five rounds of centrifugations (B), whereas the plasmon peak disappeared after three rounds of centrifugation in the case of CTAB-capped NRs (A).

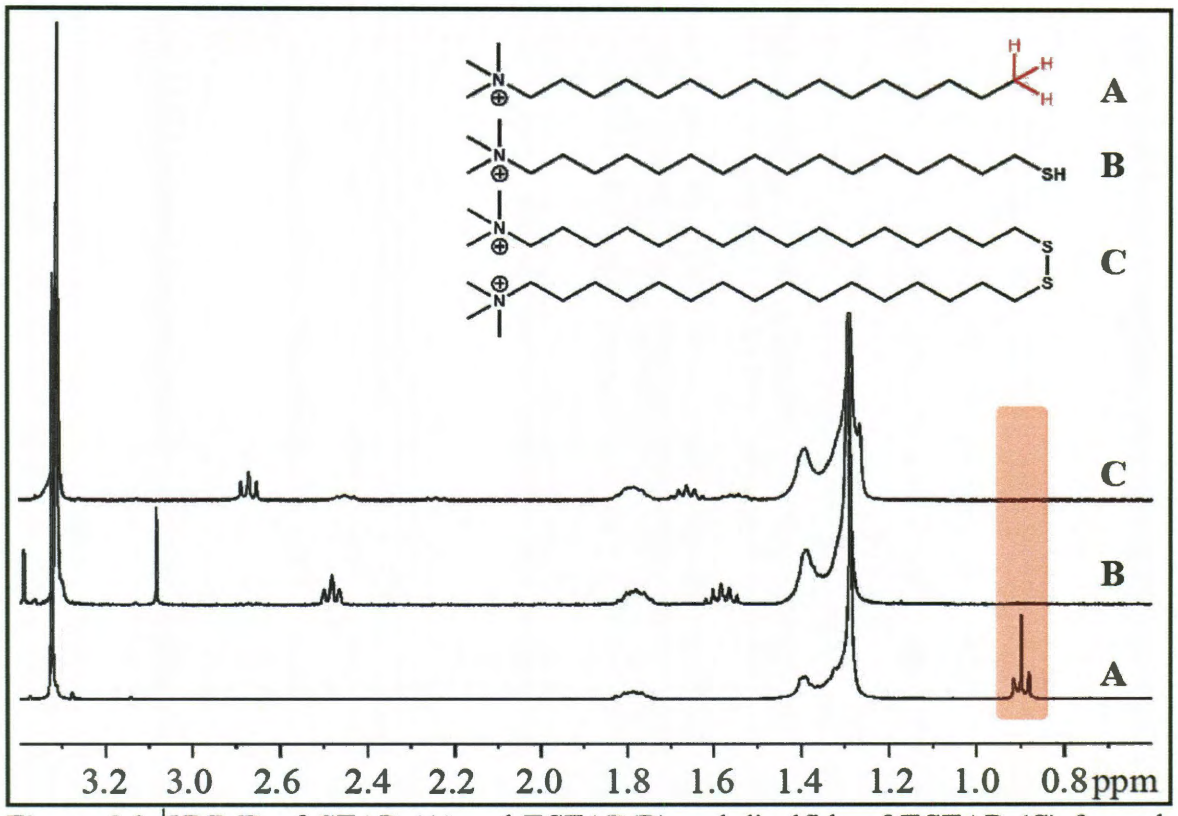

Figure 3.3 ^{1}HNMR of CTAB (A) and TCTAB(B) and disulfide of TCTAB (C) formed after oxidative dissolution of gold core. Note the absence of methyl peak at 0.93 ppm in B, and C.

We also performed SEM imaging to determine the morphology of nanorods after the ligand exchange. Figure 3.4 A and B show the SEM images of CTAB- and TCTAB-coated gold nanorods, respectively. The shape and size of NRs remain unchanged. However, CTAB-capped gold nanorods are organized in ordered arrays where as TCTAB-capped gold nanorods are packed randomly. This is consistent with the previous studies, which show that free CTAB directs the ordered assembly of gold nanostructures into colloidal crystals.[47]

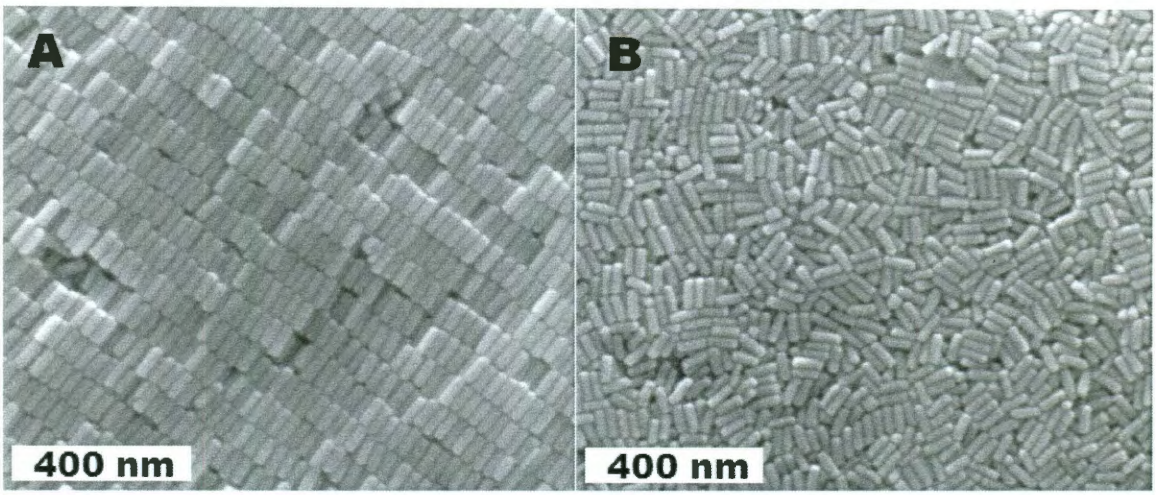

Figure 3.4 SEM images of CTAB-capped (A) and TCTAB-capped (B) gold nanorods. Samples were prepared by drying a drop of their aqueous solution on a silicon wafer.

3.2.3 *In vitro* cytotoxicity studies of TCTAB-functionalized nanorods

Previous research have shown that the cytotoxicity of CTAB-AuNR is mostly due to the presence of free CTAB in solution.[30] However, it is difficult to distinguish between the unbound free CTAB and surface bound CTAB molecules as they are involved in a dynamic equilibrium. Our systematic characterization proved that in case of TCTAB-coated gold nanorods, both surface bound and free CTAB were completely removed. Therefore, it is expected that these NRs will show reduced cytotoxicity. The cytotoxicity study was performed using 15,000 breast cancer cell count standard MTT assay. The cytotoxicity was quantified by calculating the IC_{50} value which is defined as the concentration of nanorods required for 50 percent cell death. CTAB-AuNRs showed high cytotoxicity (IC_{50} = 18 μg/mL) and at 100 μg/mL concentration almost all the cells died. On the other hand, TCTAB-AuNRs were virtually nontoxic as we could not calculate the IC_{50} value (cell viability ~ 90%) (Figure 3.5).

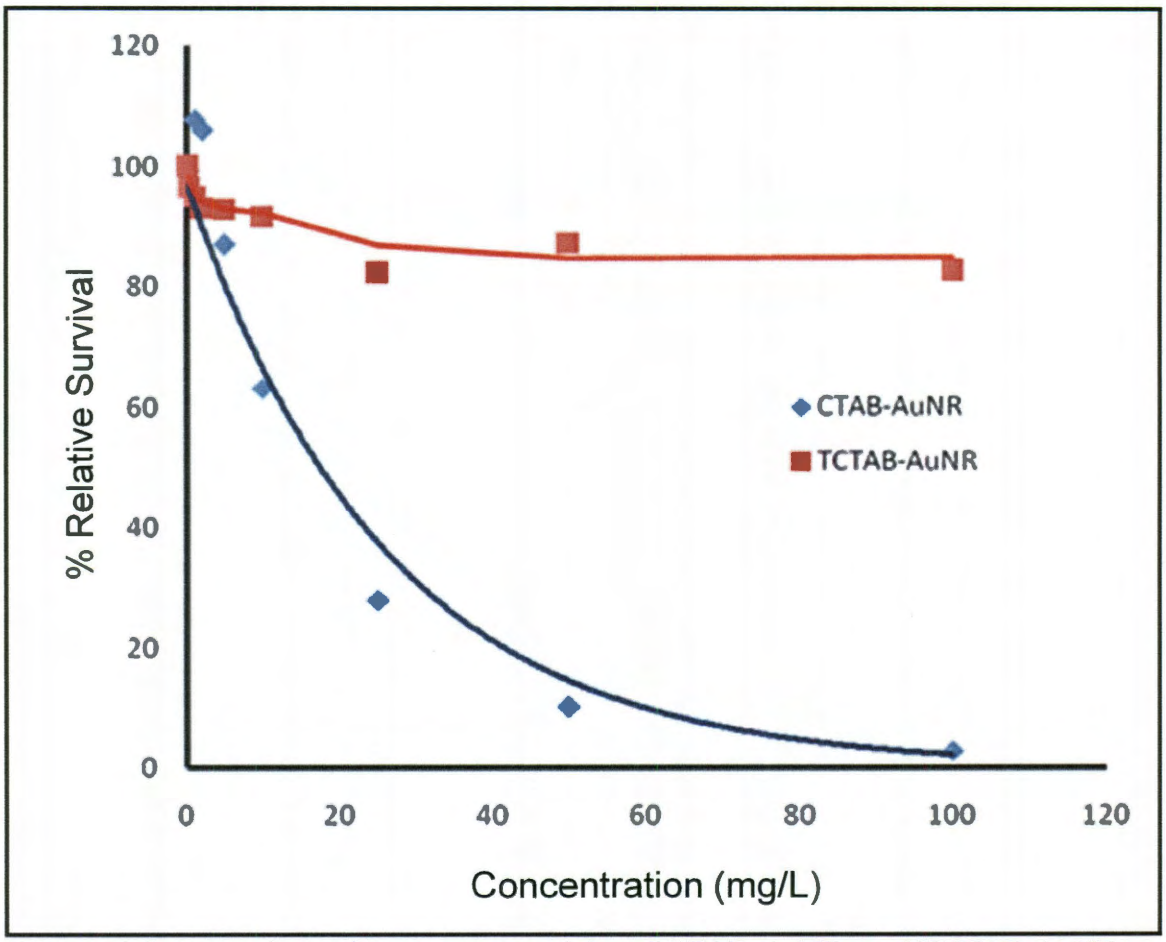

Figure 3.5 Comparison of *in vitro* cytotoxicity of CTAB-AuNRs and TCTAB-AuNRs.

This result is consistent with the previous assertions that the surface charge is not a key factor for the cytotoxicity of nanoparticle systems.[30] This experiment also suggests that the TCTAB-coated NRs should be ideal candidates for layer-by-layer assembly with polyelectrolytes. Previous research showed that highly cytotoxic polyelectrolyte-CTAB complex easily detaches from NR surface because of the non-covalent nature of gold-CTAB bond.[33] This problem will no longer exist in case of TCTAB-AuNRs as the thiol is covalently anchored to the gold surface.

3.2.4 Cellular uptake studies of TCTAB functionalized nanorods

While performing cytotoxicity experiments we observed that TCTAB-AuNR treated cells become purple, which indicates the association of thiolated NRs with the cells. This is expected because positively charged AuNRs are strongly attracted to the plasma membrane of cancer cells. To determine the location of NRs we performed bright field optical microscopy experiments. For that purpose, cells treated with the AuNR-TCTAB were first fixed on a substrate and then the substrate was investigated using reflective mode of an optical microscope. We were able to see large number of tiny bright spots indicating the presence of NRs inside the cells ((Figure 3.6). However, these NRs are relatively small in size and their optical scattering intensity is quite low.

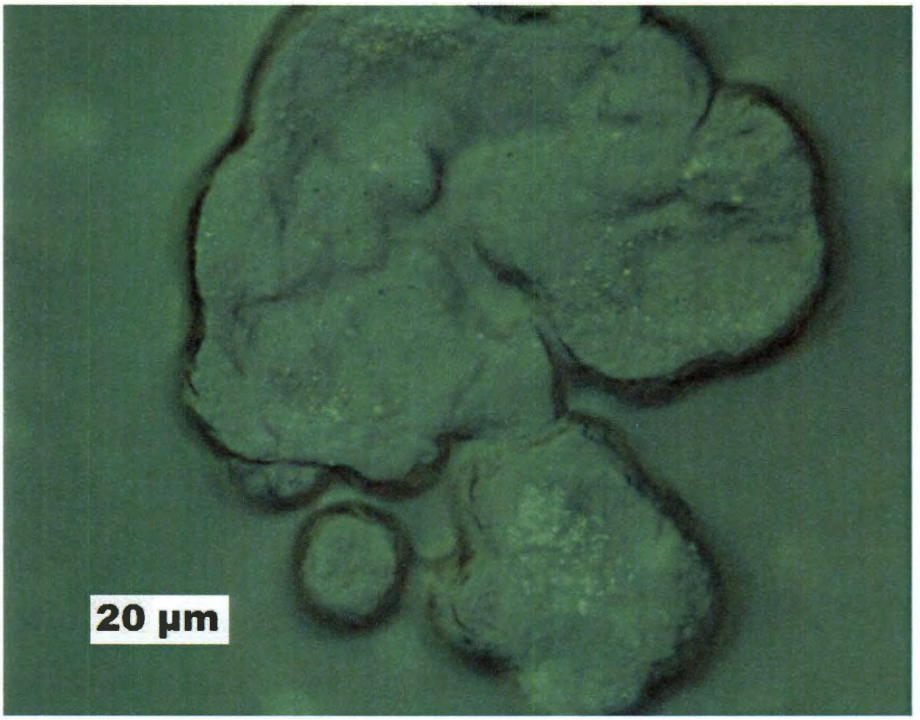

Figure 3.6 Gold nanorods (bright spots) inside breast cancer cells.

To improve the contrast and scattering, we investigated cellular uptake of larger gold microrods (800x 200 nm). Gold microrods were first prepared in the presence of CTAB and then CTAB bilayer was replaced by TCTAB by the ligand exchange

procedure mentioned in chapter 3.2.2. TCTAB-AuMRs showed virtually no cytotoxicity and they were efficiently taken by cancer cells. Additionally, their lager size allowed us to locate individual microrods by optical microscopy and SEM. Figure 3.7 shows the bright field and dark field optical images of gold microrods inside the cells. SEM imaging (Figure 3.8) was also carried out to determine whether microrods are adhered to the cell membrane or residing inside the cells. The SEM sample was prepared by fixing the cells on a glass slide followed by sputtering a 5 nm film of metallic gold. Both SEM and optical image clearly proved that the AuMRs are indeed internalized by the cells. Moreover, they are excluded from the nucleus which indicates endosomal uptake of gold microrods.

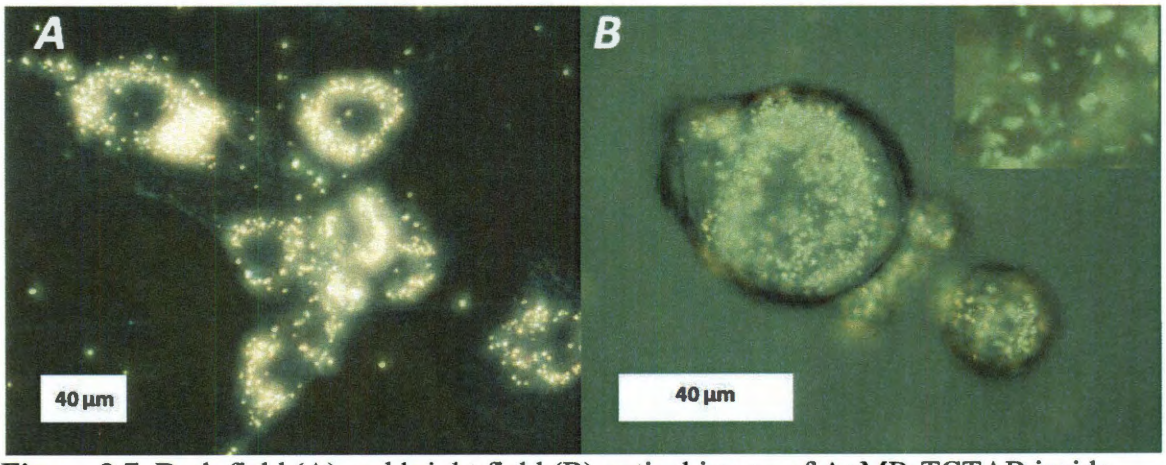

Figure 3.7 Dark field (A) and bright field (B) optical image of AuMR-TCTAB inside breast cancer cells. Cropped image (inset) showing individual microrods.

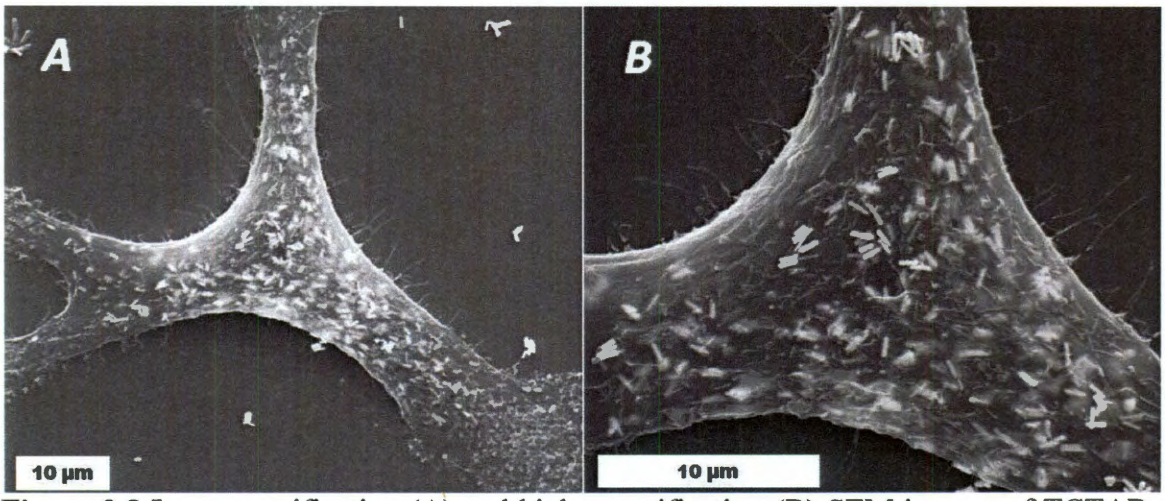

Figure 3.8 Low magnification (A) and high magnification (B) SEM images of TCTAB-AuMR inside breast cancer cells.

As a control TCTAB-AuMRs were compared to widely used thiolated polyethylene glycol (PEG-SH) stabilized rods. PEG-SH coated rods are neutral in nature and their cell uptake is poor.[44] Figure 3.9 shows the dark field optical image of both PEG-AuMR and TCTAB-AuMR treated cells. TCTAB-AuMR treated cells appeared much brighter because of the efficient internalization of metallic nanostructures which strongly scatter visible light.

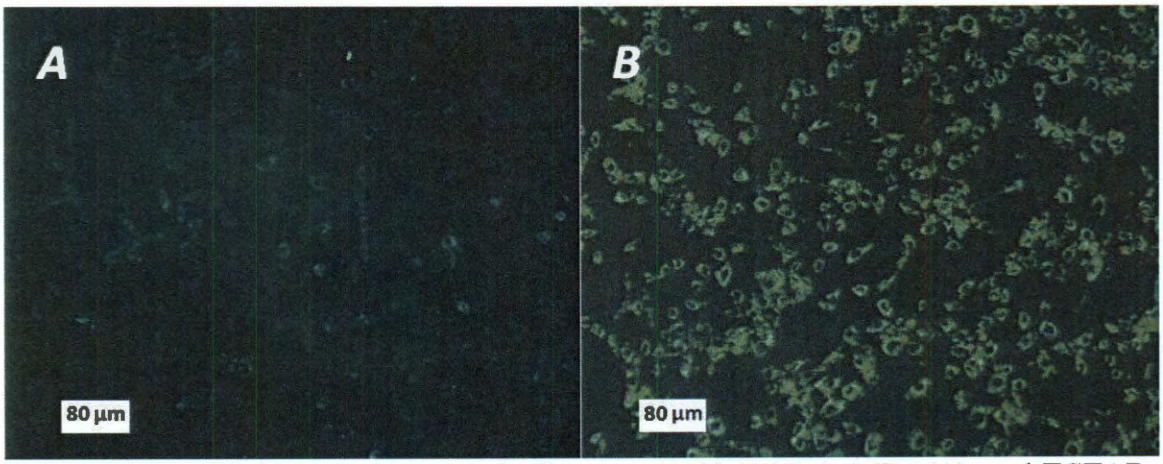

Figure 3.9 Dark field optical image of cells treated with PEG-AuMRs (A), and TCTAB-AuMRs (B).

The estimated amount of uptake was 20 % based on the ICP-OES data obtained by dissolving cells which had been treated with thiolated gold nanorods. Remarkably, proliferation of the cells did not stop in spite of having such a high content of gold inside them. These results show that the surface coating on the nanorods plays an important role for cellular uptake of gold nanostructures. In addition, strong light scattering of metallic nanostructures can be used for locating them inside the cells. No additional florescent probe or biomarker is required for this purpose. Rapid delivery and effective internalization of gold nanostructures inside the cells may also be useful for drug delivery and cancer therapeutics.

3.3 Conclusion

In this chapter we have demonstrated a novel way to synthesize highly stable, functionalized gold nanorods by exchanging CTAB with its thiolated analogue TCTAB. Complete removal of CTAB was also confirmed by NMR spectroscopy. TCTAB capped AuNRs shows high cellular uptake while maintaining very low cytotoxicity. This new type of nanorods can be potentially used for cancer therapy, drug, and gene delivery.

3.4 Experimental Section

Gold (III) chloride ($HAuCl_4 \cdot 3H_2O$), 1,11-dibromoundecane, hexadecane-1, 16-diol, sodium methoxide and ethanol solution of trimethylamine were purchased from Aldrich Chemical Co. *N*-bromosuccinamide (NBS) and triphenylphosphine (Ph_3P) were purchased from TCI America. Cell culture supplies were purchased from ATCC, Inc. MTT analysis was performed using a GeneMate ELx800 absorbance reader (BioTek) using 690 nm filter cut-off. Unless otherwise stated, all chemicals were used without further purification. SEM imaging was done by FEI Quanta 400 ESEM FEG instrument

in high vacuum mode. Optical microscopy images were obtained in reflective mode on a Nikon microscope. ^{1}HNMR spectra were recorded in CD_2Cl_2 or $CDCl_3$ solutions on a Bruker 400 MHz spectrometer. Size Exclusion Chromatrography (SEC) analysis was performed on a Waters Breeze 1515 series liquid chromatograph.

3.4.1 Synthesis of 1,16-dibromohexadecane 2

The synthesis of **6** was carried out according to the procedure describe elsewhere.[48] A 50 mL solution of triphenylphosphine (3.93 g, 15 mmol) in anhydrous THF was added to a stirred solution of *N*-bromosuccinamide (2.67 g, 15 mmol) in 50 mL THF at 0 °C. Upon vigorous stirring, a solution of hexadecane-1, 16-diol **1** (1 g, 3.9 mmol) in 25 mL THF was slowly added to the mixture of NBS and Ph_3P. The resulting solution was warmed to room temperature and then heated at 60 °C for 3.5 hours. THF was removed by rotary evaporation and the residue was re-crystallized form ethanol to obtain 1.1 g of **2** as white powder (70 % isolated yield).

^{1}H NMR ($CDCl_3$, 400 MHz): δ 1.26-1.46 (m, 24 H), 1.85 (q, 4H), 3.41 (t, 4H).

3.4.2 Synthesis of 16-bromo-1-hexadecanethioacatate 3

One gram (2.60 mmol) of **2** was dissolved in 40 mL methanol in a three-neck flask and the solution was degassed for one hour. Separately, 124 mg of sodium methoxide was dissolved in 12 mL dry, ice-cold methanol and mixed with 204 mg (2.6 mmol) of thiolacetic acid. This mixture was transferred into a funnel. The solution in the three-neck flask was refluxed under argon atmosphere and the content in the funnel was slowly added to the solution over the course of 4 hours. After the reaction was complete, the content of the flask was cooled to room temperature and methanol was removed

under reduced pressure. The yellow oil was further purified by column chromatography (20 % ethyl acetate in hexane) to obtain 480 mg of **3** (50 % yield).

3.4.3 Synthesis of 16-bromo-1-hexadecanethiol 4

To a stirred solution of **3** (400 mg, 1.05 mmol) in 10 mL of dry methanol, 4 mL of acetyl chloride was added drop-wise and the reaction mixture was kept at 50 °C for 4 hours. After the reaction was complete, 200 mL of CH_2Cl_2 was added to the reaction mixture and excess acetyl chloride and HCl were removed by multiple extractions with DI water. The mixture was dried over sodium sulfate. Methylene chloride was evaporated under reduced pressure to obtain 284 mg of **4** as colorless oil (80 % isolated yield).

^{1}H NMR ($CDCl_3$, 400 MHz): δ 1.26-1.46 (m, 25H), 1.60 (m, 2H), 1.85 (q, 2H), 2.52 (q, 2H), 3.41 (t, 2H).

3.4.4 Synthesis of thiocetylltrimethyl ammonium bromide (TCTAB) 5

To a solution of **4** (284 mg, 0.85 mmol) in 5 mL of ethyl acetate, excess amount of 4.2 M ethanol solution of trimethylamine was added. The mixture was vigorously stirred under argon for 4 days. The resulting white precipitate was filtered and the washed several times with ethyl acetate to remove excess trimethyl amine. The residue was vacuum dried to obtain 270 mg of **5** (80 % isolated yield).

^{1}H NMR ($CDCl_3$, 400 MHz): δ 1.26-1.46 (m, 25H), 1.60 (m, 2H), 1.85 (m, 2H), 2.52 (q, 2H), 3.5 (s, 9H), 3.55-3.7 (m, 2H).

3.4.5 Ligand exchange of AuNRs with TCTAB

Gold nanorods were prepared by the procedure described elsewhere.[49] The concentration of gold nanorods in the growth solution was roughly 0.22 mg/mL. Nine milliliters of this solution was centrifuged at 13,000 rpm for 10 min. The supernatant was

carefully removed using a pipette and precipitate was redispersed in 0.5 mL of DI water. The resulting NR solution was treated with an aqueous solution of TCTAB prepared by dissolving 10 mg of TCTAB in 1.5 mL DI water. After stirring the mixture at room temperature for 12 h, the solution was centrifuged at 13,000 rpm for 10 min. The supernatants were discarded and the precipitate was washed four times with pure water to remove excess thiol and CTAB. Finally, the precipitate was dissolved in 4 mL of pure water and kept as 0.5 mg/mL stock solution. Appropriate amount of NR stock solution was first lyophilized to obtain a powder. The powder was then treated with a methanol solution of KCN and the resulting solution was analyzed by ^{1}HNMR spectroscopy.

3.4.6 Ligand Exchange of gold microrods

The solution of CTAB-capped AuMRs was kept at 27°C for 12 hours to precipitate the MRs from the solution. The supernatant was carefully removed and the brown precipitate was washed two times with 0.1 M CTAB solution to remove excess of gold ions and ascorbic acid. The purified MRs solution was treated with an aqueous solution of TCTAB prepared by dissolving 10 mg of TCTAB in 1.5 mL of DI water. The solution was quickly sonicated for 3 sec and kept at 27 °C for 12 h without any stirring. After 12 h the supernatant was carefully removed and freshly prepared aqueous thiol solution (2 mL, 5 mg/mL) was added again. The vial was kept at 27 °C for additional 12 h. The mixture was centrifuged of obtain AuMRs as dark brown precipitate. The precipitate was washed multiple times with pure water to remove any residual thiol and CTAB. Finally, TCTAB capped AuMRs were dissolved in pure water and kept as stock solution (0.5 mg/mL).

3.4.7 MTT assay experiment

Breast cancer cells (MCF-7) were plated in 96-well plates at a concentration of 15,000 cells per well and allowed to attach for 24 hours. After the attachment, 100 μL of media containing gold nano/microrods was added to each well. After 24 hours of treatment, a solution of MTT in PBS (25 μL, 5 mg/mL) were added to each well and incubated at 37°C for 3 hours. The media was then removed and blue formazan metabolite was dissolved in 100 μL of DMSO. Absorbance values were recorded by plate reader (Gene Mate, Bio Tek) equipped with 570 nm filter.

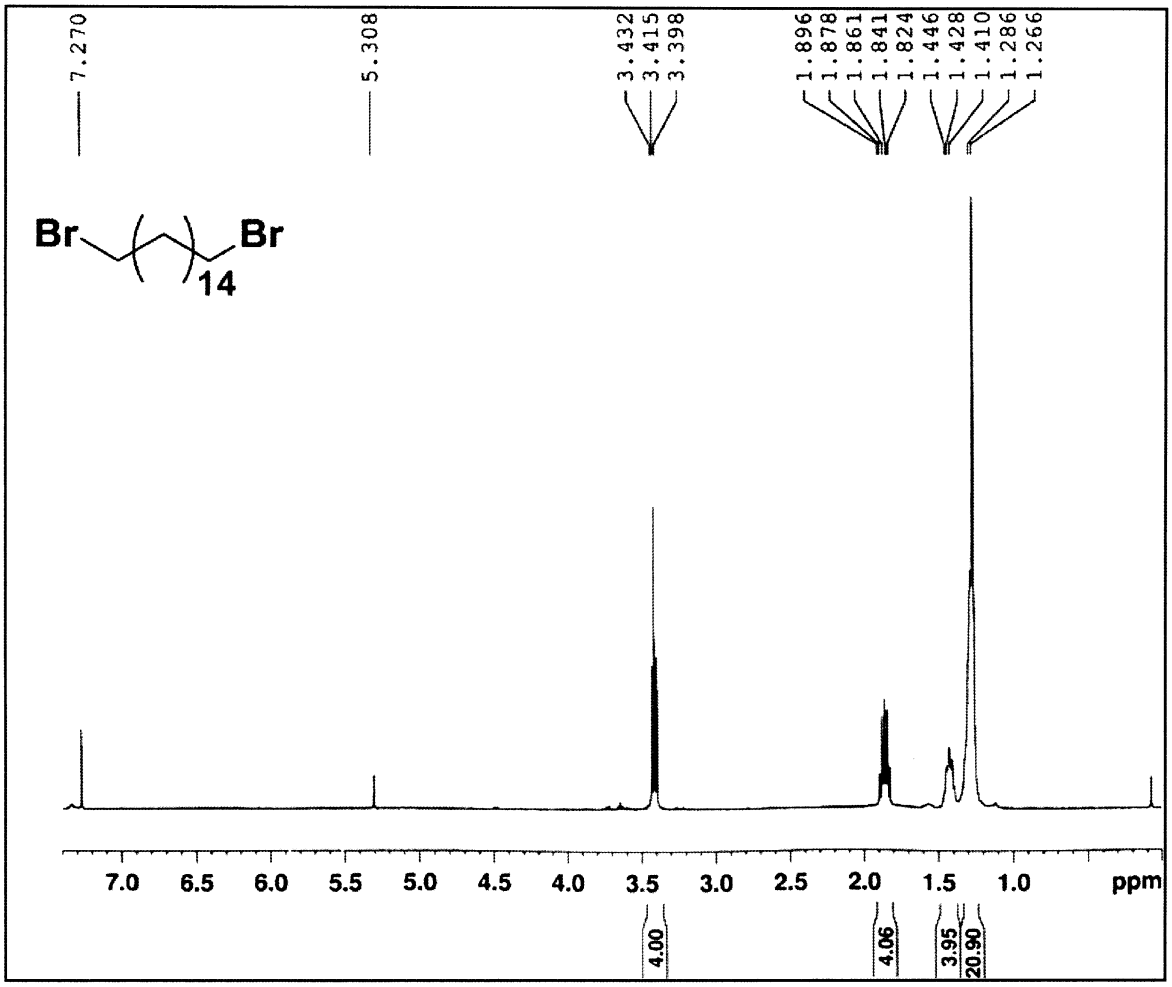

Figure 3.10 ^{1}H NMR of compound **2**

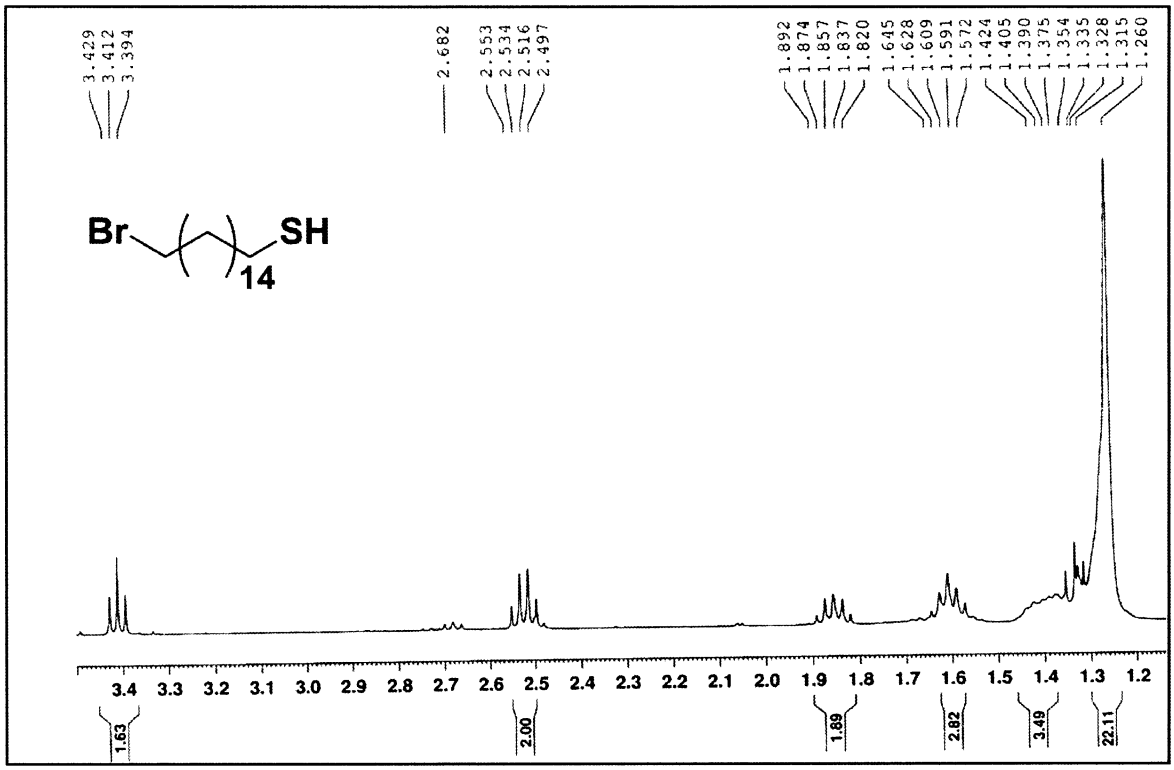

Figure 3.11 ^{1}H NMR of compound **4**

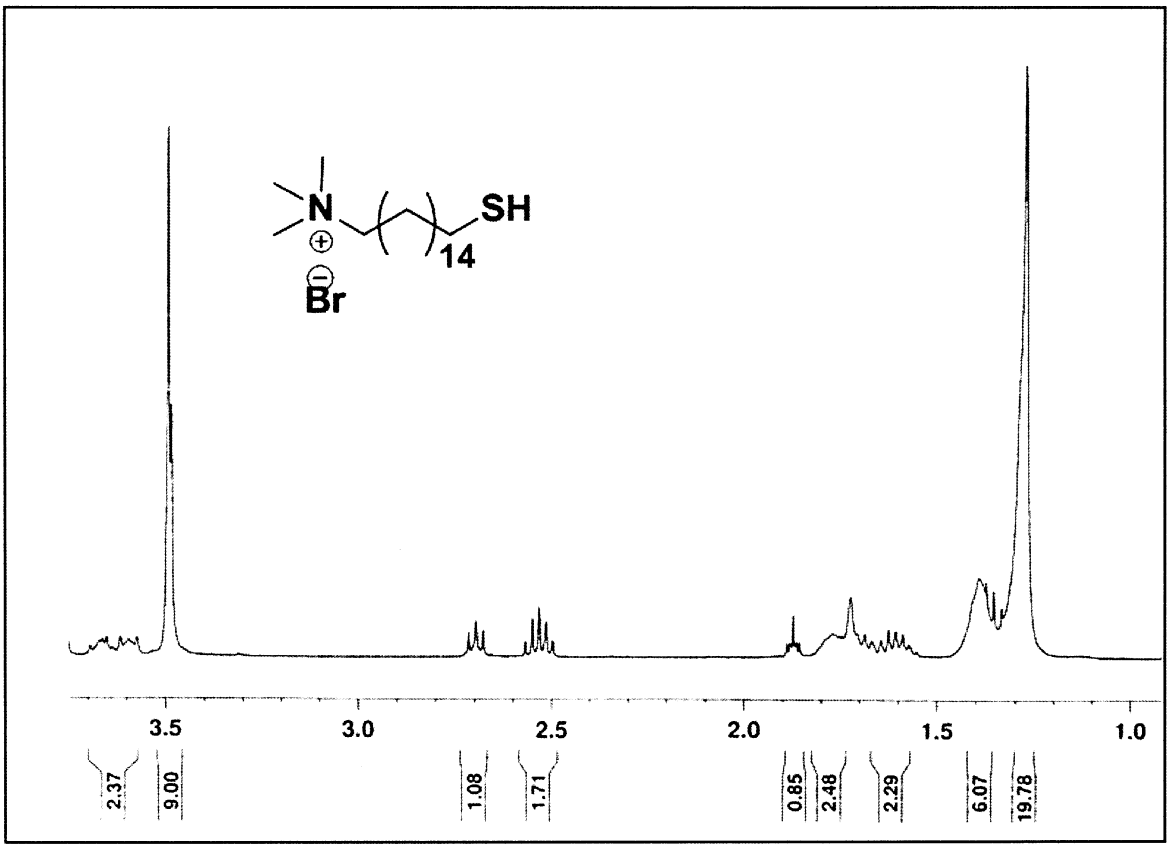

Figure 3.12 ^{1}H NMR of compound **5**

References

(1) Boisselier, E.; Astruc, D. *Chem. Soc. Rev.* **2009**, *38*, 1759.

(2) Huang, X. H.; Neretina, S.; El-Sayed, M. A. *Adv. Mater.* **2009**, *21*, 4880.

(3) Link, S.; El-Sayed, M. A. *J. Phys. Chem. B* **1999,** *103*, 8410.

(4) Nikoobakht, B.; El-Sayed, M. A. *Chem. Mater.* **2003**, *15*, 1957.

(5) Jana, N. R.; Gearheart, L.; Murphy, C. J. *J. Phys. Chem. B* **2001**, *105*, 4065.

(6) Wu, H.-Y.; Huang, W.-L.; Huang, M. H. *Cryst. Growth Des.* **2007**, *7*, 831.

(7) Wu, H.-Y.; Chu, H.-C.; Kuo, T.-J.; Kuo, C.-L.; Huang, M. H. *Chem. Mater.* **2005**, *17*, 6447.

(8) Wei, Z.; Mieszawska, A. J.; Zamborini, F. P. *Langmuir* **2004**, *20*, 4322.

(9) Khanal, B. P.; Zubarev, E. R. *J. Am. Chem. Soc.* **2008**, *130*, 12634.

(10) Lu, X.; Yavuz, M. S.; Tuan, H.-Y.; Korgel, B. A.; Xia, Y. N. *J. Am. Chem. Soc.* **2008**, *130*, 8900.

(11) Pazos-Perez, N.; Baranov, D.; Irsen, S.; Hilgendorff, M.; Liz-Marzan, L. M.; Giersig, M. *Langmuir* **2008**, *24*, 9855.

(12) Critchley, K.; Khanal, B. P.; Gorzny, M. L.; Vigderman, L.; Evans, S. D.; Zubarev, E. R.; Kotov, N. A. *Adv. Mater.* **2010**, *22*, 2338.

(13) Solis, D.; Chang, W.-S.; Khanal, B. P.; Bao, K.; Nordlander, P.; Zubarev, E. R.; Link, S. *Nano Lett.* **2010**, *10*, 3482.

(14) Xiang, C.; Kim, J. Y.; Penner, R. M. *Nano Lett.* **2009**, *9*, 2133.

(15) Kim, F.; Sohn, K.; Wu, J.; Huang, J. *J. Am. Chem. Soc.* **2008**, *130*, 14442.

(16) Wang, H. F.; Huff, T. B.; Zweifel, D. A.; He, W.; Low, P. S; Wei, A.; Cheng, J. X. *Proc. Natl. Acad. Sci. USA* **2005**, *102*, 15752.

(17) Durr, N. J.; Larson, T.; Smith, D. K.; Korgel, B. A.; Sokolov, K.; Ben-Yakar, A. *Nano Lett.* **2007**, *7*, 941.

(18) Murphy, C. J.; Gole, A. M.; Stone, J. W.; Sisco, P. N.; Alkilany, A. M.; Goldsmith, E. C.; Baxter, S. C. *Acc. Chem. Res.* **2008**, *41*, 1721.

(19) Qiu, L.; Larson, T. A.; Vitkin, E.; Guo, L.; Hanlon, E. B.; Itzkan, I.; Sokolov, K.; Perelman, L. T. *Biomed. Opt. Exp.* **2010**, *1*, 135.

(20) Ding, H.; Yong, K.-T.; Rot, I.; Pudavar, H. E.; Law, W. C.; Bergey, E. J.; Prasad, P. N. *J. Phys. Chem. C* **2007**, *111*, 12552.

(21) Liao H.; Nehl, C. L.; Hafner, J. H. *Nanomedicine* **2006**, *1*, 201.

(22) Hu, M.; Chen, J. Y.; Li, Z. Y.; Au, L.; Hartland, G. V.; Li, X. D.; Marquez, M.; Xia, Y. N. *Chem. Soc. Rev.* **2006**, *35*, 1084.

(23) Huang, X.; El-Sayed, I. H.; Qian, W.; El-Sayed, M. A. *J. Am. Chem. Soc.* **2006**, *128*, 2115.

(24) Oyelere, A. K.; Chen, P. C.; Huang, X; El-Sayed, I. H; El-Sayed, M. A. *Bioconjugate Chem.* **2007,** *18*, 1490.

(25) Huff, T. B.; Tong, L.; Zhao, Y.; Hansen, M. H.; Cheng, J. -X.; Wei, A. *Nanomedicine* **2007**, *2*, 125.

(26) Huang, Y.-F.; Sefah, K.; Bamrungsap, S.; Chang, H. -T.; Tan, W. *Langmuir* **2008**, *24*, 11860.

(27) Guo, R.; Zhang, L.; Qian, H.; Li, R.; Jiang, X.; Liu, B. *Langmuir* **2010**, *26*, 5428.

(28) Lal, S.; Clare, S. E.; Halas, N. J. *Acc. Chem. Res.* **2008**, *41*, 1842.

(29) Nikoobakht, B.; El-Sayed, M. A. *Langmuir.* **2001**, *17*, 6368.

(30) Alkilany, A.; Nagaria, P.; Hexel, C. R.; Shaw, T. J.; Murphy, C. J.; Wyatt, M. D. *Small* **2009**, *5*, 701.

(31) Gole, A.; Murphy, C. J.; *Chem. Mater.* **2005**, *17*, 1325.

(32) Huang, H. C.; Barua, S.; Kay, D. B.; Rege, K. *ACS Nano* **2009**, *3*, 2941.

(33) Leonov, P. A.; Zheng, J.; Clogston, J. D.; Stern, S. T.; Patri, A. K.; Wei, A. *ACS Nano* **2008**, *2*, 2481.

(34) Ding, H.; Yong, K.-T.; Roy, I.; Pudavar, H. E.; Law, W. C.; Bergey, E. J.; Prasad, P. N. *J. Phys. Chem. C* **2007**, *111*, 12552

(35) Parab, H. J.; Chen, H, M.; Lai, T. -C.; Huang, J. H.; Chen, H. C.; Liu, R. -S.; Hsiao, M.; Chen, C, -H.; Tsai, D, -P.; Hwu, Y. -K. *J. Phys. Chem. C* **2009**, *113*, 7574.

(36) Niidome, T.; Yamagata, M.; Okamoto, Y.; Akiyama, Y.; Takahashi, H.; Kawano, T.; Katayama, Y.; Niidome, Y. *J. Controlled Release* **2006**, *114*, 343.

(37) Huff, T. B.; Hansen, M. N.; Zhao, Y.; Cheng, J. X.; Wei, A. *Langmuir* **2007**, *23*, 1596.

(38) Li, J. L.; Day, D.; Gu, M. *Adv. Mater.* **2008**, *20*, 3866.

(39) Rostro-Kohanloo, B. C.; Bickford, L. R.; Payne, C. M.; Day, E. S.; Anderson, L. J.; Zhong, M.; Lee, S.; Mayer, K. M.; Zal, T.; Adam, L.; Dinney, C. P. N.; Drezek, R. A.; Westand, J. L.; Hafner, J. H. *Nanotechnology* **2009**, *20*, 434005.

(40) Nie, Z. H.; Fava, D.; Kumacheva, E.; Zou, S.; Walker, G. C.; Rubinstein, M. *Nat. Mater.* **2007**, *6*, 609.

(41) Pierrat, S.; Zins, I.; Breivogel, A.; Sonnichsen, C. *Nano Lett.* **2007**, *7*, 259.

(42) Gentili, D.; Ori, G.; Franchini, M. C. *Chem. Commun.* **2009**, 5874.

(43) Zhou, W.; Shao, J.; Jin, Q.; Wei, Q.; Tang, J.; Ji, J. *Chem. Commun.* **2010**, *46*, 1479.

(44) Nativo, P.; Prior, I. A.; Brust, M. *ACS Nano*, **2008**, *2*, 1639.

(45) Bain, C. D.; Troughton, B. E.; Tao, Y.–T.; Evall, J.; Whitesides, G. M.; Nuzzo, R. G. *J. Am. Chem. Soc.* **1989**, *111*, 321.

(46) Terrill, R. H.; Postlethwaite, T. A.; Chen, C. –H.; Poon, C.-D.; Terzis, A.; Chen, A.; Hutchison, J. E.; Clark, M. R.; Wignall, G.; Londono, J. D.; Superfine, R.; Favo, M.; Johnson, C. S.; Samulski, E. T.; Murray, R. W. *J. Am. Chem. Soc.* **1995**, *117*, 12537.

(47) Ming, T.; Kou, X. S.; Chen, H. J.; Wang, T.; Tam, H. L.; Cheah, K. W.; Chen, J. Y.; Wang, J. F. *Angew. Chem. Int. Ed.* **2008**, *47*, 9685.

(48) Franceschi, S.; Andreu, V.; Viguerie, N. D.; Riviere, M.; Lattes, A.; Moisand, A. *New J. Chem.* **1998**, 225.

(49) Khanal, B. P.; Zubarev, E. R. *Angew. Chem. Int. Ed.* **2007**, *46*, 2195.

Chapter IV

Self-Assembly of Gold Nanostructures- Formation of Well-Defined 3D Colloidal Crystals

4.1 Introduction

In recent past gold nanorods have gained much attention for their widespread applications in bio-medical imaging,[1-6] medical diagnostics[7-18] and chemical sensing.[19-26] Similar to other noble metal nanostructures, gold nanorods show strong absorption and scattering due to collective oscillation of electrons on NR surface, also known as surface plasmon resonance.[11,27-30] The plasmon peak can be fine tuned by changing the shape, size, and aspect ratio of gold nanorods. [11,31-34] In addition, it is important to find out ways to organize the nanorods into finite structures as it offers the preparation of engineered materials with unique optical and electronic properties. The controlled organization of nanomaterials can be achieved by using self-assembly technique.[35-47] Self-assembly is a "bottom-up" technique which promotes the organization of individual components to form ordered structures without the influence of external forces. Two- and three-dimensional superlattices of colloidal particles, also known as colloidal crystals are useful for preparing photonic bandgap materials,[48-51] optical switches,[52-54] and sensor devices.[55] While thousands of colloidal crystals made of spherical building blocks have been reported,[49,51,56] there are very few examples of colloidal crystals constructed from anisotropic *rod-like* particles.[57,58] If created, such structures would have *direction-dependent* macroscopic properties (optical, electrical, and mechanical) and would represent a fundamentally new type of nanomaterials.

El-Sayed and co-workers first reported assemblies of gold nanorods prepared on a TEM grid by slow evaporation of solvent.[59] Liquid crystalline ordering was also observed by Murphy *et al.* for high aspect ratio gold nanorods with penta-twinned cross-section.[60] Very recent advances in this area include smectic-like arrays of AuNRs organized from aqueous solutions,[61] and vertically standing superlattices.[62-66] Many reports in the literature also highlight examples of the nanorods assemblies, which are based on non-covalent interactions,[67-69] polymer-induced self-corralling,[70] external electric fields,[71] tip-selective functionalization,[72-73] and breath figures technique.[74] In spite of this recent progress, colloidal crystallization of gold nanorods remains a challenge and finding a method to prepare *mesoscopically* or even *macroscopically* large colloidal single crystals is still an elusive goal. One critically important feature required for the assembly of rod-shaped particles into large colloidal superstructures is their narrow size distribution both in terms of their diameter and length. While the diameter of gold nanorods (AuNRs) is normally very uniform, the length distribution is very difficult to control. This is the main reason why superlattices made of inorganic NRs are often quite small and rarely exceed several microns in lateral dimensions.[75] In addition the nature of surfactant present on the nanoparticles surface plays critical role for the colloidal crystallization. Gold nanorods prepared by "seed mediated growth method" are stabilized by cationic surfactant CTAB. CTAB not only acts as a template for one dimensional growth, but also provides the stability of AuNRs by forming a dynamic bilayer on nanorod surface.[59-60] It also facilitates the formation of ordered arrays of gold nanorods by balancing the attractive depletion force and electrostatic repulsion.[59,61]

In this chapter we describe colloidal crystallization of spherical gold nanoparticles and anisotropic gold nanorods. Faceted three dimensional colloidal crystals of monodisperse gold nanoparticles (~ 6 nm) were prepared by slow precipitation technique. In addition, we report the application of evaporation induced self-assembly technique for the preparation of near-macroscopic colloidal crystals of CTAB-capped gold nanorods (25 x 75 nm). When an aqueous solution of CTAB-coated NRs were allowed to dry on a silicon surface, nanorods spontaneously self-assembled into three dimensional superlattices. In these colloidal crystals NRs are hexagonally close packed and oriented parallel to the substrate. In addition, we found that the orientation of individual nanorods in a colloidal crystal can be altered from side-on to tip-on by changing the nature of the substrate. Our systematic studies reveal that the crystallization process is essentially a co-crystallization between the NRs and free CTAB surfactant present in the media.

4.2 Results and Discussion

4.2.1 Colloidal crystallization of gold nanoparticles

To study the colloidal crystallization of gold nanoparticles, we prepared decanethiol capped near-monodisperse gold nanoparticles (~6 nm) by annealing a solution of 1-3 nm decanethiolated gold particles in neat decanethiol (Figure 4.1).[76] The hydrophobic decanthiol ligand renders these particles highly soluble of in organic solvents like THF, toluene, and methylene chloride. However, they are not soluble in polar organic solvent like methanol and DMF. Colloidal crystallization of the particles was carried out by slowly diffusing methanol into the THF solution of the particles using the set up shown in Figure 4.2. When methanol concentration reaches a critical value, particles start forming small individual aggregates which may be considered as the

nucleation step of the colloidal crystallization. These aggregates are small enough to remain suspended in the solution and they continue growing in all directions until they become too heavy to remain suspended. The final morphology of the colloidal crystal will be determined by the shape of the small aggregates formed at the early stage of crystallization. After 72 hours the supernatant becomes clear and colorless indicating the completion of crystallization. The dark brown precipitate was transferred to a sample stub for SEM imaging.

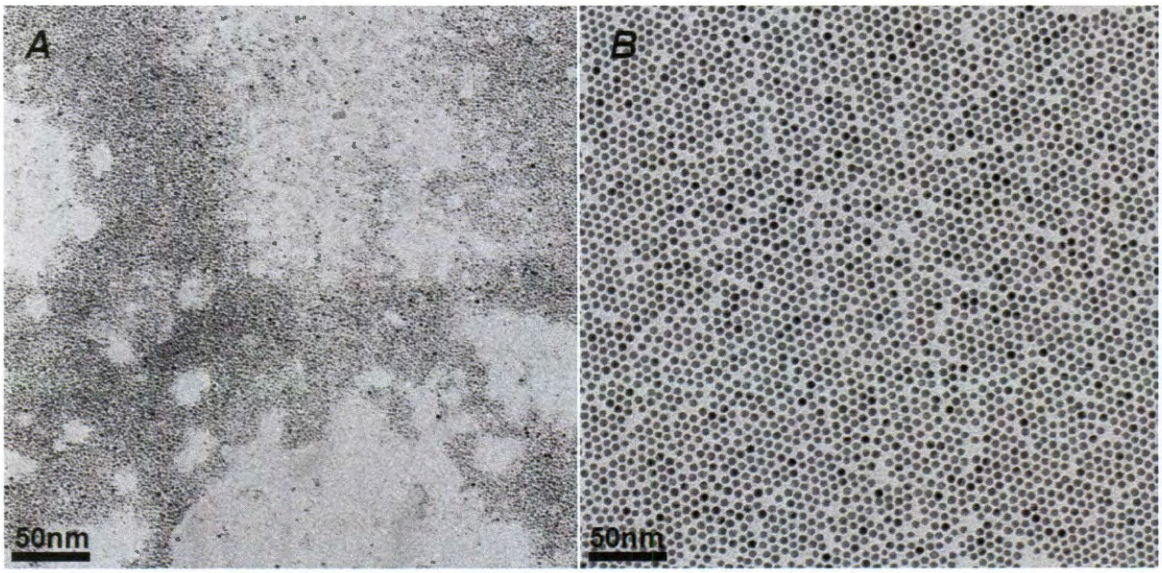

Figure 4.1 Transmission electron microscopy image of decanethiol-coated 1-3 nm (A) and 6 nm (B) gold nanoparticles.

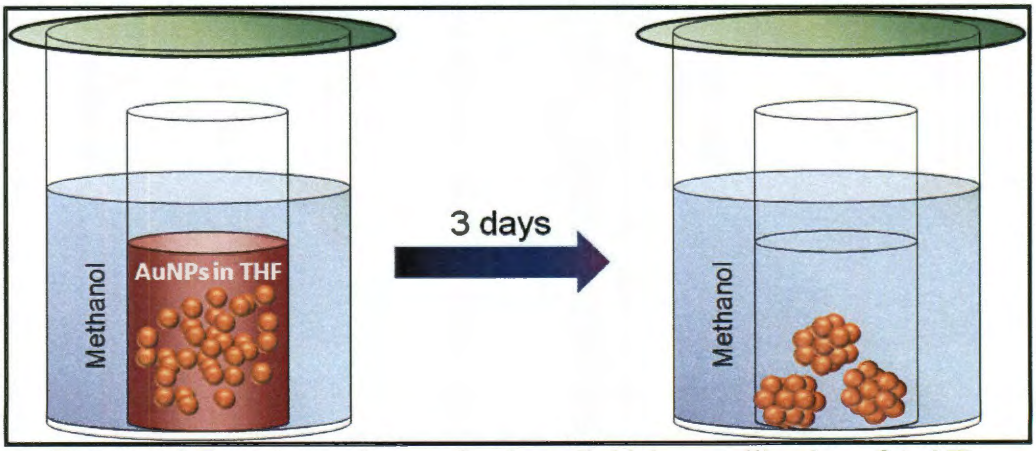

Figure 4.2 Experimental setup for the colloidal crystallization of AuNPs

SEM investigation showed the formation of faceted three-dimensional colloidal crystals of varying shapes and sizes (300 nm to 3 μm) (Figure 4.3). To resolve individual positions of the AuNPs, we performed high resolution SEM (HRSEM) imaging. HRSEM images (Figure 4.3C and Figure 4.3D) prove that the nanoparticles are ordered in hexagonal closed packed lattice structures that are analogous to atomic face centered cubic (FCC) structure where AuNPs take the position of the atoms and interdigitated decanethiols act as soft "molecular mortar" responsible for the overall structural integrity. The calculated interparticle distance was less than 1.5 nm which again supports the full interdigitation of decanethiols between two nanoparticles. The interdigitation of decanthiol ligand can be explained by the strong covalent anchoring of alknethiols to gold surface which promotes their *all trans* conformation.[77,78]

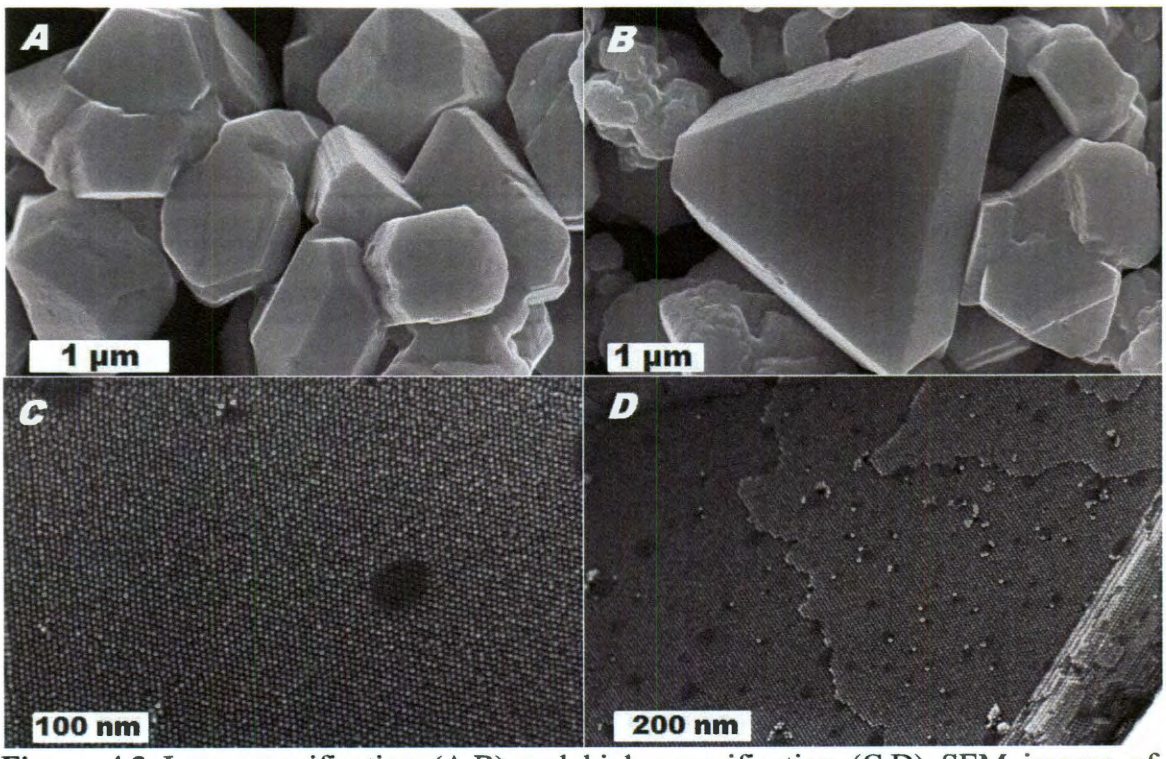

Figure 4.3 Low magnification (A,B) and high magnification (C,D) SEM images of colloidal crystals of 6 nm gold nanoparticles.

Crystallization of gold nanoparticles results in the formation of both single crystalline and polycrystalline colloidal crystals. However, formation of amorphous aggregates was not observed. Our repeated attempts for the preparation of larger colloidal crystals by increasing the concentration of gold nanoparticles were not successful. As the concentration of the nanoparticles increases, higher numbers of nucleation sites become available and eventually more colloidal crystals are formed. Still, overall dimensions of the crystals did not increase significantly. We also observed that the nature of the solvent does not have profound effect on the crystallization as colloidal crystals can be successfully prepared from toluene and chloroform solution of nanoparticles. The crystallization is also reversible in nature as colloidal crystals can be easily re-dissolved in chloroform or THF without changing their optical property.

4.2.2 Colloidal crystallization of monodisperse gold nanorods

Conventional AuNRs synthesized by Murphy and El-Sayed procedure are stabilized by a cationic surfactant CTAB.[59,60] These rods can be assembled into liquid crystal like aggregates with either nematic or smectic-like order. The absence of long range order is due to the size polydispersity of the nanorods. It is to be noted that thickness of anisotropic gold nanostructures can be controlled precisely but the length polydispersity is really difficult to avoid. Previous work in our group identified the conditions for a 1000-fold increase in the amount of NRs synthesized in one batch (Figure 4.4). This is achieved by slow deposition of Au (I) ions on top of pre-synthesized gold nanorods. This process leads to an amplification of the NRs dimensions, which reach 75 nm in length and 25 nm in diameter. Most importantly, the size distribution of NRs becomes much narrower (σ ~3 %). [79]

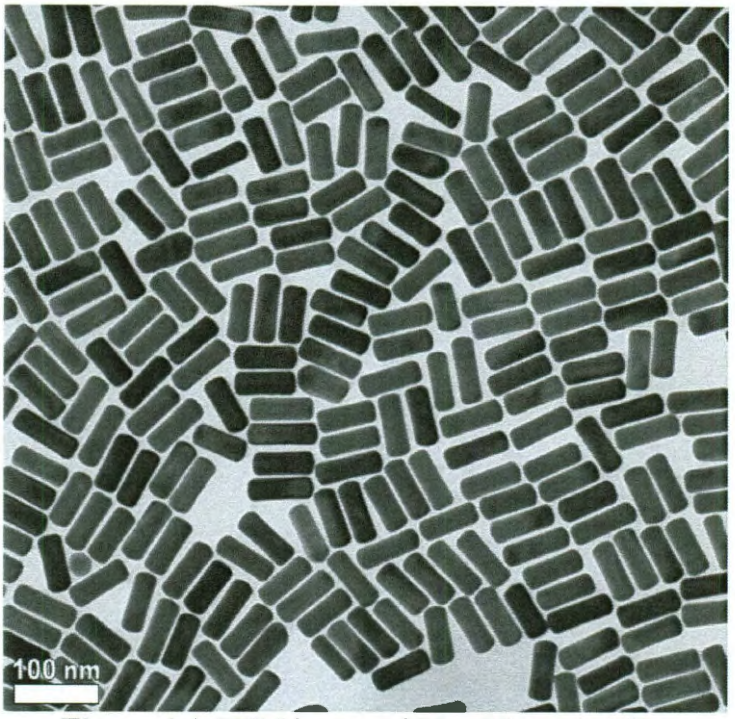

Figure 4.4 TEM image of 25 x 75 nm AuNRs

The crystallization of amplified AuNRs which are nearly monodisperse could potentially yield true colloidal single crystals. Our initial attempts of crystallization by diffusing a poor solvent like DMF and methanol into the aqueous solution of AuNRs resulted in the removal of CTAB bilayer from NR surface and an irreversible agglomeration of AuNRs was observed. It is to be noted that unlike spherical gold nanoparticles, direct synthesis of alkanethiol-capped NRs is not possible. Although alkanethiol capped nanorods can be prepared by exchanging CTAB with alkanethiols, their stability and solubility in organic solvents is quite poor.

At this point we explored the evaporation-induced self-assembly technique to crystallize monodisperse NRs. We hypothesize that CTAB on gold surface will act as the directing agent for the crystallization of NRs. We also hypothesize that size monodispersity of these nanorods will promote pure crystalline order as opposed to the liquid crystalline order observed in case of polydisperse AuNRs. The growth solution of

AuNR contains a large amount of free CTAB (36.5 mg/mL) which can interfere with the crystallization of gold nanorods and subsequent SEM imaging. For that purpose, NR stock solution was centrifuged once and the precipitate was redispersed in pure water. The centrifugation reduces CTAB concentration up to 40 times without disturbing the solubility of the NRs. The mass of CTAB in the solution was still twice the mass of gold nanorods as determined by inductively coupled plasma (ICP) and thermo gravimetric analysis (TGA). When a droplet of NR stock solution was allowed to dry on a silicon wafer, faceted colloidal crystals of gold nanorods were formed. Figure 4.5 shows the SEM image of prepared colloidal crystals measuring up to 4 microns in lateral dimensions. These colloidal crystals have hexagonal closed packed (HCP) order which is governed by the cylindrical shape of gold nanorods. It is to be noted that nanorods in the crystals are oriented in a side-on fashion.

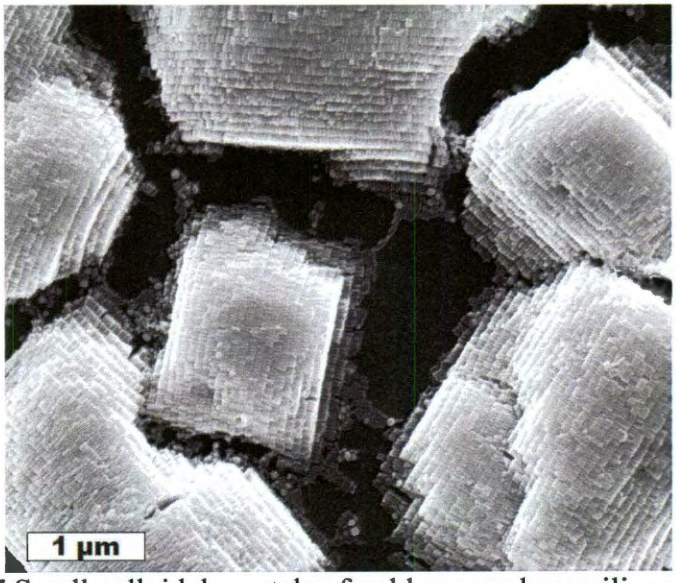

Figure 4.5 Small colloidal crystals of gold nanorods on silicon substrate.

SEM investigation (Figure 4.5) clearly indicates that amplified AuNRs can be self-assembled to prepare colloidal crystals having true crystalline order. The only problem is that these colloidal crystals are still fairly small. In order to prepare colloidal

crystals of larger dimension, we decided to decrease the rate of evaporation of solvent. Intuitively, one can speculate the reduction of evaporation rate would give the NRs more time to self-assemble and hence structures with larger dimension can be prepared. For that purpose the drying process was carried out in a humid atmosphere (Figure 4.6). The high water vapor pressure significantly reduces the rate of evaporation and the drying time increases up to 6 times.

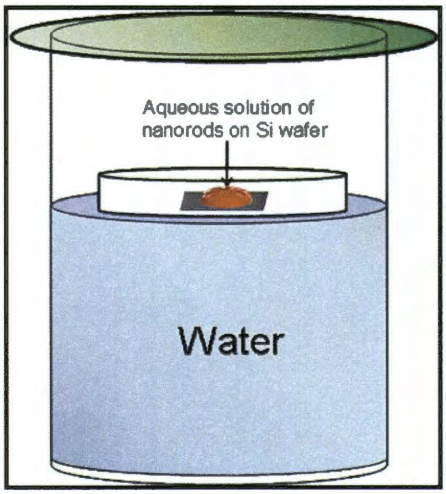

Figure 4.6 Slow drying of aqueous solution of gold nanorods on silicon substrate.

Optical microscopy image (Figure 4.7A) of the dried sample shows the formation of discrete assemblies measuring up to 100 microns in one dimension. The structures have a characteristic shape of elongated trapezoids and rectangles. Further structural investigation by SEM proved that these structures are colloidal single crystals of gold nanorods (Figure 4.7B and Figure 4.7C). The length of the colloidal crystal shown in Figure (4.7B) is 160 μm and its width is 14 μm. Therefore, the size of the crystals was increased up to 50 times and reached nearly a macroscopic level by reducing the rate of solvent evaporation.

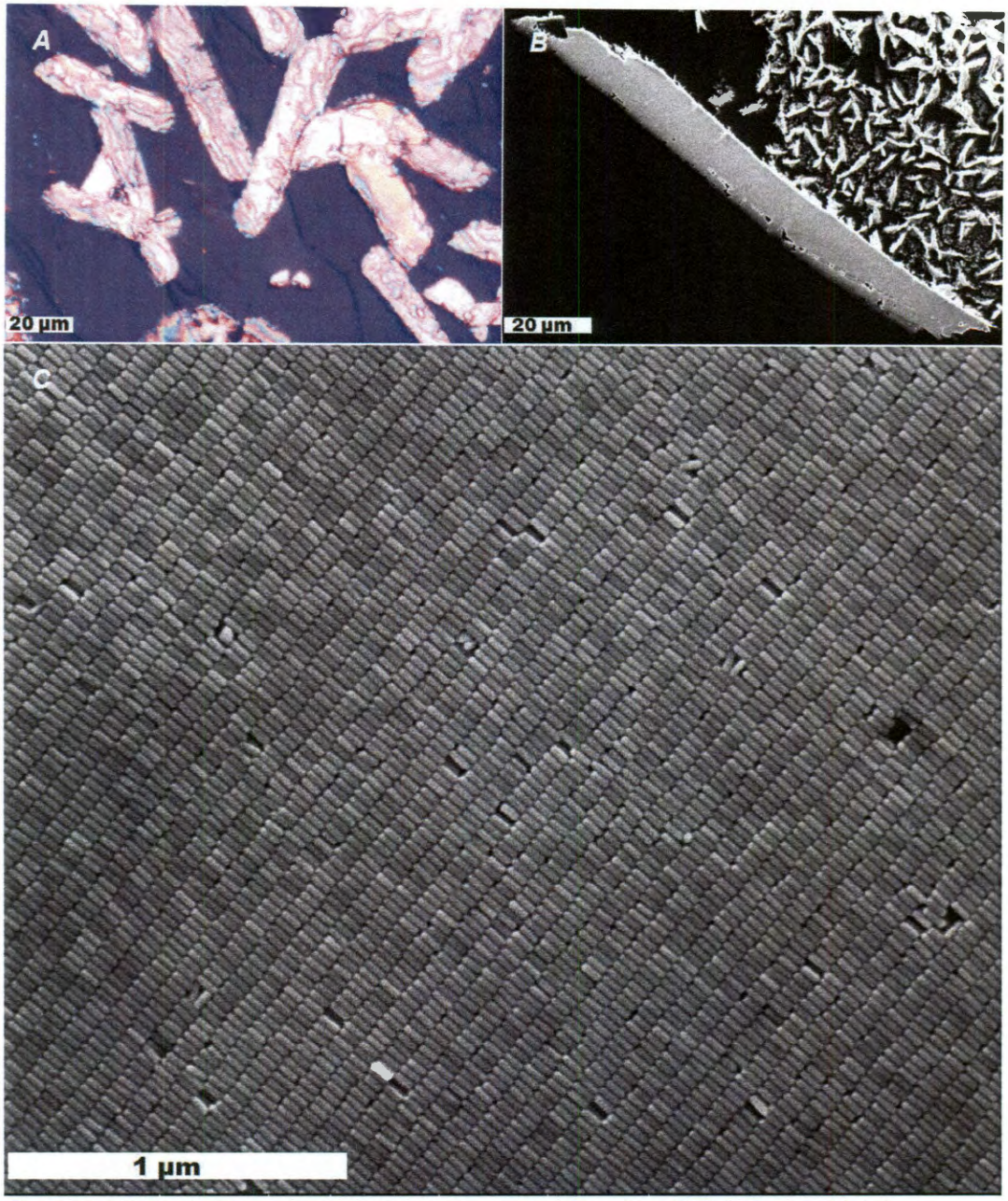

Figure 4.7 Optical microscopy (A), low magnification SEM (B), and high magnification SEM (C) images of ~ 160 micron long colloidal single crystal of gold nanorods

Most importantly, the orientational and positional order of individual NRs is preserved throughout the entire 160x 14 µm structure, which makes it a true colloidal single crystal. To the best of our knowledge, this is by far the largest size of colloidal single crystals comprised of rod-shaped building blocks. Unlike other assemblies, the

crystal is not a 2D monolayer structure. We were able to determine the third dimensionality of the crystal by tilting the sample during SEM imaging (Figure 4.8). It measures almost two microns in thickness, which corresponds to ~80 layers of NRs. Tilted SEM image also confirms hexagonal packing between two successive layers. Thus, the colloidal crystals that form under these conditions are three-dimensional objects comprising tens of millions of highly ordered gold NRs.

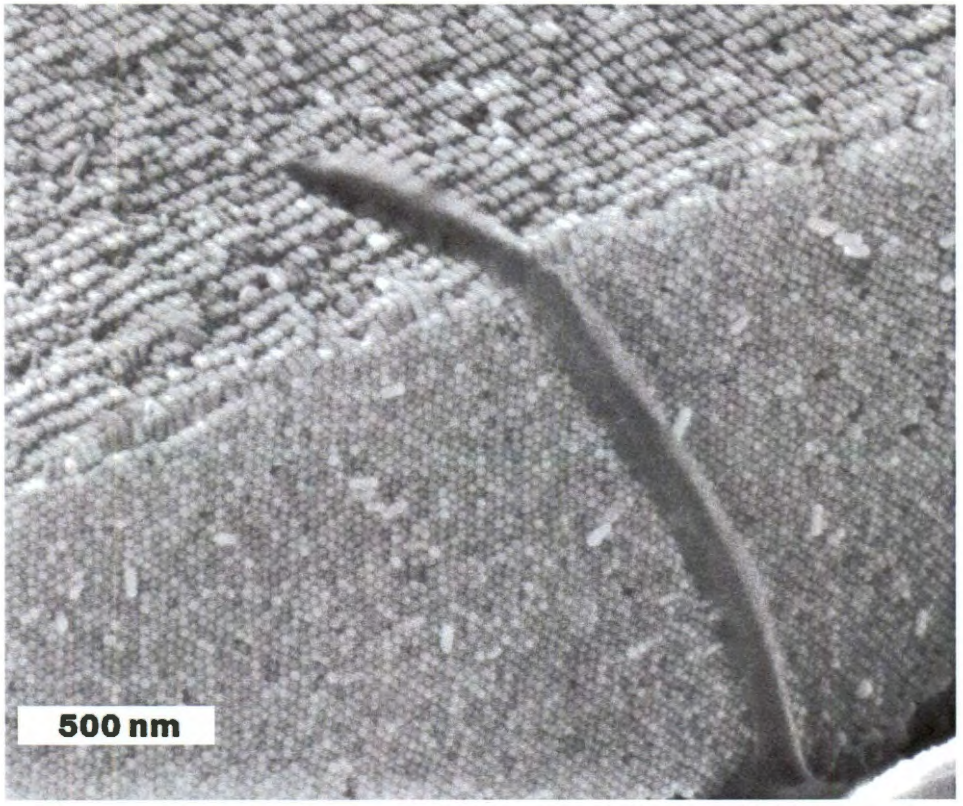

Figure 4.8 Tilted SEM image showing the side of a colloidal crystal.

Remarkably, the crystallization process can be monitored by simple bright field optical microscopy. Metallic nanostructures are capable of scattering bright light and their position and movement can be easily visualized using a bright light source. Optical imaging revealed spontaneous formation of small aggregates of gold nanorods at the water-silicon-air triple interface during the initial stage of drying. Size of these

aggregates increased in lateral dimensions as the drying continued (Figure 4.9). This is also known as *coffee ring* effect where the difference in rate of solvent evaporation drives the accumulation of the solute, i.e. nanorods, around the edge of the droplet. [61] Slow drying of the solvent ensures long range order between NRs. The interparticle distance in a crystal is about 3 nm, which corresponds to a bilayer of CTAB. That means when two nanorods each having bilayers of CTAB come in close proximity, one of the two bilayers is excluded and NRs are attached together via spontaneous interdigitation of another CTAB bilayer. Essentially, this interdigitated bilayer of CTAB is the soft "molecular mortar" necessary for structural integrity of colloidal crystals.

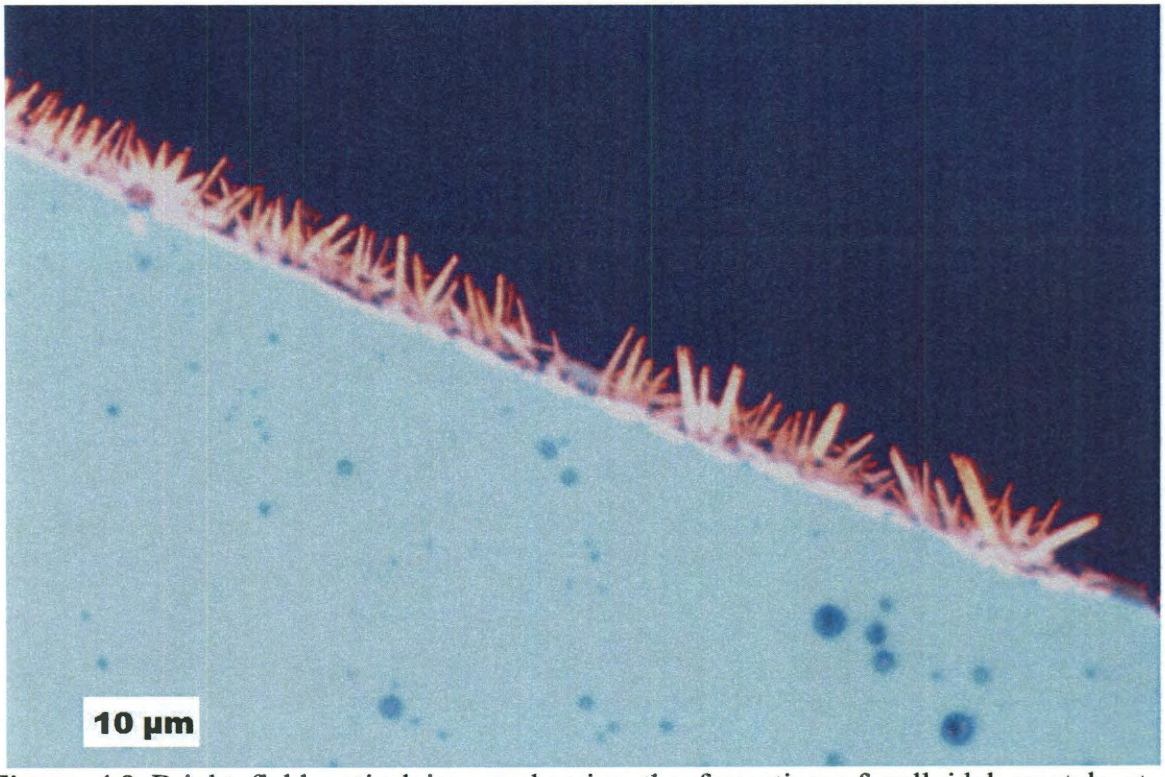

Figure 4.9 Bright field optical image showing the formation of colloidal crystals at water-silicon-air interface.

4.2.3 Controlling the orientation of AuNRs in a colloidal crystal

We also explored the opportunity to control the orientation of NRs in colloidal crystal. Commercially available silicon is coated with a thin layer of silicon oxide, which makes the substrate hydrophilic in nature. The measured contact angle of water on Si wafer is ~25°. The low water contact angle is responsible for the side-on orientation of NRs. One would expect that increase in the contact angle may switch the orientation from parallel to perpendicular. When a thin layer (~1.5 μm) of a positive photoresist (diazonaphthoquinone, S1813) is spin-coated on the wafer, the water contact angle increases to ~75°. When the aqueous solution of gold nanorods was slowly dried on resist-coated wafer, all the NRs self-assembled to form vertically standing superlattice as illustrated in Figure 4.10.

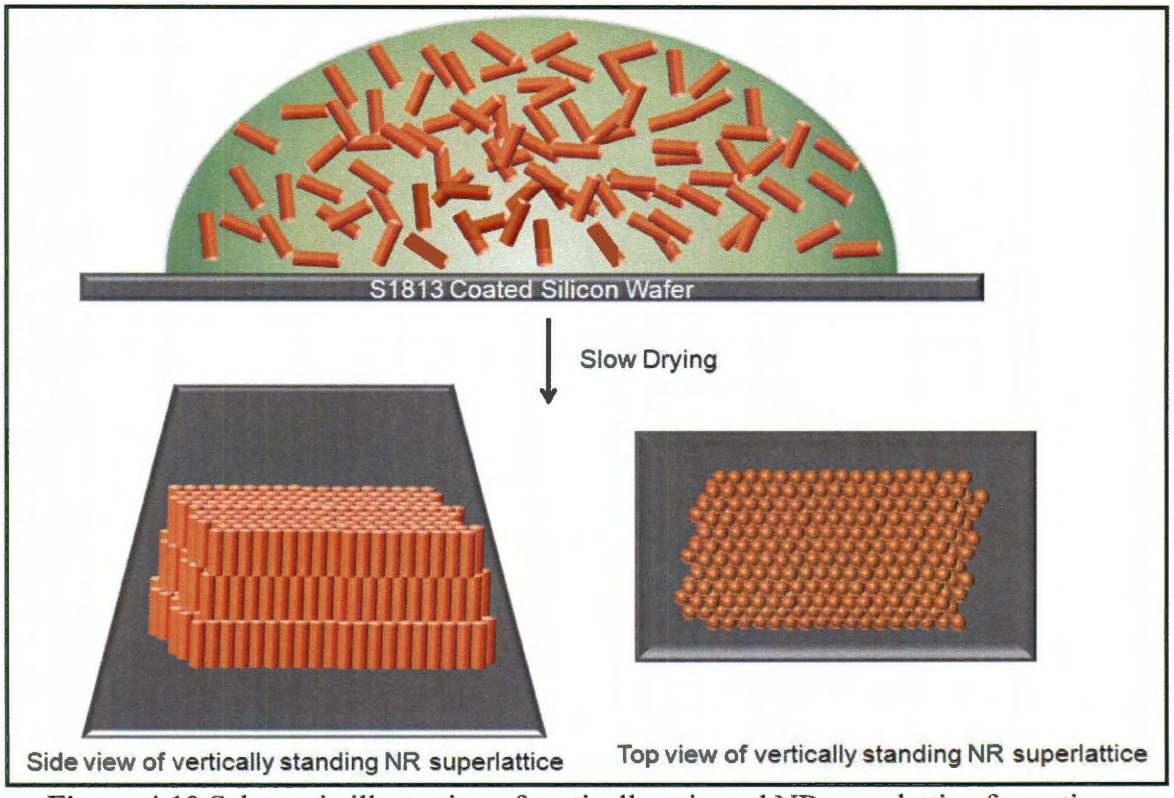

Figure 4.10 Schematic illustration of vertically oriented NR superlattice formation.

Figure 4.11A and 4.11B show the top view of a colloidal single crystal, which was grown on a silicon wafer spin-coated with S1813 resist. These colloidal crystals have extremely large domains without any grain boundaries. Importantly, the SEM imaging of an edge of such colloidal crystal reveals that the orientational and positional order of NRs remains consistent throughout the entire structure (Fig. 4.11C). There are approximately 15 hexagonal layers of NRs packed in an ABAB fashion similar to classical HCP lattice. The tips of NRs from layer A positioned on top of the interstitial voids in adjacent layer B. This assembly process was also observed on other hydrophobic substrates as we were able to prepare vertically standing nanorods arrays on S1813 coated ITO and carbon surface.

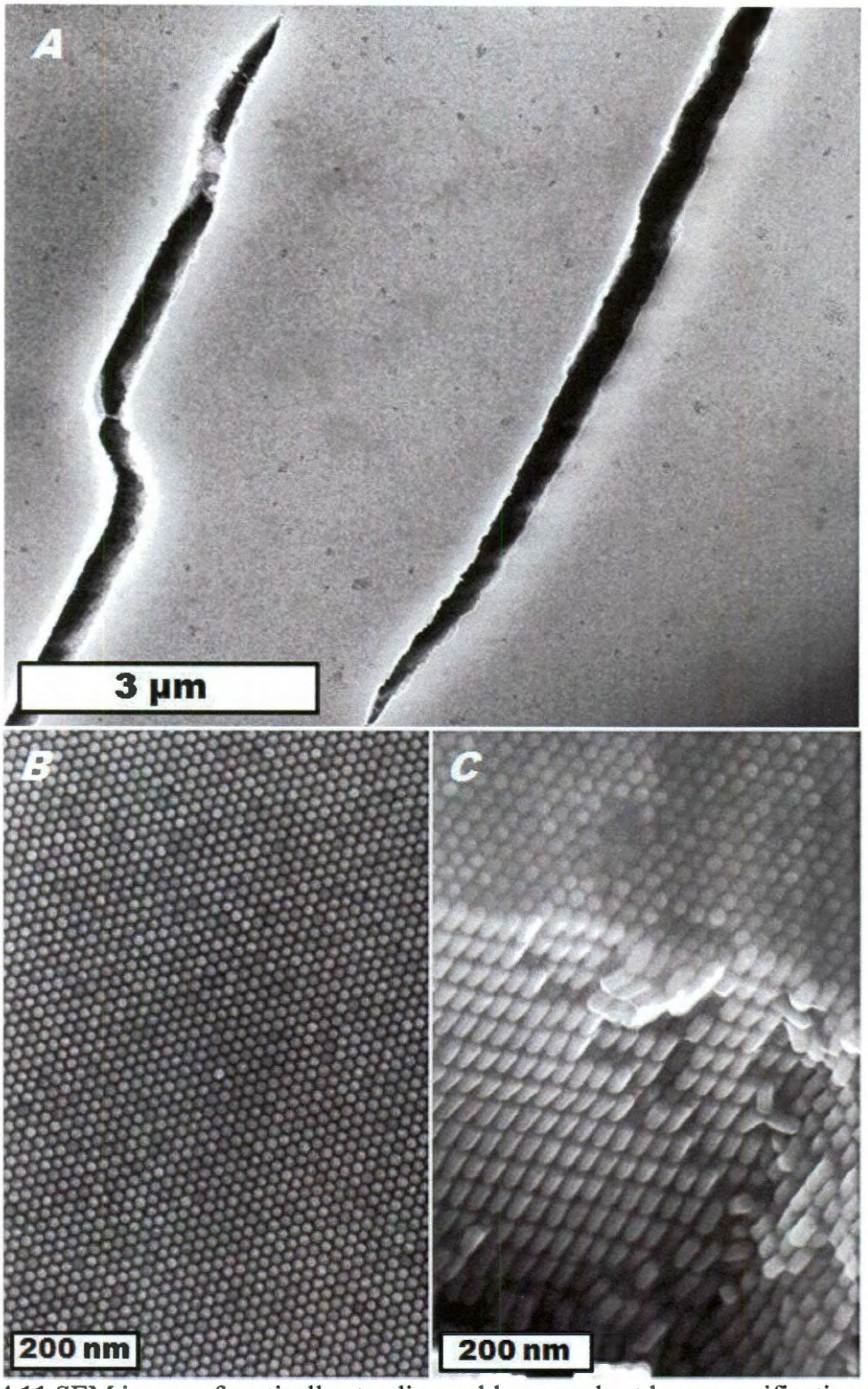

Figure 4.11 SEM image of vertically standing gold nanorods at low magnification (A), and high magnification (B), and cross-sectional view of colloidal single crystal (C).

These findings indicate that the nature of the substrate strongly affects the initial stages of crystallizations. The first layer of the colloidal crystal may form and grow in lateral dimensions while in direct contact with the substrate. Alternatively, small aggregates can initially form in solution and only then land on the substrate. In both cases, however, the orientation of rods is controlled by the interactions between the CTAB molecules residing on the nanorods and the underlying substrate. It can be envisioned that the interactions between the ionic compound CTAB and a highly hydrophobic coating on the substrate is significantly less favorable than the interactions between the rods (CTAB-CTAB). In an attempt to minimize the former and to maximize the latter type of interactions, the initial nuclei (probably, disk-shaped aggregates of rods) should stand on their tips and keep adding rods from solution via side-by-side packing, resulting in a lateral growth. Once the first layer forms, it can serve as a template for the second layer because it has a significant degree of order. In addition, its top surface is coated with hydrophilic CTAB which is much more preferable for the incoming rods than the rest of the hydrophobic substrate.

4.2.4. Role of free CTAB in colloidal crystallization of nanorods

CTAB is known to affect the assembly of nanostructures by counterbalancing attractive depletion forces and electrostatic repulsion. Our systematic investigation showed that the overall concentration of CTAB present in the aqueous solution of nanorods has a strong influence on the formation of colloidal crystals. Also, CTAB concentration is critically important for directing the orientation of NRs with respect to the substrate. Thermogravimetric analysis of CTAB-capped gold nanorods showed that the weight fraction of CTAB present in solution is almost twice the weight fraction of the

nanorods. This implies that the amount of free CTAB in the drying solution is many orders of magnitude greater than that contained in the bilayers that encapsulate NRs. It is worth noting that CTAB is not only an ionic molecule, but is also a crystallizable compound. It is possible that the observed colloidal self-assembly involves a co-crystallization of free CTAB and CTAB-coated NRs. This is consistent with the SEM microscopy observation which shows that some interstitial voids between the NRs measure up to 10 nm, which is significantly larger than the thickness of CTAB bilayer (4 nm) (Figure 4.12).

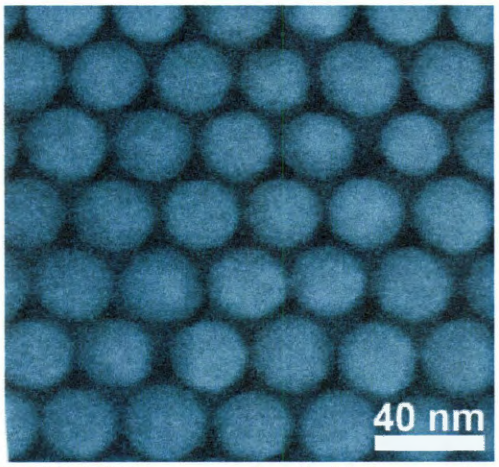

Figure 4.12 HRSEM image of colloidal crystal of Au NRs.

In order to prove that CTAB is important for colloidal crystallization, the removal of CTAB excess is necessary. The attachment of CTAB to the NR surface is purely non-covalent in nature and its continuous removal by centrifugation destroys the dynamic bilayer essential for the stability and solubility of gold nanorods. To solve this problem we decided to synthesize a thiolated CTAB analogue thiocetyltrimethyl ammonium bromide (TCTAB). Thiolated CTAB is structurally similar to conventional CTAB, but it has a pendant thiol group which is capable of forming a strong covalent bond with the gold (Figure 4.13). Importantly, the presence of ammonium salt will provide necessary

water solubility. These NRs would still be positively charged like CTAB-coated NRs and the electrostatic forces involved in crystallization should remain the same.

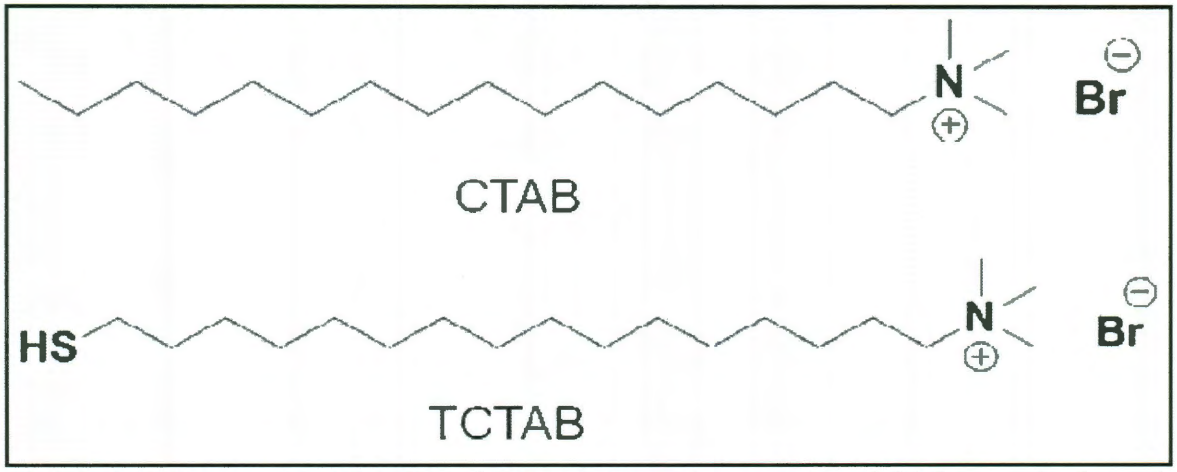

Figure 4.13 Structures of CTAB and TCTAB. Note the presence of thiol group in the end of the alkyl tail.

Thiol monolayer capped AuNRs were prepared by adding a solution of CTAB-coated AuNRs into an aqueous solution of free TCTAB ligand. Covalent binding of thiol to the gold surface allowed us to remove the free CTAB from the media by multiple rounds of centrifugation. The complete removal of free CTAB is confirmed by NMR and TGA.

Remarkably, when a stock solution of TCTAB-AuNRs was dried on a silicon substrate, no crystallization was observed (Figure 4.14A). However, colloidal crystallization can be induced by introducing small amount of free CTAB into the aqueous solution of TCTAB-AuNRs (Figure 4.14B). This control experiment not only proves that free CTAB is responsible for colloidal crystallization, but also proves that the crystallization process requires a mixture of soft "molecular mortar" and hard colloidal particles.

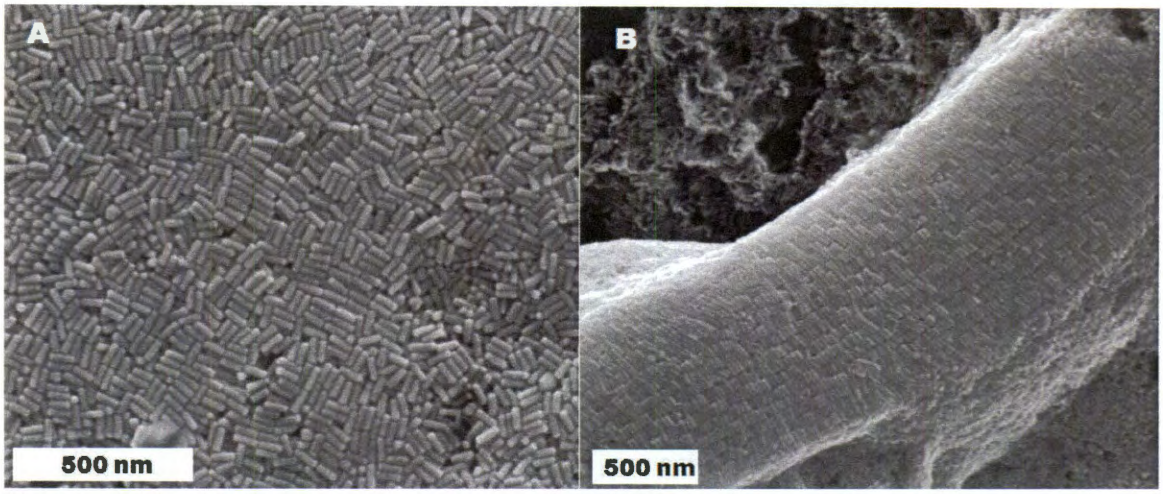

Figure 4.14 (A) Random aggregates of TCTAB-AuNRs, (B) ordered assembly of TCTAB AuNRs obtained by the addition of free CTAB.

Another important control experiment was performed by using polyethylene glycol (PEG-SH) functionalized gold nanorods. Unlike TCTAB, PEG does not have any charge and PEGylated NRs are neutral in nature. However, just like CTAB, PEG is also a crystallizable compound. If the process is indeed a co-crystallization of NRs with free organic compound present in the media, then PEG-functionalized NRs should also form colloidal crystals in the presence of free PEG. Figure 4.15A shows the SEM image of pure PEG-coated nanorods on a silicon substrate, which do not undergo any crystallization upon slow drying of their aqueous solution. However, addition of free PEG (0.5 mg/mL) induced the crystallization (Figure 4.15B). This control experiment further suggests that the presence of free crystallizable organic compounds templates the crystallization of gold nanorods.

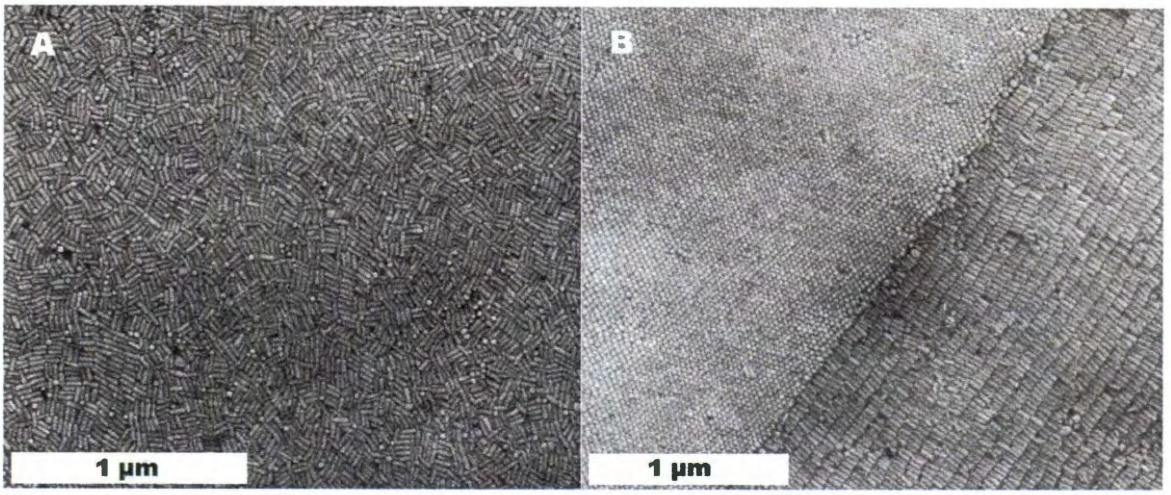

Figure 4.15 (A) Random aggregates of pure PEG-AuNRs, (B) ordered assembly of PEG-AuNRs obtained by the addition of free PEG molecules.

4.3 Conclusions

In summary, we described the colloidal crystallization of spherical gold nanoparticles and anisotropic gold nanorods. In addition, vertically oriented superlattices of gold nanorods were obtained by their spontaneous organization on hydrophobic substrates. Our systematic investigation also proved that colloidal assembly of gold nanorods is a co-crystallization process of gold nanorods and free organic compound present in solution. These studies offer important insights for the design and preparation of superlattices composed of anisotropic building blocks

4.4 Experimental Section

Unless otherwise stated, all the chemicals were purchased from commercial sources and they were used without any further purification. SEM imaging was done by FEI Quanta 400 ESEM FEG instrument in high vacuum mode. Gold films were prepared by e-beam evaporator and sputter coater. Optical microscopy images were obtained in reflective mode on a Nikon microscope. ^{1}HNMR spectra were recorded on solution of CD_2Cl_2 or $CDCl_3$ on a Bruker 400 MHz spectrometer. TEM imaging was done using

JEOL 1230 high contrast microscope operating at 100 KV accelerating voltage. TEM samples of gold nanoparticles were prepared by dipping a carbon-coated copper TEM grid into the THF or $CHCl_3$ solution of nanoparticles. TEM samples of gold nanorods were prepared by dipping a carboncoated copper TEM grid into their aqueous solution.

4.4.1 Synthesis of 1-decanethiol-capped gold nanoparticles

Decanethiol functionalized gold nanoparticles (~2 nm in diameter) were prepared by two-phase synthesis described by Brust and co-workers.[80] In a typical synthesis, 120 mg of gold (III) chloride was dissolved in 10 mL of DI water. In a separate vial, 730 mg of tetraoctylammonium bromide was dissolved in 27 mL of toluene. These two solutions were mixed and stirred vigorously until the gold chloride was completely transferred into the organic layer. To this organic layer, 65 mg of 1-decanethiol was added, and then a freshly prepared aqueous solution of sodium borohydride (123 mg in 8.5 mL water) was added slowly into the mixture. The organic layer turned dark brown during the reduction. After 5 min of stirring, an excess of methanol was added, and the gold nanoparticles were centrifuged at 1200 rpm for 5 min. Purified particles were dissolved in THF and kept as a stock solution.

4.4.2 Synthesis of monodisperse 6 nm gold nanoparticles

Ten milligrams of decanethiol-capped, 2 nm gold particles were dissolved in 3 g of neat 1-decanethiol. The solution was transferred into an 8 mL vial and capped with a teflon-coated cap. The vial was heated to 175 $^{\circ}$C and kept at that temperature for 1 h. During this annealing process, the solution became dark red, indicating the overall increase in the size of the gold nanoparticles. The solution was treated with excess

methanol, and the particles were centrifuged at 1200 rpm for 5 min. The precipitate containing decanethiol-capped 6 nm gold nanoparticles was dissolved in THF.

4.4.3 Synthesis of the colloidal crystals of gold nanoparticles

A solution was prepared in an 8 mL vial by dissolving 2 mg of decanethiol-capped gold nanoparticles in 2 mL of dry THF. Separately, a methanol bath was prepared by putting ~ 100 mL of methanol in a 250 mL beaker. The vial was carefully placed inside the methanol bath and the beaker was tightly covered. The whole chamber was kept undisturbed for 3 days. After 3 days the solution inside the vial became clear and dark brown precipitate was observed. The vial was carefully removed from the methanol bath and supernatant was removed. The dark brown precipitate was transferred to an SEM sample stub for imaging.

4.4.4 Preparation of colloidal crystals having side-on orientation of gold nanorods

Monodisperse gold nanorods were prepared by slightly modifying the procedure describe elsewhere.[79] Aqueous solution of gold nanorods was centrifuged once and re-dispersed in appropriate amount of DI water to make a stock solution (~1 mg/mL). A piece of silicon wafer (1 cm^2) was thoroughly cleaned with acetone and dried by blowing nitrogen. The wafer was placed on a Petri dish. The Petri dish was kept floating on top of water in a 250 mL beaker containing 200 mL of water. A droplet of stock solution of gold nanorods (30 μL) was placed on top of the wafer and the beaker was covered with a lid. The whole setup was kept undisturbed at room temperature for 12 h during which water evaporated and a golden rim formed. The substrate was washed with warm water and prepared for the SEM imaging.

4.4.5 Preparation of colloidal crystals having tip-on orientation of gold nanorods

A piece of silicon wafer (1 cm^2) was thoroughly cleaned with acetone and dried by blowing nitrogen. A positive photoresist S1813 (Microchem Corp.) was spin-coated at 6,000 rpm onto the wafer. The substrate was annealed at 125 $^{\circ}C$ for 10 min. After that, two drops of aqueous solution of nanorods were placed on it and dried using the procedure described above.

4.4.6 Ligand exchange of CTAB-coated gold nanorods with TCTAB

The concentration of gold nanorods in the growth solution was roughly 0.22 mg/mL. Nine milliliters of this solution was centrifuged at 13,000 rpm for 10 min. The supernatant was carefully removed using a pipette and precipitate was re-dispersed in 0.5 mL of DI water. The resulting NR solution was treated with an aqueous solution of TCTAB prepared by dissolving 10 mg of TCTAB in 1.5 mL DI water. After stirring the mixture at room temperature for 12 h, the solution was centrifuged at 13,000 rpm for 10 min. The supernatants were discarded and the precipitate was washed four times with pure water to remove excess thiol and CTAB. Finally, the precipitate was dissolved in 2 mL of pure water and kept as 1 mg/mL stock solution.

4.4.7 Ligand exchange of CTAB-coated gold nanorods with thiol-terminated PEG

The concentration of gold nanorods in the growth solution was roughly 0.22 mg/mL. Nine milliliters of this solution was centrifuged at 13,000 rpm for 10 min. The supernatant was carefully removed using a pipette and precipitate was re-dispersed in 0.5 mL of DI water. The resulting NR solution was treated with an aqueous solution of PEG-SH prepared by dissolving 10 mg of thiol-terminated PEG (MW 2000 g/mol) in 1.5 mL DI water. After stirring the mixture at room temperature for 12 h, the solution was

centrifuged at 13,000 rpm for 10 min. The supernatants were discarded and the precipitate was washed four times with pure water to remove excess thiol and CTAB. Finally, the precipitate was dissolved in 2 mL of pure water and kept as 1 mg/mL stock solution

References

(1) Wang, H. F.; Huff, T. B.; Zweifel, D. A.; He, W.; Low, P. S; Wei, A.; Cheng, J. X. *Proc. Natl. Acad. Sci. USA* **2005**, *102*, 15752.

(2) Durr, N. J.; Larson, T.; Smith, D. K.; Korgel, B. A.; Sokolov, K., Ben-Yakar, A. *Nano Lett.* **2007**, *7*, 941.

(3) Qiu, L.; Larson, T. A.; Vitkin, E.; Guo, L.; Hanlon, E. B.; Itzkan, I.; Sokolov, K.; Perelman, L. T. *Biomed. Opt. Exp.* **2010**, *1*, 135.

(4) Ding, H.; Yong, K.-T.; Rot, I.; Pudavar, H. E.; Law, W.C.; Bergey, E. J.; Prasad, P. N. *J. Phys. Chem. C* **2007**, *111*, 12552.

(5) Murphy, C. J.; Gole, A. M.; Stone, J. W.; Sisco, P. N.; Alkilany, A. M.; Goldsmith, E. C.; Baxter, S. C. *Acc. Chem. Res.* **2008**, *41*, 1721.

(6) El-Sayed, I. H; Huang, X.; El-Sayed, M. A. *Nano Lett.* **2005**, *5*, 829.

(7) Huang, X.; El-Sayed, I. H.; Qian, W.; El-Sayed, M. A. *J. Am. Chem. Soc.* **2006** 128, 2115.

(8) Oyelere, A. K.; Chen, P.C.; Huang, X; El-Sayed, I. H; and. El-Sayed, M. A. *Bioconjugate Chem.* **2007,** *18*, 1490.

(9) Huff, T. B.; Tong, L.; Zhao, Y.; Hansen, M. H.; Cheng, J.-X.; Wei, A. *Nanomedicine* **2007**, *2*, 125.

(10) Chen, C. C.; Lin, Y. P.; Wang, C. W., Tzeng, H. C.; Wu, C. H.; Chen, Y. C.; Chen, C. P.; Chen, L. C.; Wu, Y. C. *J. Am. Chem. Soc.* **2006**, 128, 3709.

(11) Huang, X. H.; Neretina, S.; El-Sayed, M. A. *Adv. Mater.* **2009**, *21*, 4880.

(12) Tong, L.; Wei, Q.; Wei, A.; Cheng, J. -X. *Photohem. Photobiol.* **2009**, *85*, 21.

(13) Yu, C.; Nakshtri, H.; Irudayaraj, J. *Nano Lett.* **2007**, *7*, 2300.

(14) Tong, L.; Zhao, Y.; Huff, T. B.; Hansen, M. N.; Wei, A.; Cheng, J. X. *Adv. Mater.* **2007**, *19*, 3136

(15) Perez-Juste, J.; Pastoriza-Santos, I.; Liz-Marzan, L. M.; Mulvaney, P. "*Coord. Chem. Rev.* **2005**, *249*, 1870.

(16) Cole, J. R.; Mirin, N. A.; Knight, M.W.; Goodrich, G.P.; Halas, N. J. *J. Phys. Chem. C* **2009**, *113*, 12090.

(17) Boisselier, E.; Astruc, D. *Chem. Soc. Rev.* **2009**, *38*, 1759.

(18) Murphy, C. J.; Gole, A. M.; Hunyadi, S. E.; Stone, J. W.; Sisco, P. N.; Alkilany, A.; Kinard, B. E. ; Hankins, P. *Chem. Commun.* **2007**, 544.

(19) Wang, Y.; Lee, K.; Irudayaraj, J. *Chem. Commun.* **2010**, *46*, 613.

(20) Gole, A.; Murphy, C. J. *Langmuir* **2005**, *21*, 10756.

(21) Nehl, C. L.; Liao H.; Hafner, J. H. *Nano Lett.* **2006**, *6*, 683.

(22) Hu, M.; Chen, J. Y.; Li, Z. Y.; Au, L.; Hartland, G. V.; Li, X. D.; Marquez, M.; Xia, Y. N. *Chem. Soc. Rev.* **2006**, *35*, 1084.

(23) Jain, P. K.; El-Sayed, M. A. *Nano Lett.* **2008**, *8*, 4347.

(24) Castellana, E. T.; Gamez, C. R.; Gomez, M. E.; Russell, D. H. *Langmuir* **2010**, *26*, 6066.

(25) Yu, C.; Irudayaraj, J. *Anal. Chem.* **2007**, *79*, 572.

(26) Sudeep, P. K.; Joseph, S. T. S.; Thomas, K. G. *J. Am. Chem. Soc.* **2005**, *127*, 6516.

(27) El-Sayed, M. A. *Acc. Chem. Res.* **2001**, *34*, 257.

(28) Link, S.; El-Sayed, M. A. *Inter. Rev. Phys. Chem.* **2000**, *19*, 409.

(29) Burda, C.; Chen, X. B.; Narayanan, R.; El-Sayed, M. A. *Chem. Rev.* **2005**, *105*, 1025.

(30) Haes, A. J.; Stuart, D. A.; Nie, S. and Van Duyne, R. P. *J. Fluoresc.* **2004**, *14*, 355.

(31) Nikoobakht, B.; El-Sayed, M. A. *Chem. Mater.* **2003**, *15,* 1957.

(32) Murphy, C. J.; Orendorff, C. J. *Adv. Mater.* **2005**, 17, 2173.

(33) Gao, J. X.; Bender, C. M.; Murphy, C. J. *Langmuir* **2003**, *19*, 9065

(34) Khanal, B. P.; Zubarev, E. R. *J. Am. Chem. Soc.* **2008**, *130*, 12634.

(35) Li, F.; Josephson, D. P.; Stein, A. *Angew. Chem. Int. Ed.* **2011**, *50*, 360.

(36) Ozin, G. A.; Hou, K.; Lotsch, B. V.; Cademartiri, L.; Puzzo, D. P.; Scotognella, F.; Ghadimi, A. Thomson, J. *Mater. Today* **2009**, *12*, 12.

(37) Mirkin, C. A.; Letsinger, R. L.; Mucic, R. C.; Storhoff, J. J. *Nature* **1996**, *382,* 607.

(38) Alivisatos, A. P.; Johnsson, K. P.; Peng, X.; Wilson, T. E.; Loweth, C. J.; Bruchez, M. P., Jr.; Schultz, P. G. *Nature* **1996**, *382*, 609.

(39) Mirkin, C. A. *Inorg. Chem.* **2000**, *39*, 2258.

(40) Boal, A. K.; Ilhan, F.; DeRouchey, J. E.; Thurn-Albrecht, T.; Russell, T. P.; Rotello, V. M. *Nature* **2000**, *404*, 746.

(41) Murray, C. B.; Kagan, C. R.; Bawendi, M. G. *Science* **1995**, *270,* 1335.

(42) Motte, L.; Billoudet, F.; Lacaze, E.; Pileni, M. P. *Adv. Mater.* **1996**, *8*, 1018.

(43) Schmitt, J.; Decher, G.; Dressick, W. J.; Brandow, S. L.; Geer, R. E.; Shashidar, R.; Calvert, J. M. *Adv. Mater.* **1997**, *9*, 61.

(44) Heath, J. R.; Knobler, C. M.; Leff, D. V. *J. Phys. Chem. B* **1997**, *101*, 189.

(45) Li, M.; Schnablegger, H.; Mann, S. *Nature* **1999**, *402*, 393.

(46) Velev, O. *Science* **2006**, *312*, 376.

(47) Kalsin, A.; Fialkowski, M.; Paszewski, M.; Smoukov, S. K.; Bishop, K. J. M.; Grzybowski, B. A. *Science* **2006**, *312*, 420.

(48) Vlasov, Y. A.; Bo, X. Z.; Sturm, J. C.; Norris, D. J. *Nature* **2001**, *414*, 289.

(49) Jiang, P.; Ostojic, G. N.; Narat, R.; Mittleman, D. M.; Colvin, V. L. *Adv. Mater.* **2001**, *13*, 389.

(50) García-Santamaría, F.; Ibisate, M; Rodríguez, I.; Meseguer, F.; and López, C. *Adv. Mater.* **2003**, *15*, 788.

(51) Jiang, P.; Bertone, J. F.; Colvin, V. L. *Science* **2001**, 291, 453-457.

(52) Noda, S.; Chutinan, A., Imada, M.; *Nature* **2000**, *407*, 608.

(53) Nelson, E. C.; García-Santamaría, F.; Braun, P. V. *Adv. Funct. Mater.*, **2008**, ***18***, 1983.

(54) Rinne, S. A.; García-Santamaría, F.; Braun, P. V, *Nature Photonics **2008**, **2***, 52.

(55) Potyrailo, R.A.; Ding, Z.; Butts, M. D.; Genovese, S. E.; Deng, T.; *IEEE Sensors Journal*, **2008**, *8*, 815.

(56) Velev, O. D.; Jede, T. A.; Lobo, R. F.; Lenhoff, A. M. *Nature* **1997**, *389*, 447.

(57) Talapin, D. V.; Shevchenko, E. V.; Murray, C. B.; Kornowski, A.; Forster, S.; Weller, H. *J. Am. Chem. Soc.* **2004**, *126*, 12984.

(58) Schilling, T.; Frenkel, D. *Phys. Rev. Lett.* **2004**, *92*, 085505.

(59) Nikoobakht, B.; Wang, Z. L.; El-Sayed, M.A. *J. Phys. Chem. B* **2000**, *104*, 8635.

(60) Jana, N.R.; Gearheart, L. A.; Obare, S. O.; Johnson, C. J.; Edler, K. J.; Mann, S.; Murphy, C. J. *J. Mater. Chem.* **2002**, *12*, 2909.

(61) Ming, T.; Kou, X.S.; Chen, H. J.; Wang, T.; Tam, H.L.; Cheah, K.W.; Chen, J. Y.; Wang, J. F. *Angew. Chem. Int. Ed.* **2008**, *47*, 9685.

(62) Guerrero-Martínez, A.; Pérez-Juste, J.; Carbó-Argibay, E.; Tardajos, G.; Liz-Marzán, L.M. *Angew. Chem. Int. Ed.* **2009**, *48*, 9484.

(63) Zhao, N.; Liu, K.; Greener, J.; Nie, Z. H.; Kumacheva, E. *Nano Lett.* **2009**, *9*, 3077.

(64) Ahmed, S.; Ryan, K.M. *Nano Lett.* **2007**, *7*, 2480.

(65) Zhang, X. M.; Imae, T. *J. Phys. Chem. C* **2009**, *113*, 5947.

(66) Robinson, R. D.; Sadtler, B.; Demchenko, D. O.; Erdonmez, C. K.; Wang, L. W.; Alivisatos, A. P. *Science* **2007**, *317*, 355.

(67) Wijaya, A.; Hamad-Schifferli, K. *Bioconjugate Chem.* **2007**, *18*, 1490.

(68) Nakashima, H.; Furukawa, K.; Kashimura, Y.; Torimitsu, K. *Langmuir* **2008**, *24*, 5654.

(69) Chan, Y. T.; Li, S. N.; Moorefield, C. N.; Wang, P. S.; Shreiner, C. D.; Newkome, G. R. *Chem. Eur. J.* **2010**, *16*, 4164.

(70) Gupta, S.; Zhang, Q.; Emrick, T.; Russell, T. P. *Nano Lett.* **2006**, *6*, 2066.

(71) Ryan, K. M.; Mastroianni, A.; Stancil, K. A.; Liu, H.; Alivisatos, A. P. *Nano Lett.* **2006**, *6*, 1479.

(72) Nie, Z. H.; Fava, D.; Kumacheva, E.; Zou, S.; Walker, G. C.; Rubinstein, M. *Nat. Mater.* **2007**, *6*, 609.

(73) Liu, K.; Nie, Z. H.; Zhao, N. N.; Li, W.; Rubinstein, M.; Kumacheva, E. *Science* **2010**, *329*, 197.

(74) Khanal, B. P.; Zubarev, E. R. *Angew. Chem. Int. Ed.* **2007**, *46*, 2195.

(75) Pietrobon, B.; McEachran, M.; Kitaev, V. *ACS Nano* **2009**, *3*, 21.

(76) Lin, X. M.; Wang, G. M.; Sorensen, C. M.; Klabunde, K. J. *J. Phys. Chem. B* **1999**, *103*, 5488.

(77) Prasad, B. L. V.; Stoeva, S. I.; Sorensen, C. M.; Klabunde, K. J. *Chem. Mater.* **2003**, *15*, 935.

(78) Badia, A.; Singh, S.; Demers, L.; Cuccia, L.; Brown, G. R.; Lennox, R. B. *Chem. Eur. J.* **1996**, *2*, 359.

(79) Alvarez-Puebla, R. A.; Agarwal, A.; Manna, P.; Khanal, B. P.; Aldeanueva-Potel, P.; Carbo-Argibay, E.; Pazos-Perez, N.; Vigderman, L.; Zubarev, E. R.; Kotov, N. A.; Liz-Marzan, L. M. *Proc. Natl. Acad. Sci. U.S.A.* **2011**, *108*, 8157.

(80) Brust, M.; Fink, J.; Bethell, D.; Schiffrin, D. J.; Kiely, C. *J. Chem. Soc. Chem. Commun.* **1995**, 1655.

Chapter V

Controlled Self-assembly of Anisotropic Gold Nanostructures

5.1 Introduction

Controlled organization of nanostructures into ordered assemblies opens up avenues for designing advanced functional materials. In that respect self-assembly becomes extremely important because it provides us the ability to arrange nanostructures into ordered arrays without the influence of external forces.[1-18] Anisotropic gold nanostructures such as gold nanorods and gold nanowires are of great interest because of their unique optical and electronic properties.[19-30] For that reason, structures made of periodic arrays of these nanostructures may find extensive applications in bio-medical imaging,[31-36] sensors,[37-40] and flexible electronics.[41-48] Our investigation of CTAB capped AuNRs shows that slow evaporation of their aqueous solution leads to the formation of 3D colloidal crystals of gold nanorods. However, the colloidal crystals formed by this process are not of similar shape and size. So, it is important to find new ways of controlling the morphology of self-assembled structures on a substrate as it will enable us to study physicochemical properties of periodic arrays of monodisperse structures.[49-53]

Shape and size of self-assembled structures can be controlled by combined use of "top-down" and "bottom-up" assembly technique.[54-62] First, a patterned substrate is designed by conventional photolithographic techniques and then nanostructures are self-assembled inside the etched patterns.[54-62,68-70] This confinement approach offers the possibility of controlling the self-assembled structures by changing the dimensions of the pattern.[54-62] There are several reports in the literature highlighting the wet assembly[54-61] and dry assembly[62] of spherical microparticles on top of a lithographically patterned

substrate. In addition, the microcontact printing technique has been used for the controlled assembly of nanoparticles by creating patterned hydrophobic and hydrophilic sites on a gold substrate.[63-67] Nanostructures can also be self-assembled on top of such substrates using non covalent interactions.[63-67] However, there are only few reports describing the assembly of anisotropic nanostructures using these techniques.[68-70] If prepared, these assembled structures may offer the preparation of hybrid superstructures with anisotropic optical, electronic, and mechanical properties. These properties can be further exploited to design bio-sensing devices and conductive surfaces with high efficiency and high reproducibility.

In this chapter, we describe the use of substrate patterning to control the morphologies of self-assembled structures on silicon substrates. When an aqueous solution containing CTAB capped gold nanorods was dried on a patterned substrate, virtually all the nanostructures accumulated inside the lithographically etched pattern. The process was found to be highly selective as no deposition was found on the photoresist-coated area. Additionally, we describe the assembly of anisotropic gold nanostructures using the microcontact printing technique. Finally, we report the evaporation induced self assembly (EISA) of ultra long gold nanowires to form two dimensional periodic arrays.

5.2 Results and Discussions

5.2.1 Design of the patterned substrate by photolithography

Orientation of rods and the spatial distribution of colloidal crystals depend on the hydrophilicity of substrate. Therefore, one can expect that if a periodic hydrophilic/hydrophobic contrast is created on the surface, the NRs may primarily

accumulate on the hydrophilic sites (due to more favorable interactions with CTAB-bilayer molecules). Photolithography is a widely used technique for creating hydrophobic/hydrophilic contrast on a solid substrate. First, a hydrophobic photoresist (S1813) coated silicon wafer was exposed to UV irradiation. Removal of the resist from the UV-treated areas exposes slightly hydrophilic surface of silicon. Commercially available silicon wafers have thin layer of silicon oxide coating which makes them hydrophilic in nature. Essentially, the patterned substrate has periodic arrays of hydrophilic silicon oxide surface separated by a hydrophobic background of S1813 film (Figure 5.1).

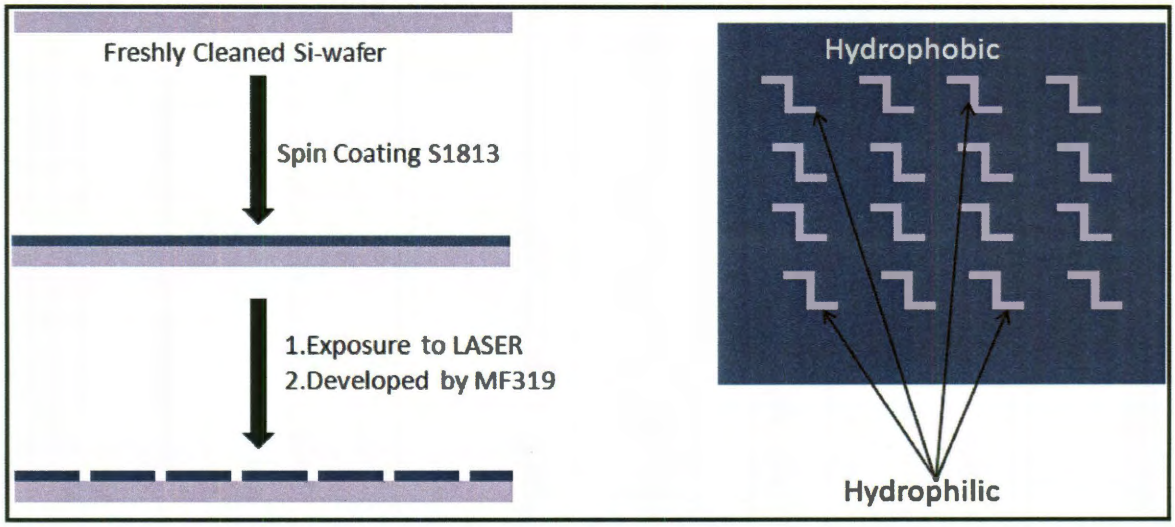

Figure 5.1 Design of patterned substrate by photolithography.

5.2.2 Self-assembly of gold nanorods on patterned substrates

Self-assembly of nanoparticles on patterned substrates is not only directed by hydrophilic interaction, but also by the capillary forces and gravitational sedimentation. Our initial trials for selective deposition of amplified NRs (75nm X 25nm) inside lithographically etched patterns were not successful. Amplified gold nanorods are highly soluble in water and their rate of sedimentation is quite low. In addition, when their

aqueous solution was dried on patterned substrates, the *coffee ring* effect drove the accumulation of NRs around the edge of the drying water droplet.[18] Therefore, most of the nanorods were deposited around the perimeter of the droplet forming a golden rim and virtually no deposition was observed on top of the pattern which is at the center of the droplet. In order to avoid this problem, we decided to use over amplified gold microrods (800nm X 200nm) (Figure 5.2). These microrods (MRs) are significantly heavier than amplified NRs and they undergo sedimentation from their aqueous solution at much faster rate. The "coffee ring" formation does not occur as these MRs sediment before the water droplet dries. When an aqueous solution of these rods was dried on a solid substrate, uniform deposition was observed. Additionally, large size of these microrods helps in characterizing the assembly process by optical microscopy and SEM. However, a balance must be maintained between the solubility and the rate of sedimentation of the MRs. The sedimentation process should not be too fast as it reduces the selectivity of the assembly process. We observed that AuMRs having length more than 1.2 microns did not work for the self-assembly experiment. Size monodispersity of the MRs should also be maintained to obtain self-assembled structures with long range order.

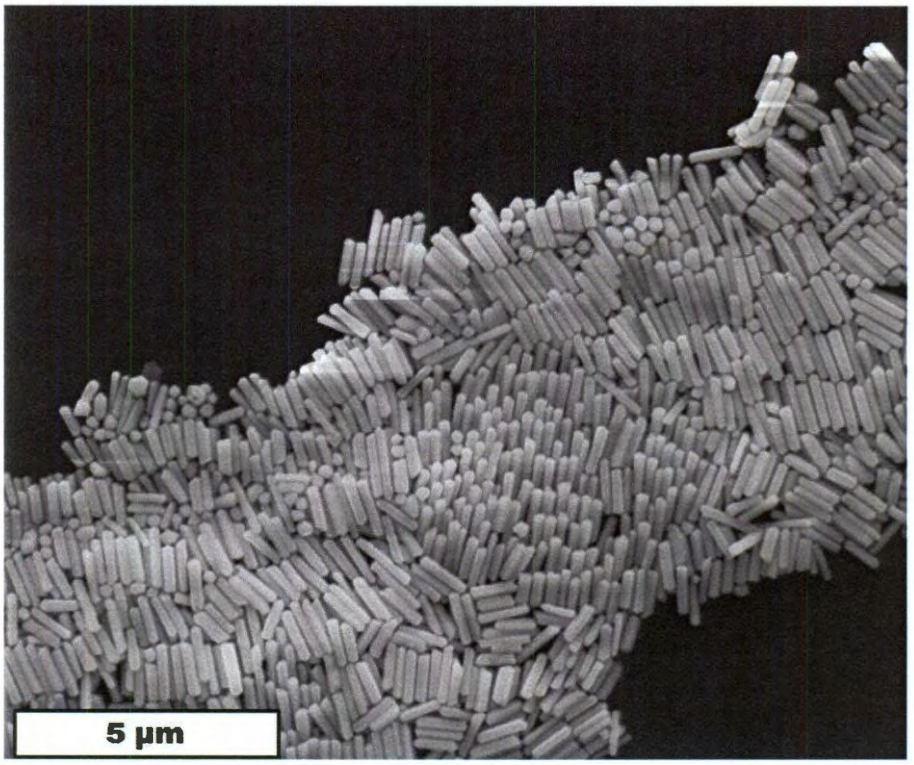

Figure 5.2 SEM image of gold microrods (800nmX200nm)

When colloidal crystals are grown on flat substrates, their orientation is random and size distribution is broad. For many applications it is desirable to control these parameters. For the self-assembly experiment an aqueous solution of CTAB-functionalized MRs is cast onto the patterned surface having "Z" shaped etched areas and allowed to dry slowly. SEM imaging showed that MRs are deposited exclusively on the Z-shaped bare silicon surface (Figure 5.3) and virtually no deposition was found on top of the photoresist coated area. This high selectivity proves that MRs are strongly attracted to the hydrophilic area. This is truly a long range assembly as it persisted over the entire pattern. The selectivity of the assembly does not depend on the shape of the micropattern. In addition to high selectivity, we also observed that MRs confined inside the pattern are oriented vertically with respect to the substrate (Figure 5.4). This

assembly process is similar to template assisted self assembly process (TASA) which uses a fluid cell to control the dewetting of the liquid.

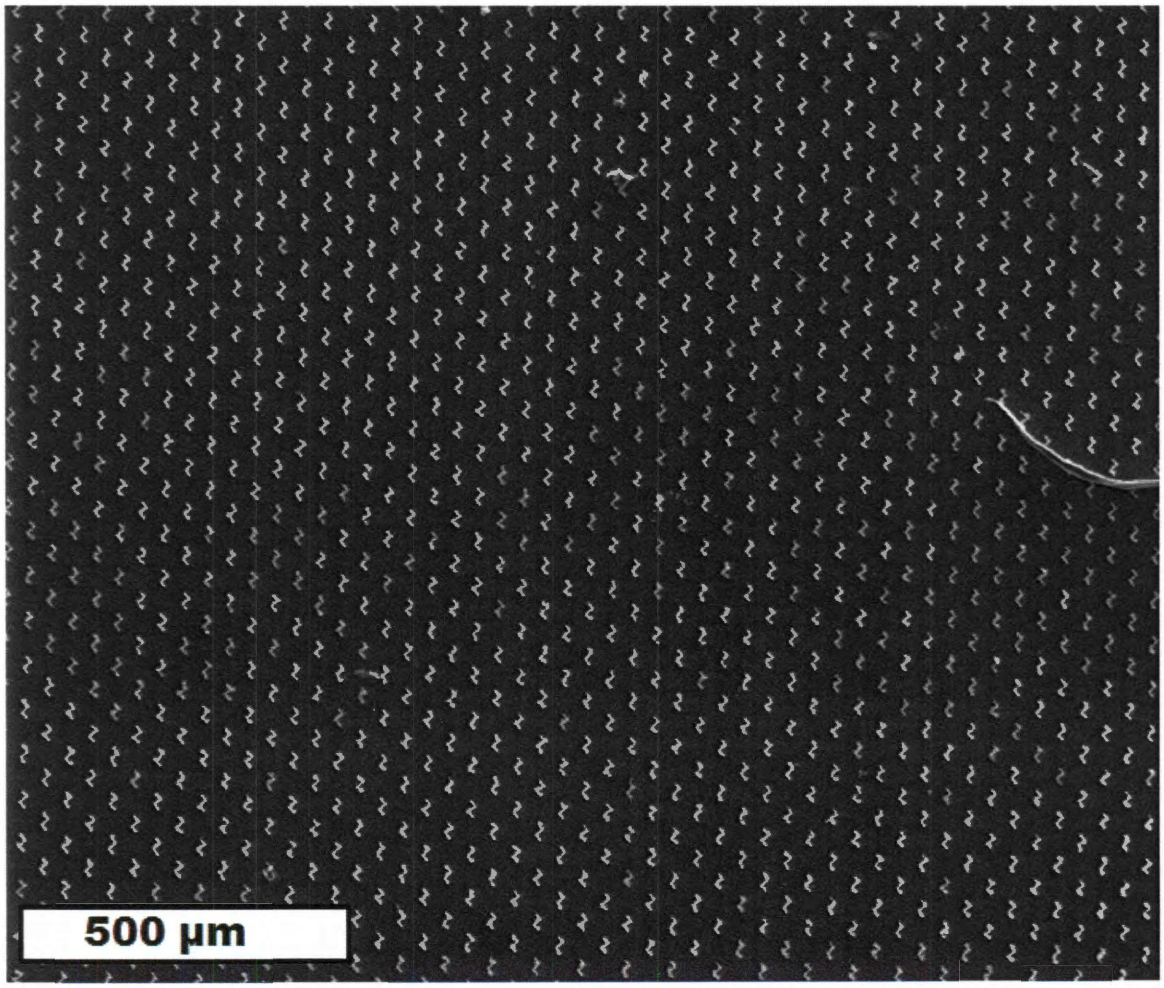

Figure 5.3 Low magnification SEM image of periodic arrays of AuMRs on patterned substrate.

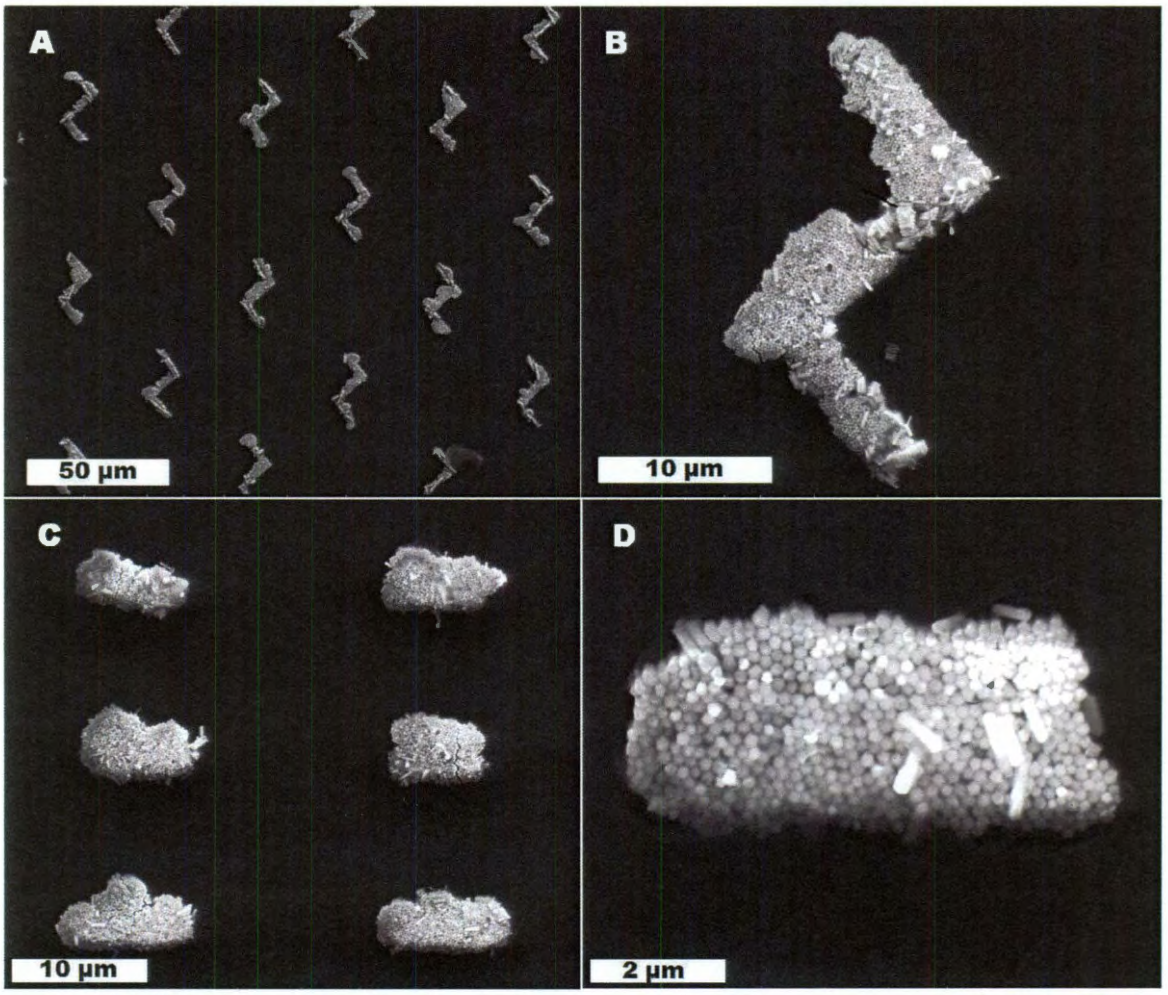

Figure 5.4 SEM images (A,C) of periodic arrays of AuMRs on patterned substrate. High magnification SEM images (B,D) showing vertical orientation of gold microrods.

It can be hypothesized that the slow drying of water droplet is causing dewetting when the thickness of the water film reaches a critical value (several microns). As a result, a continuous film of water solution brakes into *microscopic droplets* covering the hydrophilic features of the pattern (Figure 5.5). Due to the ionic nature of CTAB, MRs followed the water phase and concentrated in the hydrophilic areas. As the drying of microdroplets continues, the NRs self-assembled into vertically oriented structures confined inside the etched micropattern.

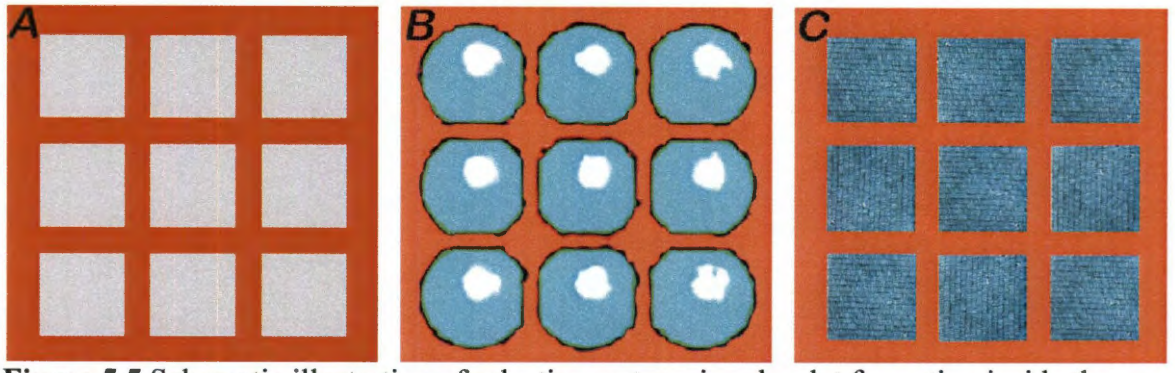

Figure 5.5 Schematic illustration of selective water microdroplet formation inside the hydrophilic areas (gray) against hydrophobic background of photoresist coated silicon(red). Subsequent evaporation results in their assembly inside the hydrophilic wells.

To explore this phenomenon in detail we decided to try a pattern where we have mixture of shapes, both straight lines and curves. Figure 5.6 shows an SEM image of a photolithographic micropattern (letters R-I-C-E) .When a dilute solution of gold microrods was cast on this patterned substrate and allowed to dry slowly all MRs spontaneously migrated and became confined in the interior of the letters, and there was virtually no deposition of rods in the photoresist-coated hydrophobic background. In this case, the microrods self-assembled parallel to the substrate in a side-to-side fashion and formed 1D strands that comprise hundreds of rods and measure up to 20 μm in length making up a "firewood pile" pattern. It is possible that the MRs assemble during the late stage of the drying of the water droplet confined inside the etched pattern. However, it is also possible that these parallel packed strands form before the dewetting occurs and they preferentially sediment inside the hydrophilic areas (R-I-C-E pattern). Although there was no long range ordering due to the polydispersity of rods and fairly complex shape of the letters, the high selectivity of MRs was particularly remarkable and persisted over the entire pattern (Figure. 5.6A). However, this experiment clearly shows the possibility to control the size and orientation of MR assemblies on the surface.

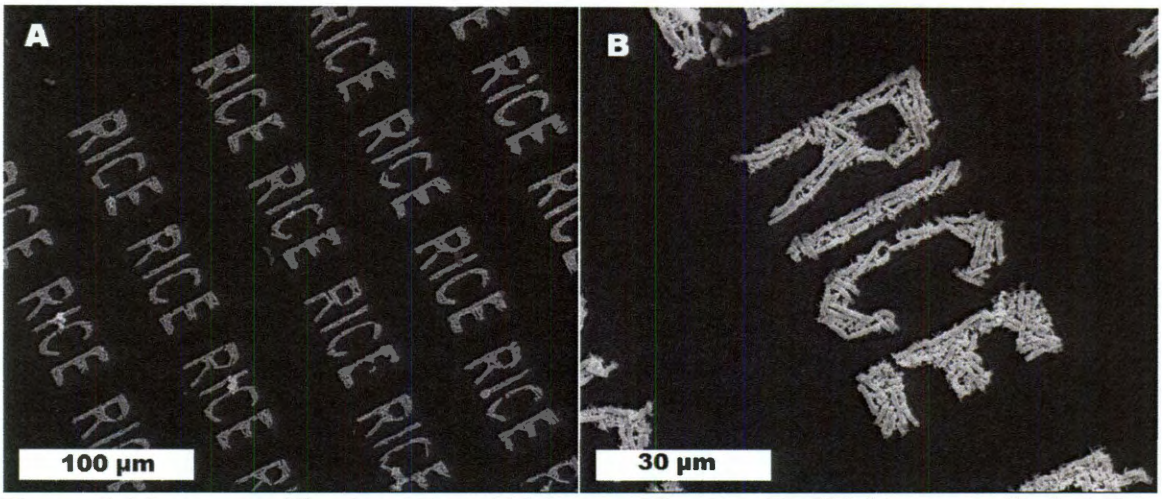

Figure 5.6 Low magnification (A) and high magnification (B) SEM images of R-I-C-E made of MRs.

5.2.3: Design of the patterned substrate using microcontact printing technique

In addition to photolithography, microcontact printing technique is a well known method for creating hydrophobic/hydrophilic contrast on a substrate. This is achieved by selectively creating alternating self-assembled monolayers (SAMs) of hydrophilic and hydrophobic thiols on a gold surface. An elastomeric polydimethylsiloxane (PDMS) stamp with imprinted photolithographic pattern is generally used as a mold to print the thiol (hydrophobic or hydrophilic) ink at specific areas of the substrate (Figure 5.7). Most importantly, the chemical functionality of the SAMs can be changed by changing the thiol. Generally, 16-mercaptohexadecanoic acid (MHDA) is used to form the hydrophilic SAM and hexadecanethiol (HDT) is used to create the hydrophobic background. This resulting substrate is chemically different from a lithographically designed pattern. However, they are similar in nature as both of them have periodic arrays of hydrophilic areas against a hydrophobic background. When MHDA is used, the hydrophilic SAM becomes carboxyl terminated, hence anionic in nature (Figure 5.8).

Anionic nature of the SAM would allow the favorable electrostatic attraction with positively charged CTAB coated NRs and their selective deposition may be observed.

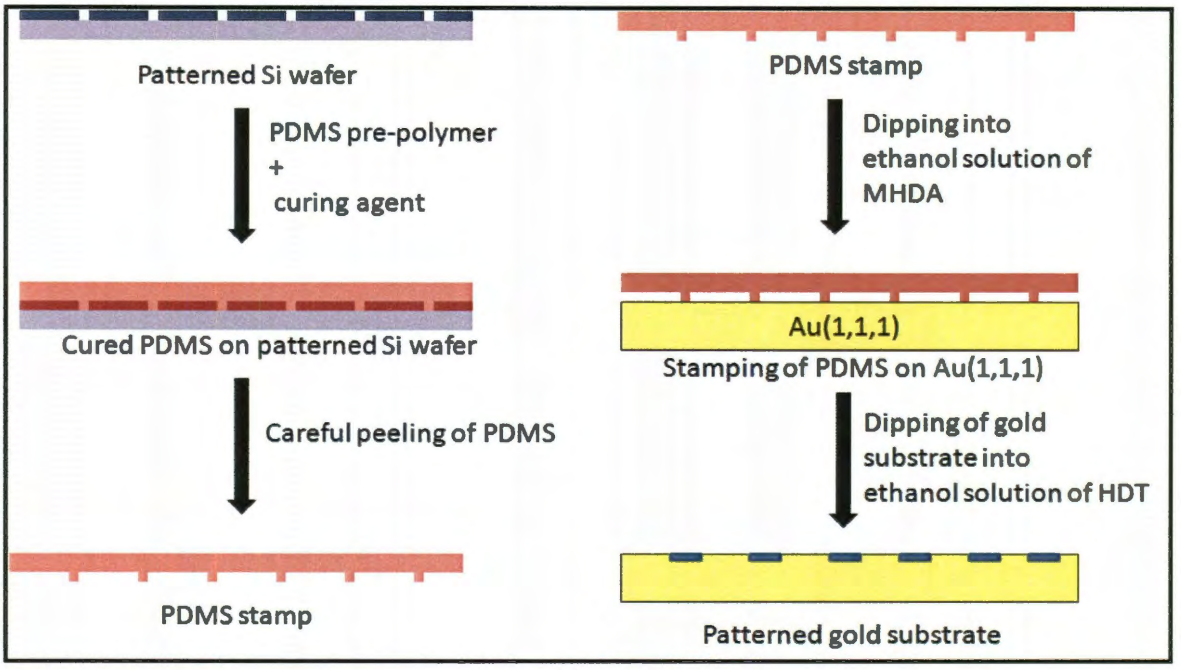

Figure **5.7** Schematic illustration of microcontact printing technique

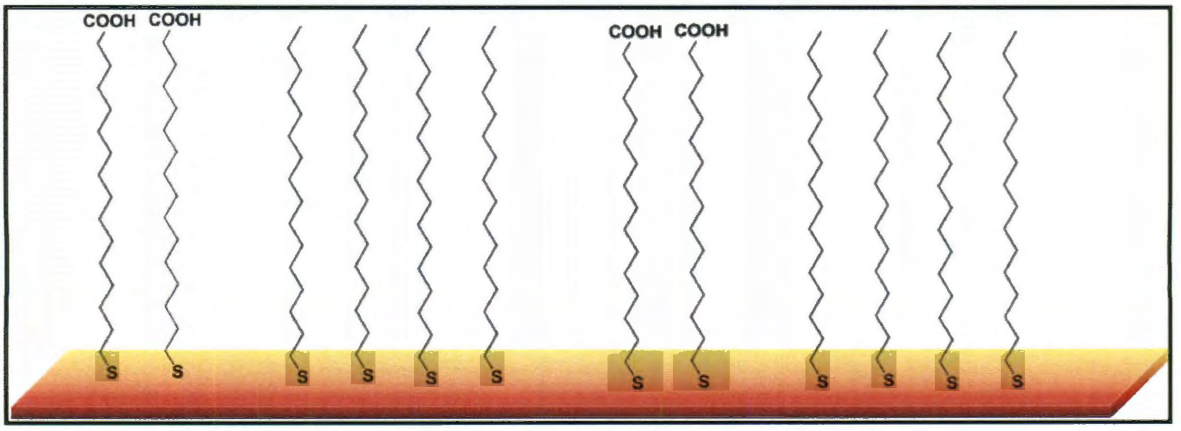

Figure 5.8 Schematic of hydrophoibic and hydrophilic SAMs on gold surface

5.2.4 Self-assembly on patterned substrate designed by microcontact printing technique

For the self-assembly experiment we placed a drop of MR solution on the patterned substrate (stripes) and checked the self-assembly process by optical microscopy. We observed rapid migration of microrods towards the hydrophilic areas on the substrate. This migration occurs right after the casting of the water droplet. Because the rate of sedimentation of these MRs is not that fast, it can be assumed that the rapid migration is due to the attractive electrostatic forces between positively charged MRs and negatively charged SAM. SEM imaging showed the selective deposition of MRs on top of the hydrophilic areas (Figure 5.9) forming monolayers of parallel packed structures. This process was found to be highly selective and there was virtually no deposition on the hydrophobic areas. In addition, MRs are oriented perpendicular with respect to the long axis of the hydrophilic pattern. The rate of sedimentation does not have a profound effect on this self-assembly. We were also able to self-assemble amplified NRs (75m x25nm) by this technique. These NRs are highly soluble in water and their rate of gravitational sedimentation is very low. When we cast a drop of their aqueous solution on top of the patterned substrate, rapid migration of these NRs toward the hydrophilic areas was observed. Unfortunately, we still observed coffee-ring formation once the solvent was evaporated. However, SEM investigation around the center of the droplet showed a strong propensity of NRs to deposit on the hydrophilic sites (Figure 5.10). This experiment proves that electrostatic force of attraction is the major driving force for the assembly of NRs on a micro patterned gold surface. Additionally, changing the shape of the hydrophilic pattern did not affect the assembly process (Figure 5.10). We observed

that increase in the concentration of NRs decreases the selectivity of this process. However, in this case nanorods deposited in the hydrophilic areas tend to pack in side-by-side fashion. Figure 5.11 shows the periodic arrays of islands made of gold nanorods. High magnification SEM image revealed that the islands are made of the parallel packed arrays of gold nanorods. These findings are particularly important as they offer the possibility to create periodic arrays of NR superlattices. Controlled organization of assembled structures may enable us to design novel biosensing devices with high reproducibility.

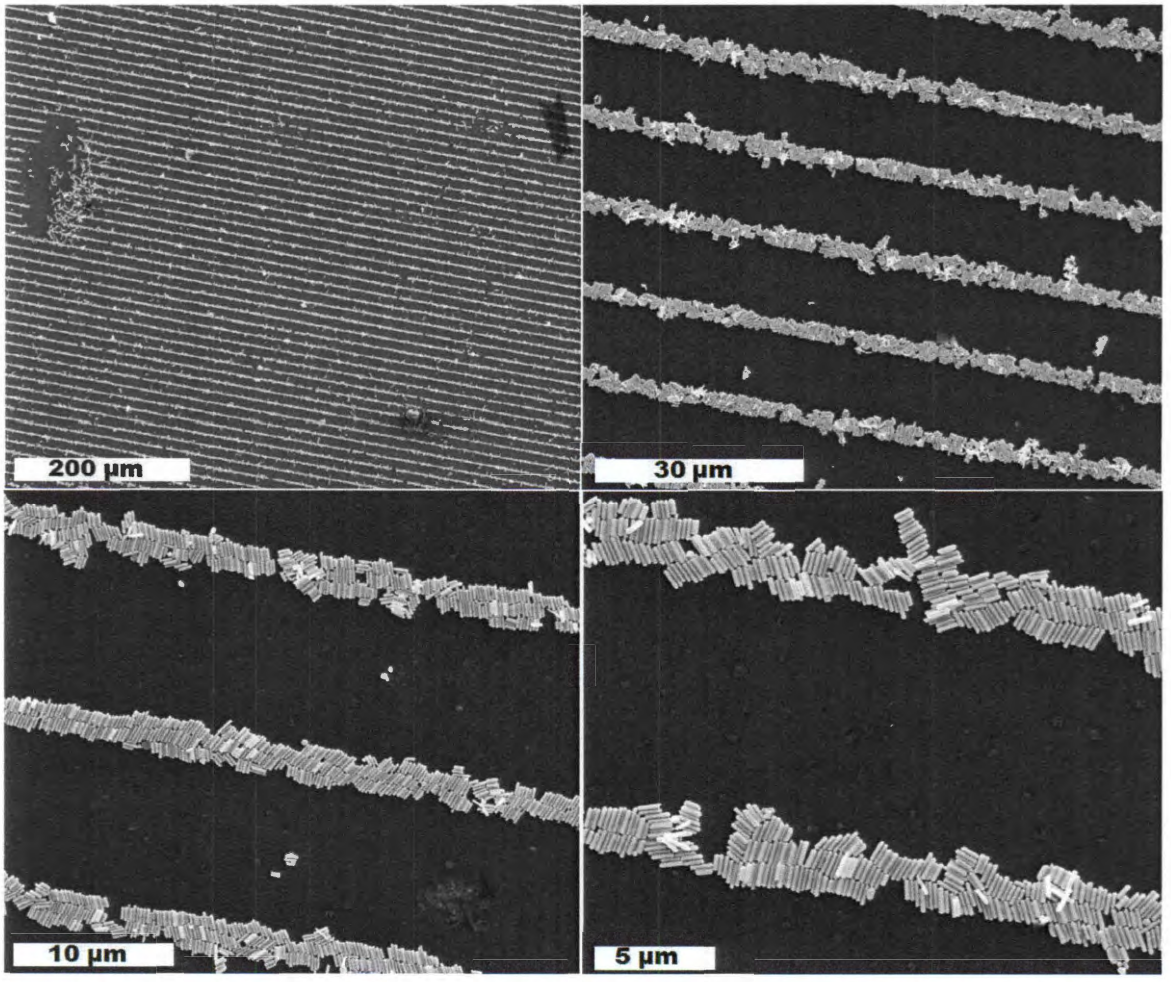

Figure 5.9 SEM images of AuMR assemblies obtained by microcontact printing.

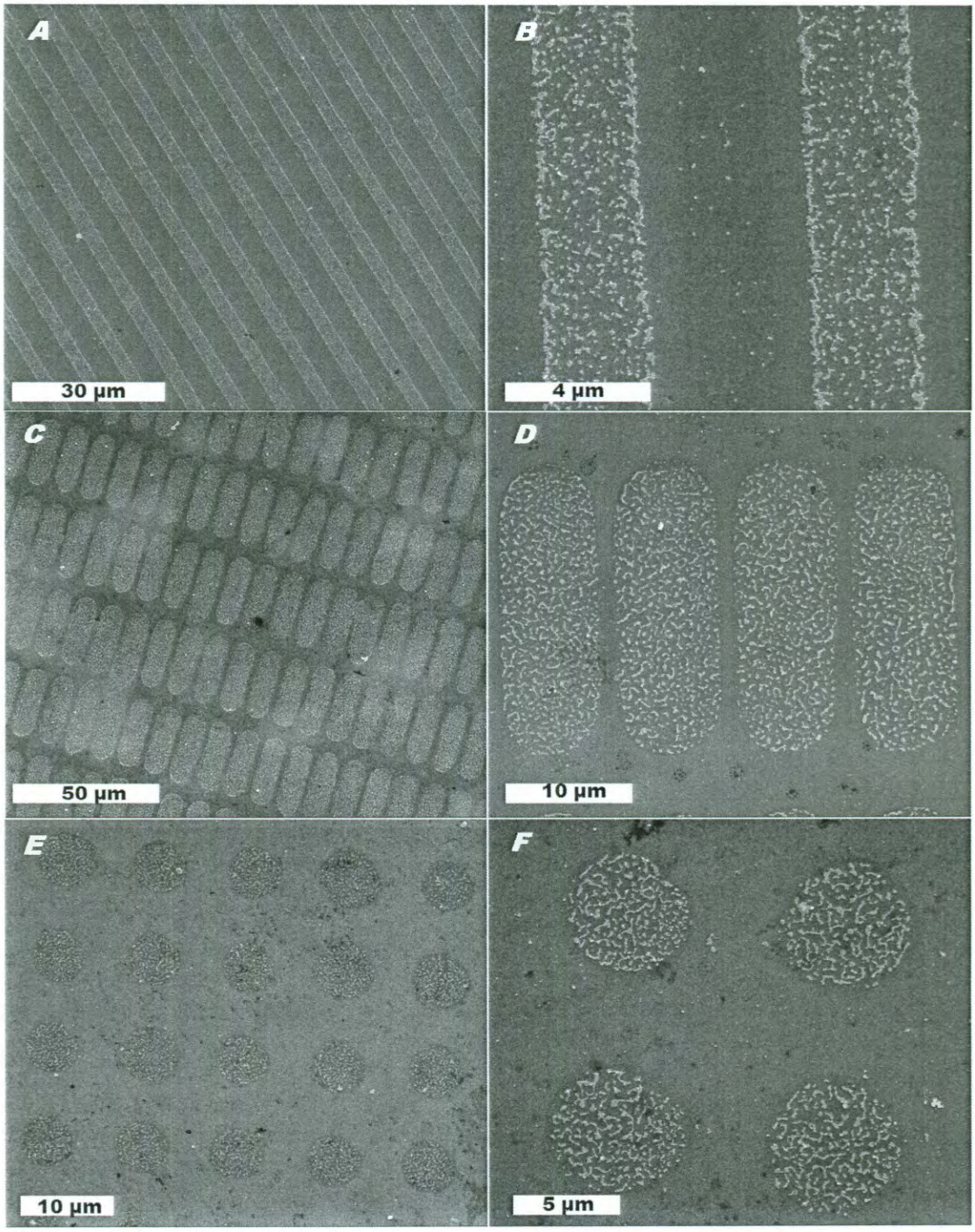

Figure 5.10 Low magnification (A) and high magnification (B) SEM image of AuNR stripes. Low magnification (C) and high magnification (D) SEM image of AuNR ovals. Low magnification (E) and high magnification (F) SEM image of AuNR circles.

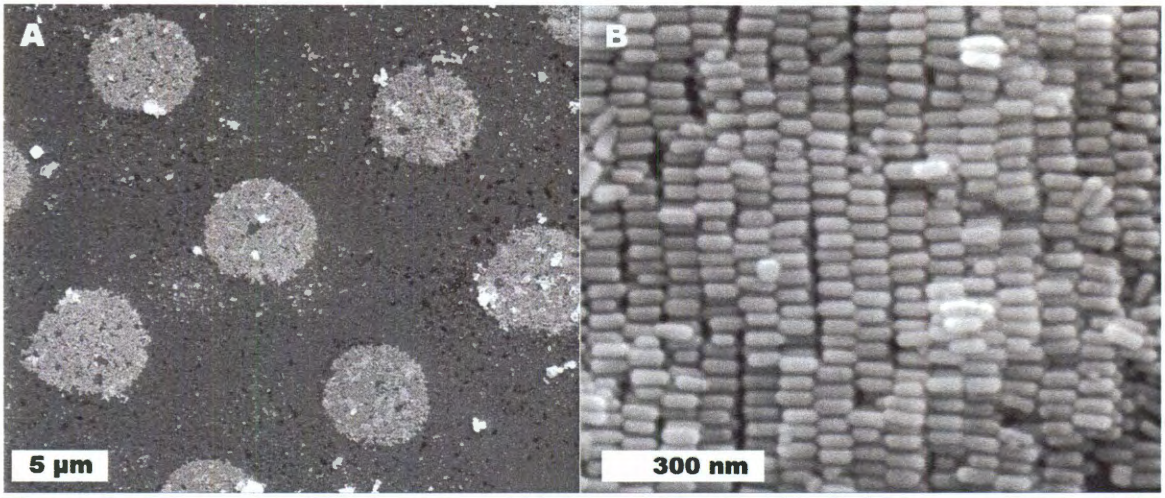

Figure 5.11 Low magnification (A) and high magnification (B) SEM image of "islands" made of parallel packed gold nanorods

A control experiment was performed by creating a periodic array of hydrophobic sites separated by hydrophilic background. In this case we used hydroxyl- or amino-terminated thiol to create the hydrophilic SAM. These thiols are not anionic and the electrostatic force of attraction between the NR and CTAB is minimal. When an aqueous solution of CTAB-capped NRs was dried on top of such substrate, ring-like assemblies were formed (Figure 5.12). Although the selectivity of this assembly process was not great, the formation of unusual ring structures from CTAB-coated NRs was particularly interesting. Selective deposition of NRs at the hydrophobic/hydrophilic interface can be attributed to the electrostatic repulsion between CTAB coated NR and positively charged hydrophilic SAM. To the best of our knowledge, this is the first example of ring-like assemblies prepared from CTAB-capped gold nanorods. In addition the NRs in these rings are packed parallel to each other and are locally organized in as "firewood pile" (Figure 5.12).

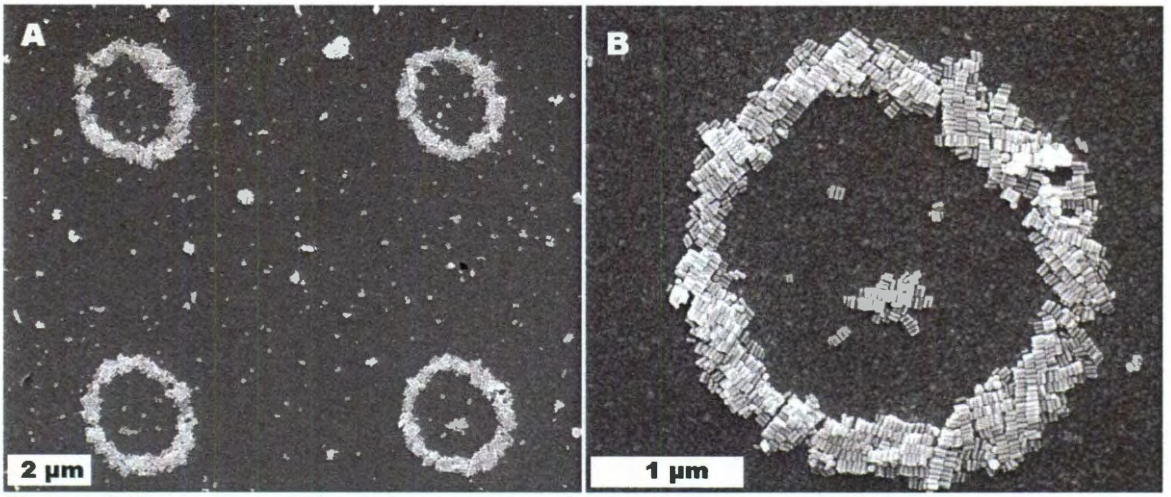

Figure 5.12 Low magnification (A) and high magnification (B) SEM image of ring-like assemblies of CTAB-capped gold nanorods.

These experiments with CTAB-coated gold nanorods prove that they can be organized in controlled fashion by creating alternating hydrophobic and hydrophilic features on a substrate. We hypothesize that the selective deposition of NRs is primarily driven by electrostatic interactions. However, it is possible that the gravitational sedimentation and capillary forces have some effect on this assembly process as we observed better selectivity for lager nanostructures. Most importantly, chemical modification of NR surface is not at all required for this process.

5.2.5 Self-assembly of polymer-functionalized gold nanorods

Previous work in our group reported ring-like assemblies of hydrophobic polymer-functionalized gold nanorods.[11] When methylene chloride solution of polystyrene-functionalized nanorods was dried on a hydrophobic substrate, all the nanorods self-assemble to form millions of ring-like assemblies. Interestingly, these assemblies are not observed when the solution is dried in a moisture free environment. When volatile solvent like methylene chloride evaporates, surface cooling results in the condensation of water vapor on the drying solvent. Optical microscopy revealed the

formation of water microdroplets on the surface of drying methyl chloride. These water microdroplets act as templates for ring formation. However, the droplets formed under these conditions coalesce rapidly and lose their size monodisperity. So, the rings became highly polydisperse in size. Controlling the size of these rings is very important as it would allow us to investigate opto-electronic properties of periodic arrays of ring-like superstructures made of anisotropic building blocks. In order to control the size of the rings, it is required to control the size of the template, i.e. the water microdroplets, which direct the assembly. Additionally, sufficient distance should be maintained between two water droplets to avoid random coalescence. When water vapor is condensed on top of a pre-cooled gold substrate with patterned hydrophobic and hydrophilic features, water droplets form exclusively on top of the hydrophilic sites. In addition, the size of the water droplets matches the size of the hydrophilic areas. Therefore, patterned arrays of hydrophilic areas promote the formation of periodic arrays of water droplets on top a gold substrate. Figure 5.13 shows the schematic illustration and optical micrograph of periodic arrays of water droplets formed under such condition. In this case, the hydrophilic areas are circular and the resulting water droplets are spherical in shape. Importantly, all of them have the same size. Uniformity of the water droplets can also be visually checked by the appearance of rainbow like pattern on the substrate.

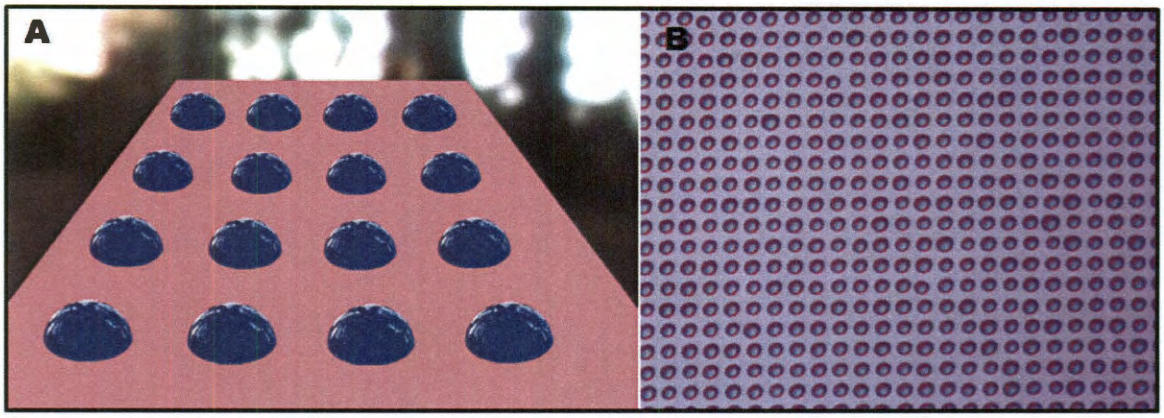

Figure 5.13 Schematic illustration (A) and optical microscopy image (B) of a periodic array of water microdroplets on patterned gold substrate.

When a drop of methylene chloride solution of polystyrene-coated nanorods was cast on top of these pre-formed water droplets and allowed to dry, all the AuNRs self-assembled to form periodic arrays of rings of gold nanorods. Because CH_2Cl_2 evaporates at a faster rate than water, each water droplet became surrounded by a thin layer of CH_2Cl_2. Polystyrene functionalized gold nanorods being highly soluble in CH_2Cl_2, remained in solution until the last portion of solvent evaporated. High hydrophobicity of the polystyrene prevented them to break the walls of the water droplets. After the drying of the water droplets, periodic arrays of ring-like assemblies were obtained. Size of these rings can be precisely controlled by changing the size of the hydrophilic areas. Figure 5.14 shows the periodic arrays of rings formed on top of a gold substrate. The diameter of these rings is 4-5 microns and the center to center distance between two rings is close to 10 microns. The orientation of nanorods in a ring is completely random.

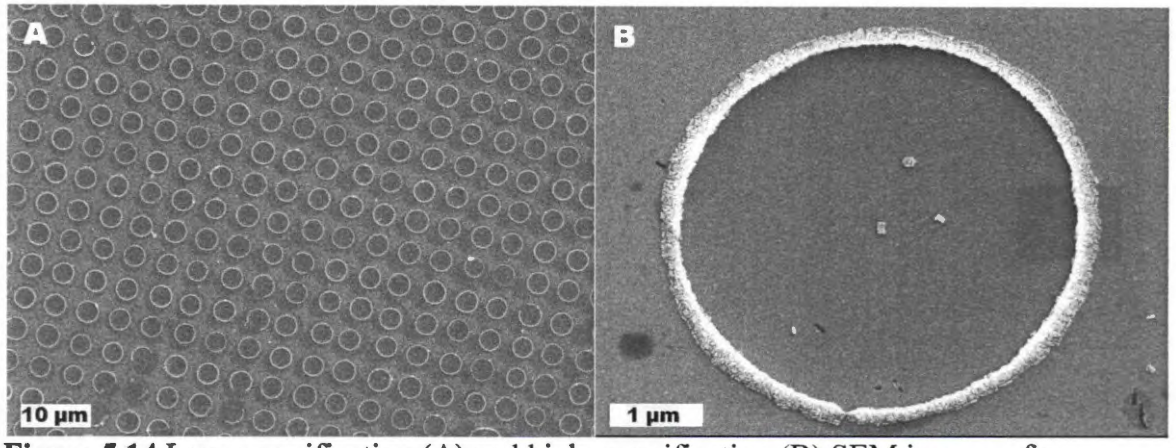

Figure 5.14 Low magnification (A) and high magnification (B) SEM images of a periodic array of rings of gold nanorods

Additionally, the shape of the patterned features can also be controlled by changing the shape of the PDMS stamp pillars. Figure 5.15 shows linear, square, and triangular assemblies obtained by this evaporative technique. Thus, a wide variety of self-assembled structures can be prepared. In the case of square and triangular assembly the edge of the assembled structures are not very sharp. This is because the water droplets formed inside square or triangular hydrophobic areas have rounded edges. Another important aspect of this assembly is that it is not limited to gold nanorods. Various types of metallic and semiconductor nanocrystals, polymers, and small organic molecules can be assembled using this technique as long as they are hydrophobic and highly soluble in volatile solvent like methylene chloride. These assemblies are also reversible in nature as the rings can be re-dissolved in CH_2Cl_2 without any agglomeration of the nanorods.

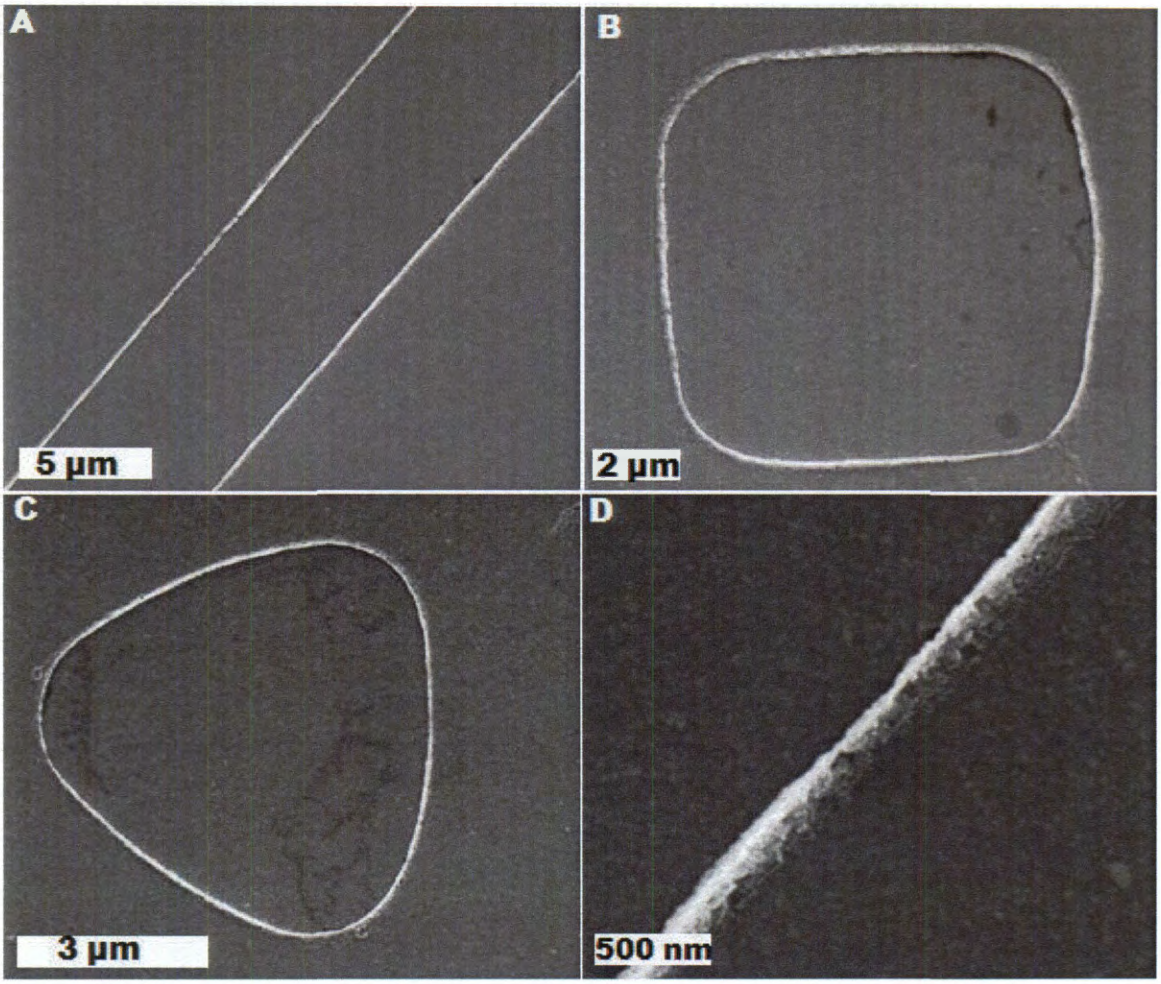

Figure 5.15 Line (A), square (B), and triangle (C) made of gold nanorods. High magnification SEM image of these assemblies is shown in (D).

An important control experiment was performed using polyethylene glycol (PEG) functionalized gold nanorods. Like polystyrene coated nanorods, PEG functionalized gold nanorods are highly soluble in organic solvent. However, they are also soluble in water because of the presence of water soluble PEG on NR surface. When a methylene chloride solution of these nanorods was dried on top of periodic arrays of water microdroplets, no rings were formed. Instead, those NRs were selectively deposited on the hydrophilic areas forming periodic arrays of "islands" of gold nanorods (Figure 5.16). During the drying process methylene chloride forms thin films around the pre-

formed water droplets. PEGylated NRs are soluble in methylelne chloride and they stay in the solution until the last portion of methylene chloride evaporates. However, since these NRs are hydrophilic in nature, they are able to penetrate the wall of the water droplet and dissolve in it. Once the water droplets evaporate, the periodic arrays of "islands" of NRs are formed. The experiment proves that the hydrophobicity of the polymer arm is critically important for the formation of ring-like assemblies. In addition, it also proves that switchable assembly can be obtained by modifying the surface of NRs.

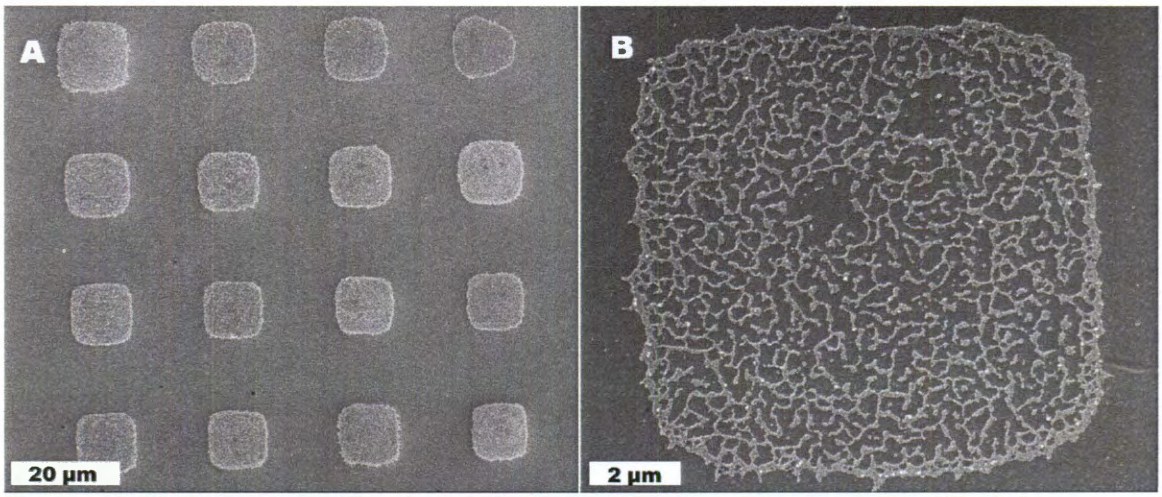

Figure 5.16 Low magnification (A) and high magnification (B) SEM images of assemblies obtained from PEG-functionalized nanorods.

5.2.6 Self-assembly of gold nanowires

Transparent conductive surfaces are essential for designing high performance solar cells, touch screen phones, and OLED dispays.[71-74] They are generally fabricated by evaporating a thin film of Indium Titanium Oxide (ITO) on top of a transparent substrate.[75,76] However, the high cost of production of ITO and its inherent brittleness have forced researchers to explore other kinds of conductive transparent materials for the fabrication of electrodes. Transparent films made of carbon nanotubes and graphene are often used for this purpose.[46,73,77-78] Although these films offer low processing temperature and high flexibility, their sheet resistance and transparency values are inferior to those of ITO. Recently, films of randomly deposited silver nanowires were also used to create conductive surface.[41-45, 78] However, in almost all cases they showed fairly low transparency and high tendency to oxidize when exposed to air atmosphere.[41-46] For that reason we focused our attention on gold nanowires that are much more stable to oxidation. In addition, we hypothesized that the organization of nanowires into periodic two dimensional network as opposed to a random network may increase the transparency and efficiency of the conductive surface. Proper organization would ensure the all the NWs are well connected with each other. This is critically important for getting a good conductivity value while maintaining high transparency of the underlying substrate (i.e. glass). It will also allow us to cover a large area using minimum amount of expensive metallic nanowires. That also means the majority of the transparent surface will not be covered by NWs and the transparency of the substrate should not decrease significantly.

For our experiments we chose CTAB-capped gold nanowires (5000 nm X 50nm) which were previously synthesized in our lab.[27] Our initial approach of self-assembly of using photolithography and microcontact printing was only partially successful. Gold nanowires having aspect ratio more than 100 have a strong propensity to form bundles and their selective sedimentation is very hard to control. However, template-assisted evaporation-induced self assembly (EISA) technique allowed us to create periodic two-dimensional networks of gold nanowires. In this procedure, a commercially available TEM grid is used as the template for directing the assembly process (Figure 5.17).

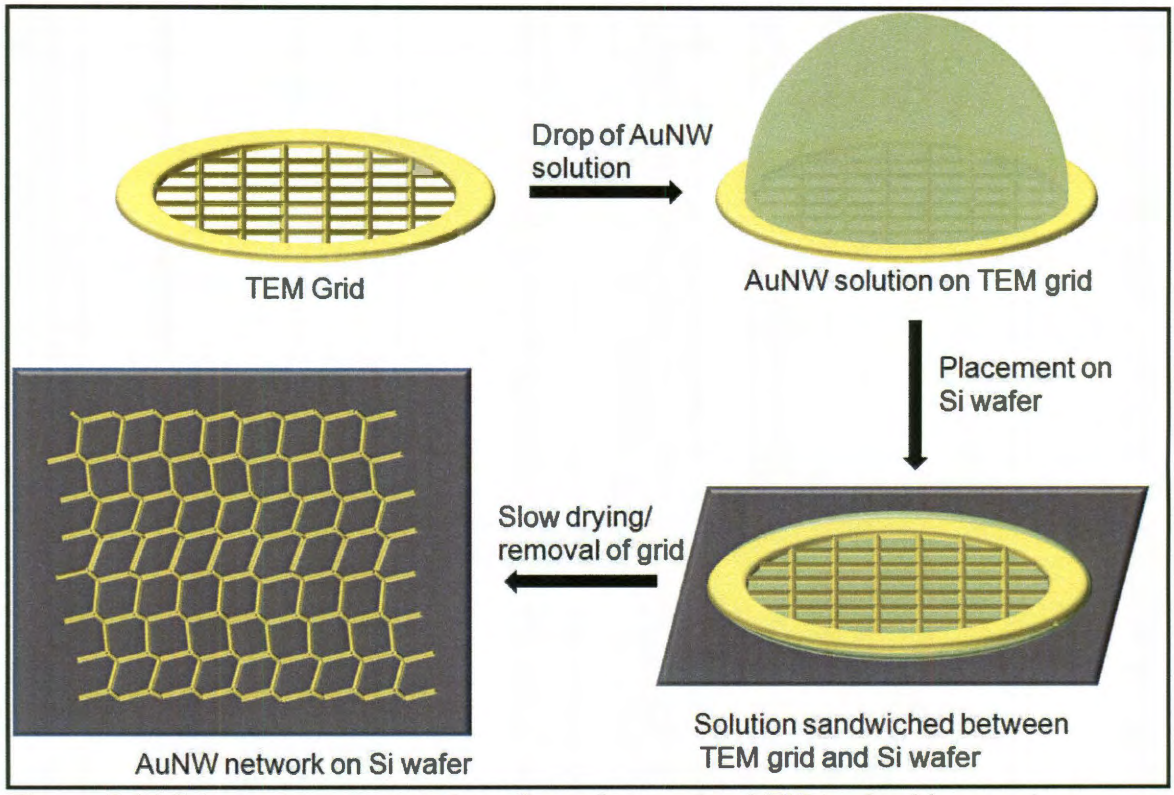

Figure 5.17 Schematic representation of template-assisted EISA of gold nanowires.

First, an aqueous solution (20 μL) of CTAB-capped gold nanowires is deposited on top of a gold TEM grid (200 or 400 mesh size) and that grid is placed on top of a silicon wafer. Due to the capillary forces the solution penetrates under the grid and slightly elevates it from the silicon substrate. Because the grid is fairly light, a thin layer

of the aqueous solution is always trapped between the grid and the underlying silicon wafer. When the majority of the solution evaporates, the residual liquid film is sandwiched between the TEM grid and the silicon substrate as illustrated in Fig. 5.17 (bottom right). The whole set up is kept under humid atmosphere and the water droplet is allowed to dry very slowly (20 h). The evaporation of water proceeds through the open windows of TEM grid and leaves the residual volume of the solution under the straight bars of the grid. This process induces the migration and accumulation of nanowires under the bars of the grid. As the slow evaporation continues, the interconnected water lines gradually shrink and align the nanowires into a continuous two-dimensional network. This periodic 2D network of AuNWs is truly a long rage assembly as it covers more than one square millimeter area (Figure 5.18).

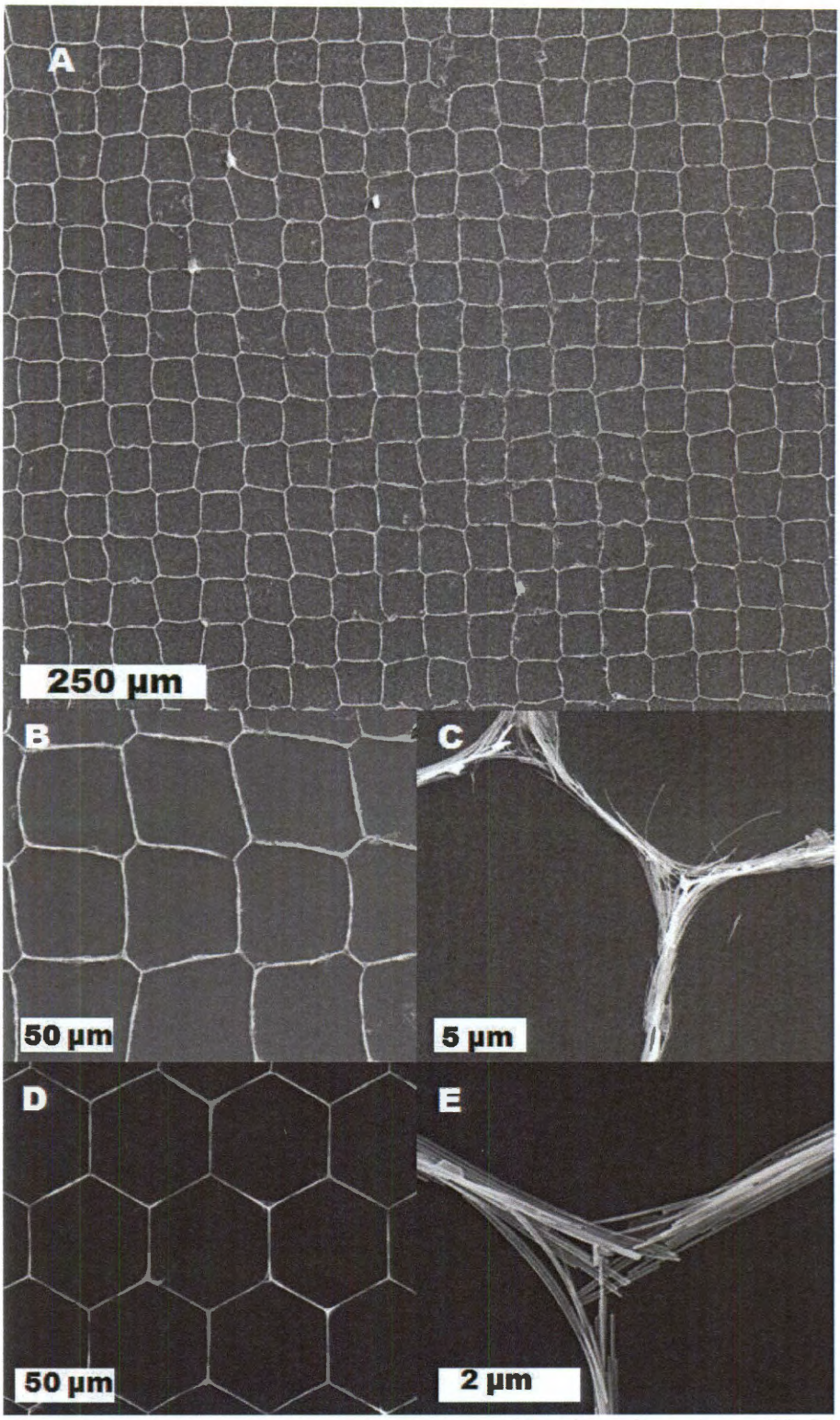

Figure 5.18 Low magnification (A) and high magnification (B and C) SEM images of AuNWs networks obtained from a TEM grid with square windows. Periodic network of AuNWs obtained from a TEM grid with hexagonal windows is shown in panels D and E.

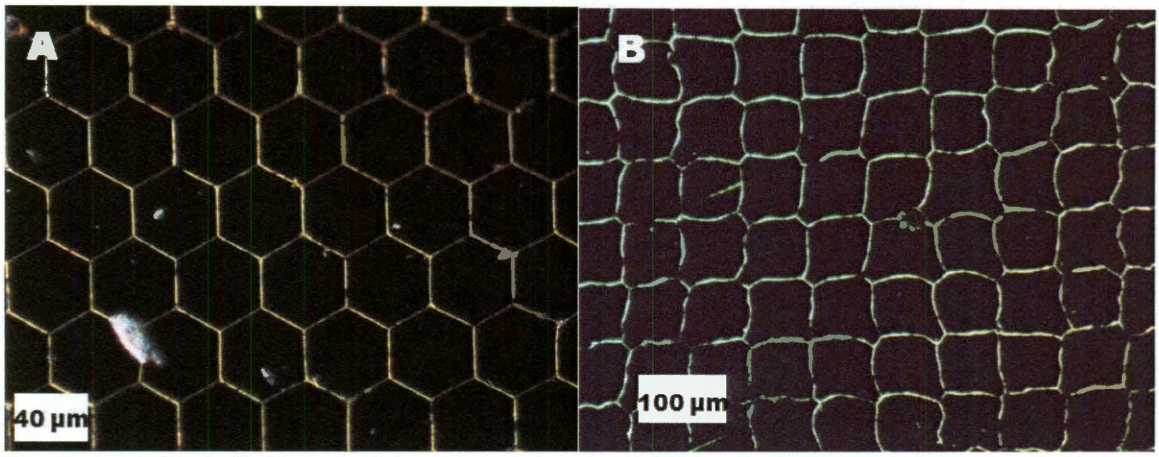

Figure 5.19 Dark field optical images of the assemblies obtained using hexagonal (A) and square (B) windows of TEM grids.

SEM imaging and optical microscopy (Fig. 5.19) clearly indicate that the periodic arrays of NW may be able to address the existing issues associated with transparent electrode fabrication. This network covers more than 1 mm^2 and it can be expected that the assembly can be extended up to many centimeters scale by using a larger template. Most importantly, high magnification SEM imaging showed that the NWs are well connected with each other. That will make this substrate highly conductive. Presence of voids in the network will ensure that the substrate maintain a high optical transparency value at all wavelengths. Our additional experiments show that the assembly proceeds in the same manner on conventional glass slides and quartz substrates. Additionally, structural robustness of gold nanowires may allow us to prepare these networks on flexible transparent substrates such as PDMS or polybutadiene elastomers.

5.2.7 Measurement of conductivity

To determine the average conductivity of the substrate, we carried out the assembly process on top of a silicon wafer, which was thermally coated with 100 nm thick silicon oxide layer. For the electrical measurements, the sample was first plasma

cleaned and then rinsed with organic solvents to remove any residual CTAB present of the surface of nanowires. The plasma treatment before the rinsing is critically important to maintain the structural integrity of these assemblies. For the electrical measurements we fabricated several electrodes by sputtering gold on top of the substrate using a 50 mesh TEM grid as a mask. The distance between two consecutive electrodes was 80 microns. Thhe conductivity was measured using a two-point probe system. The I-V curve obtained from this experiment is shown in Figure 5.20. The substrate was found to be highly conductive as it showed an average resistance of 75 ohms measure from the slope of the I-V curve.

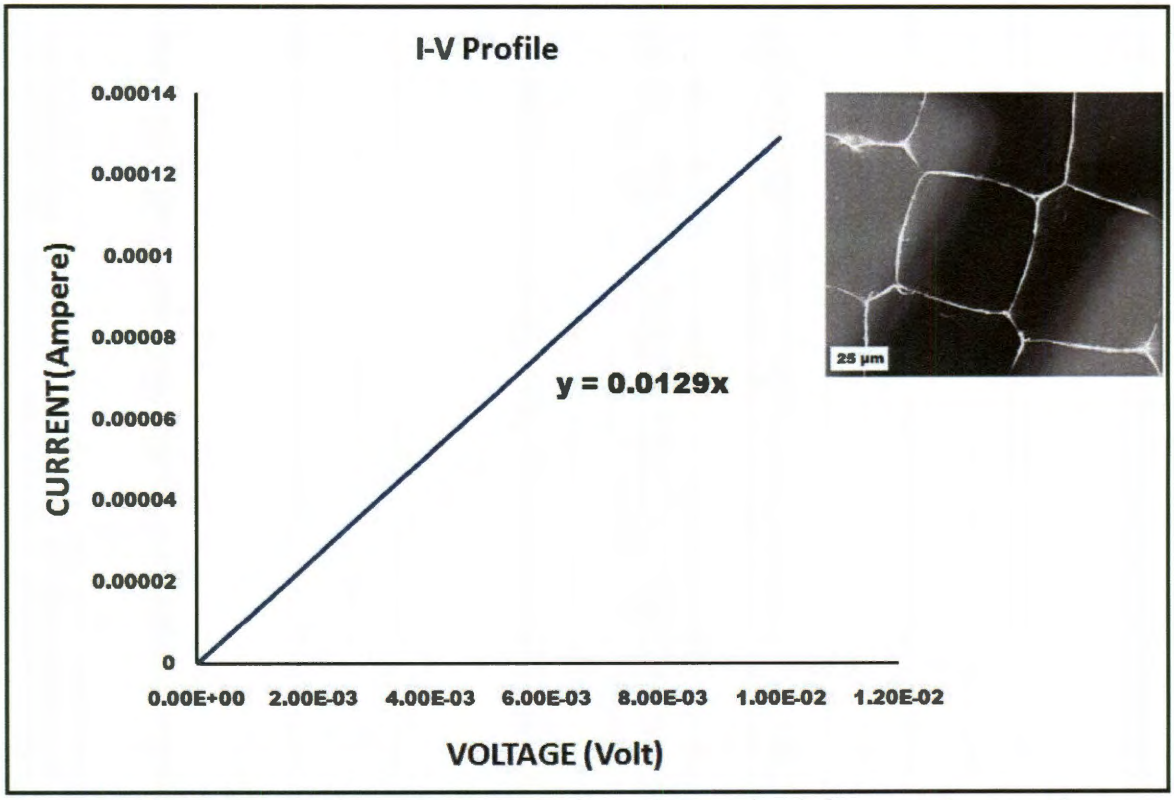

Figure 5.20 Average I-V curve obtained from the conductivity experiment using two point probe system. Gold electrodes connected by NW network (inset)

The low resistance of NW network confirms that they are indeed suitable candidate for the preparation of conductive electrodes. However, further investigation is

required to obtain sheet resistance and transparency data for these assemblies before they can be integrated into functional devices.

5.3 Conclusion

In summary, periodic arrays of anisotropic gold nanostructures are prepared by combining "top-down" and "bottom-up" techniques. The assembly process is highly selective and it was used to prepare a variety of self-assembled structures. In addition, ultra long metallic nanowires were used to prepare ordered 2D network. The controlled assembly of anisotropic nanostructures may offer an opportunity to create novel materials with unique optical and electronic properties.

5.4 Experimental Section

Unless otherwise stated, all the chemicals were purchased from commercial sources and they were used without any further purification. SEM imaging was done by FEI Quanta 400 ESEM FEG instrument in high vacuum mode. The mask making was carried out in Heidelberg DWL 66 laser writer using a 4 mm write head. Gold films were prepared by e-beam evaporator and sputter coater. Optical microscopy images were obtained in reflective mode on a Nikon microscope.

5.4.1 Pattern design by photolithography

The patterned substrate was designed by exposing a photoresist (Shipley S1813, Microchem Co.) coated silicon wafer to the UV laser light of mask maker instrument. Then, the exposed part of the resist was etched by immersing the wafer into the developer solution (Microchem MF 319) for 40 sec. The resulting substrate was checked by optical microscopy to confirm the complete etching of the resist at the exposed regions.

5.4.2 PDMS stamp design and microcontact printing

First, a patterned silicon wafer (master) was designed by optical lithography. The master was placed inside a Petri dish and 10:1 (w:w) mixture of PDMS pre-polymer (Sylgard 184, Dow Corning Corp.) and curing agent was poured on top of it and the resulting mixture was thoroughly mixed. Thee elastomer was degassed to remove the air bubbles and was cured at 70 $^{\circ}$C for 1 hour. Finally, the PDMS stamp was cut into square shape and carefully removed from the master.

A 0.002 M solution of 1-hexadecanethiol (HDT) was prepared by dissolving 25.8 mg of 1-hexadecanethiol in 50 mL anhydrous ethanol. Separately, 50 mL of 0.002 M solution of 16-mercaptohexadecanoic acid (MHDA) was prepared by dissolving 28.8 mg of MHDA in 50 mL of anhydrous ethanol. The PDMS stamp with imprinted photolithographic pattern was first dipped into MHDA solution. Then, the stamp was removed and ethanol was slowly dried by blowing nitrogen. Once dried, the stamp was pressed on top of a gold substrate and held there for 30 sec. The gold substrate was prepared by vapor deposition of 30 nm film of metallic gold on a glass slide. After the removal of the stamp, the gold substrate was dipped into the HDT solution and kept there for 40 sec. Finally, the substrate was rinsed thoroughly with pure ethanol to remove any residual thiol.

5.4.3 General procedure of self-assembly of CTAB-coated gold nanorods

Aqueous solution of gold nanorods were centrifuged once and redispersed in appropriate amount of DI water to make a stock solution (~1 mg/mL). For the self-assembly experiments, 40 μL of this solution was placed on top of the substrate. The substrate was either a lithographically patterned silicon wafer or a gold substrate having

periodic hydrophobic and hydrophilic SAMs of thiols. The substrate was kept in a humid atmosphere and the solvent was slowly dried. Once the drying was complete the substrate was first analyzed by optical microscopy and subsequently imaged by SEM.

5.4.4 Self-assembly of polystyrene-functionalized gold nanorods

Polystyrene-functionalized gold nanorods were prepared by two step procedure described elsewhere.[11] For the preparation of periodic arrays of rings, a patterned gold substrate was prepared by printing MHDA ink with a PDMS stamp having cylindrical pillars. Thus, the circular point of contacts became hydrophilic. Then the rest of the gold substrate was made hydrophobic by dipping it into 0.002 M solution of HDT. Then, the gold substrate was allowed to cool by placing it on top of an UV cuvette filled with ice-cold water. Breathing was undertaken to form a periodic array of water microdroplets on the gold surface. Immediately after that, a drop of methylene chloride solution of polystyrene-functionalized gold nanorods (0.5 mg/mL) was cast on top of the preformed array of water droplets. After methylene chloride evaporated, the gold substrate was warmed to room temperature to evaporate water microdroplets. The substrate was characterized by SEM and the formation of periodic arrays of rings was confirmed. The shape of the PDMS pillars was changed to obtain linear, trianglar, and square assemblies.

5.4.5 Self-assembly of PEG functionalized coated gold nanorods

The concentration of gold nanorods in the growth solution was roughly 0.22 mg/mL. Nine milliliters of this solution was centrifuged at 13,000 rpm for 10 min. The supernatant was carefully removed using a pipette and precipitate was redispersed in 0.5 mL of DI water. The resulting NR solution was treated with an aqueous solution of PEG-SH prepared by dissolving 10 mg of thiol-terminated PEG (MW 2000 g/mol) in 1.5 mL

DI water. After stirring the mixture at room temperature for 12 h, the solution was centrifuged at 13,000 rpm for 10 min. The supernatants were discarded and the precipitate was redispersed in pure THF and centrifuged again. This centrifugation and redispersion procedure was repeated five times to remove all the excess thiol and water. Finally, the precipitate was dissolved in 4 mL of methylene chloride and kept as 0.5 mg/mL stock solution.

5.4.6 Self-assembly of gold nanowires

CTAB capped high aspect ratio (~100) gold nanowires were synthesized by slow one dimensional growth of pentahedrally twinned gold nanorods.[27] The growth solution was kept at 27 °C for 12 hours to precipitate out the NWs from the solution. Then, the supernatant was carefully removed and the brown precipitate was washed two times with 0.1 M CTAB solution to remove excess of gold ions, ascorbic acid, and HCl. The purified NWs were re-dispersed in appropriate amount of DI water to make a stock solution (0.15 mg/mL). Gold TEM grid (SPI industries) having 400 mesh size (square or hexagonal) was used as the template for preparing periodic arrays of nanowires on a silicon substrate. About 8 μL of NW stock solution was placed at the center of the TEM grid. The grid was carefully removed from the tweezer and placed on top of a freshly cleaned silicon chip. The set up was placed inside a humid chamber and the water droplet was slowly dried. Once the drying was complete, TEM grid was carefully peeled off the substrate, which was subsequently cleaned by exposing it to oxygen plasma for 5 min. After, plasma cleaning the substrate was washed with chloroform to remove any residual CTAB.

5.4.7 Conductivity measurement of NW network

For the conductivity measurement it is required to prepare the assembly on an insulating substrate. Therefore, we carried out the assembly process on a silicon wafer which is thermally coated with insulating silicon oxide (100 nm thick). After plasma cleaning, the substrate was rinsed several times with chloroform to remove residual CTAB. We used a TEM grid (50 mesh size) as a mask to design the electrodes. The TEM grid was fixed on top the pre-formed NW network and 100 nm of gold was sputtered. The gird was then removed and the conductivity was measured using a two point probe using sweeping voltage from 0 mV to 1.2 mV.

References

(1) Murray, C. B.; Kagan, C. R.; Bawendi, M. G. *Science* **1995**, *270,* 1335.

(2) Motte, L.; Billoudet, F.; Lacaze, E.; Pileni, M. P. *Adv. Mater.* **1996**, *8*, 1018.

(3) Whitesides, G. M.; Grzybowski, B. *Science* **2002**, *295*, 2418.

(4) Schmitt, J.; Decher, G.; Dressick, W. J.; Brandow, S. L.; Geer, R. E.; Shashidar, R.; Calvert, J. M. *Adv. Mater.* **1997**, *9*, 61.

(5) Grzybowski, B. A.; Wilmer, C. E.; Kim, J.; Browne, K. P.; Bishop, K. J. M. *Soft Matter* **2009**, *5*, 1110

(6) Alivisatos, A. P.; Johnsson, K. P.; Peng, X.; Wilson, T. E.; Loweth, C. J.; Bruchez, M. P., Jr.; Schultz, P. G. *Nature* **1996**, *382*, 609.

(7) Li, M.; Schnablegger, H.; Mann, S. *Nature* **1999**, *402*, 393.

(8) Velev, O. *Science* **2006**, *312*, 376.

(9) Kalsin, A.; Fialkowski, M.; Paszewski, M.; Smoukov, S. K.; Bishop, K. J. M.; Grzybowski, B. A. *Science* **2006,** *312*, 420.

(10) Zubarev, E. R.; Xu, J.; Sayyad, A.; Gibson, J. D. *J. Am. Chem. Soc.* **2006**, *128*, 15098.

(11) Khanal, B. P.; Zubarev, E. R. *Angew. Chem. Int. Ed.* **2007**, *46*, 2195.

(12) Li, F.; Josephson, D. P.; Stein, A. *Angew. Chem. Int. Ed.* **2011**, *50*, 360.

(13) Ozin, G. A.; Hou, K.; Lotsch, B. V.; Cademartiri, L.; Puzzo, D. P.; Scotognella, F.; Ghadimi, A. Thomson, J. *Mater. Today* **2009**, *12*, 12.

(14) Mirkin, C. A.; Letsinger, R. L.; Mucic, R. C.; Storhoff, J. J. *Nature* **1996**, *382,* 607.

(15) Mirkin, C. A. *Inorg. Chem.* **2000**, *39*, 2258.

(16) Boal, A. K.; Ilhan, F.; DeRouchey, J. E.; Thurn-Albrecht, T.; Russell, T. P.; Rotello, V. M. *Nature* **2000**, *404*, 746.

(17) Heath, J. R.; Knobler, C. M.; Leff, D. V. *J. Phys. Chem. B* **1997**, *101*, 189.

(18) Ming, T.; Kou, X.; Chen, H.; Wang, T.; Tam, H.-L.; Cheah,, K.-W .; Chen,, J,-Y.; Wang, J. *Angew. Chem. Int. Ed.* **2008**, *120*, 9831.

(19) Nikoobakht, B.; El-Sayed, M. A. *Chem. Mater.* **2003**, *15*, 1957.

(20) Jana, N. R.; Gearheart, L.; Murphy, C. J. *J. Phys. Chem. B* **2001**, *105*, 4065.

(21) Wu, H.-Y.; Wan-Ling Huang, W.-L.; Huang, M. H. *Cryst. Growth Des.* **2007**, *7*, 831.

(22) Wu, H.-Y.; Chu, H.-C.; Kuo, T.-J.; Kuo, C.-L.; Huang, M. H. *Chem. Mater.* **2005**, *17*, 6447.

(23) Wei, Z.; Mieszawska, A. J.; Zamborini, F. P. *Langmuir* **2004**, *20*, 4322.

(24) Khanal, B. P.; Zubarev, E. R. *J. Am. Chem. Soc.* **2008**, *130*, 12634.

(25) Lu, X.; Yavuz, M. S.; Tuan, H.-Y.; Korgel, B. A.; Xia, Y. N. *J. Am. Chem. Soc.* **2008**, *130*, 8900.

(26) Pazos-Perez, N.; Baranov, D.; Irsen, S.; Hilgendorff, M.; Liz-Marzan, L. M.; Giersig, M. *Langmuir* **2008**, *24*, 9855.

(27) Critchley, K.; Khanal, B. P.; Gorzny, M. L.; Vigderman, L.; Evans, S. D.; Zubarev, E. R.; Kotov, N. A. *Adv. Mater.* **2010**, *22*, 2338.

(28) Solis, D.; Chang, W.-S.; Khanal, B. P.; Bao, K.; Nordlander, P.; Zubarev, E. R.; Link, S. *Nano. Lett.* **2010**, *10*, 3482.

(29) Xiang, C.; Kim, J. Y.; Penner, R. M. *Nano Lett.* **2009**, *9*, 2133.

(30) Kim, F.; Sohn, K.; Wu, J.; Huang, J. *J. Am. Chem. Soc.* **2008**, *130*, 14442.

(31) Wang, H.F.; Huff, T.B.; Zweifel, D.A.; He, W.; Low, P. S; Wei, A.; Cheng, J. X. *Proc. Natl. Acad. Sci. USA*. **2005**, *102*, 15752.

(32) Durr, N. J.; Larson, T.; Smith, D. K.; Korgel, B. A.; Sokolov, K., Ben-Yakar, A. *Nano Lett.* **2007**, *7*, 941.

(33) Qiu, L.; Larson, T. A.; Vitkin, E.; Guo, L.; Hanlon, E. B.; Itzkan, I.; Sokolov, K.; Perelman, L. T. *Biomed Opt. Exp.* **2010**, *1*, 135.

(34) Ding, H.; Yong, K.-T.; Roy, I.; Pudavar, H. E.; Law, W.C.; Bergey, E. J.; Prasad, P. N. *J. Phys. Chem. C* **2007**, *111*, 12552

(35) Nehl, C. L.; Liao H.; Hafner, J. H. *Nano Lett.* **2006**, *6*, 683.

(36) Hu, M.; Chen, J. Y.; Li, Z. Y.; Au, L.; Hartland, G. V.; Li, X. D.; Marquez, M.; Xia, Y. N. *Chem. Soc. Rev.* **2006**, *35*, 1084.

(37) Jain, P. K.; El-Sayed, M. A. *Nano Lett.* **2008**, *8*, 4347.

(38) Castellana, E. T.; Gamez, C. R.; Gomez, M. E.; Russell, D. H. *Langmuir* **2010**, *26*, 6066.

(39) Yu, C.; Irudayaraj, J. *Anal. Chem.* **2007**, *79*, 572.

(40) Sudeep, P. K.; Joseph, S. T. S.; Thomas, K. G. *J. Am. Chem. Soc.* **2005**, *127*, 6516.

(41) Sanders, A. W.; Routenberg, D. A.; Wiley, B. J.; Xia, Y.; Dufresne, E. R. and Reed, M. A. *Nano Lett.* **2006**, 6, 1822.

(42) De, S.; Higgins, T, M; Lyons, P. E.; Doherty, E. M.; Nirmalraj, P. N.; Blau, W. J.; Boland, J. J.; Coleman, J. N. *ACS Nano* **2009**, 3, 1767.

(43) Madaria, A. R.; Kumar, A.; Zhou, C. *Nanotechnology* **2011**, *22*, 245201.

(44) Yu, Z.; Zhang, Q.; Li, L.; Chen, Q.; Niu, X.; Liu, J.; Pei, Q. *Adv. Mater.* **2010**, *5*, 664.

(45) Madaria, A. R.; Kumar, A.; Ishikawa, F. N.; Zhou, C. *Nano. Res.* **2010**, *3*, 564.

(46) Jung, Y.; J.; Kar, S.; Talapatra, S.; Soldano, C.; Viswanathan, G.; Li, X.; Yao, Z.; Ou, F. S.; Avadhanula, A.; Vajtai, R.; Curran, S.; Nalamasu, O.; Ajayan, P. M. *Nano Lett.* **2006**, 6, 413.

(47) Tsai, J. T. H.; Hwang, H, -L. *J. Disp. Tech.* **2009**, *5*, 232.

(48) McAlpine, M. C.; Friedman, R. S.; Lieber, C. M. *Proc. IEEE* **2005**, *93*, 1357.

(49) Ma, D. D. D.; Lee, C. S.; Lifshitz, Y.; Lee, S. T. *Appl. Phys. Lett.* **2002**, *81*, 3233

(50) Agarwal, R.; Ladavac, K.; Roichman, Y.; Yu, G.; Lieber, C.M.; Grier, D. G. *Opt. Express* **2005** *13*, 8906.

(51) Mokkapati, S.; Beck, F. J.; Polman , A.; Catchpole. A. *Appl. Phys. Lett.* **2009**, *95*, 053115.

(52) Rybczynski, J.; Banerjee, D.; Kosiorek, A.; Giersig, M.; Ren, Z. F. *Nano Lett.* **2004**, *4*, 2037.

(53) Zhang, X.; Liu, D.; Zhang, L.; Li, W.; Gao, M.; Ren, Y.; Zeng, Q.; Niu, Z.; Zhou, W.; Xie, S. *J. Mater. Chem.* **2009**, 19, 962.

(54) Yin, Y.; Lu, Yu.; Gates, B.; Xia, Y.; *J. Am. Chem. Soc.* **2001,** *123,* 8718.

(55) Nagle, L.; Fitzmaurice, D.; *Adv. Mater.* **2003**, *15*, 933.

(56) Wang, D.; Mohwald, H. *J. Mater. Chem.* **2004**, *14*, 459.

(57) Wang, D.; Salgueirino-Maceria, V, Liz-Marzan, L. M.; Caruso, F. *Adv. Mater.*, **2002**, *14*, 908.

(58) Zheng, H.; Rubner, M. F.; Hammond, P.T.; *Langmuir* **2002**, *18*, 4505.

(59) Hwang, H.; Park, Y. -H. Park, J. -K. *Langmuir* **2009**, *25*, 6010.

(60) Schaak, R. E.; Cable, R. E.; Leonard, B. M.; Norris, B. C. *Langmuir* **2004**, *20*, 7293.

(61) Rycenga, M, Camargo, P. H. C.; Xia, Y. *Soft Mater.* **2009**, *5*, 1129.

(62) Khanh, N. N.; Yoon, K. B. *J. Am. Chem. Soc.* **2009,** *131,* 14228.

(63) Xia, Y.; Whitesides, G. M. *Angew. Chem. Int. Ed. Engl.* **1998**, *37*, 550-575.

(64) Santhanam, V.; Andres, R. P. *Nano Lett.* **2004**, 4, 41.

(65) Kinge, S.; Crego-Calama, M.; Reinhoudt, D. N. *ChemPhysChem*, **2008**, *9*, 20.

(66) Zhang, Li, Si, H. –Y, Zhang, H. –L.; *J. Mater Chem.* **2008**, *18*, 2660.

(67) Lu, G.; Li, W.; Yao, J.; Zhang, G.; Yang, B.; Shen, J. *Adv. Mater.* **2002**, *14*, 1049.

(68) Zhang, X.; Imae, T. *J. Phys. Chem. C* **2009,** *113,* 5947.

(69) Kuemin, C.; Tutz, R.; Spencer, N .D.; Wolf, H.; *Langmuir* **2011**, *27*, 6305.

(70) Zareie, m. H.; Xu, X.; Cortie, M. B.; *Small* **2007**, *3*, 139.

(71) Schmidt-Mende, L.; Fechtenkotter, A.; Mullen, K.; Moons, E.; Friend, R. H.; MacKenzie, J. D. *Science* **2001**, *293*, 5532.

(72) Bach, U.; Lupo, D.; Comte, P.; Moser, J. E.; Weissortel, F.; Salbeck, J.; Spreitzer, H.; Gratzel, M. *Nature* **1998**, *395*, 583.

(73) Wang, X.; Zhi, L.; Mullen, K. *Nano Lett.* **2008**, *8*, 323

(74) Chien, Y.; Lefevre, F.; Shih, I.; Izquierdo, R. *Nanotechnology*, **2010**, *21*, 134020.

(75) Granqvist, C. G.; Hultaker, A. *Thin Solid films* **2002**, *411*, 1.

(76) Dawar, A. L.; Joshi, J. C. *J. Mater. Sci.* **1984**, *19*, 1

(77) Li, X.; Zhu, Y.; Cai, W.; Boryslak, M.; Han, B.; Chen, D.; Piner, R. D.; Colombo, L.; Ruoff, R. S. *Nano Lett.* **2009**, *9*, 4359.

(78) Hecht, D. S.; Hu, L.; Irvin, G. *Adv. Mater.* **2011**, *23*, 1482

Chapter VI

Synthesis of Hybrid Gold on Cadmium Sulfide Nanostructures

6.1 Introduction

Controlled synthesis of anisotropic metallic and semiconductor nanostructures has opened avenues for the preparation of novel materials that have widespread applications in biomedical science and photovoltaic devices.[1-26] In addition to single material nanostructures, synthesis of multicomponent nanostructures is also an important task as it offers the preparation of materials that have distinctly different properties from individual components.[27,28] There are numerous reports in the literature highlighting synthesis of multicomponent hybrid core-shell materials by chemical combination of two or more different nanostructures.[28-34] There are also several examples describing selective growth of metals on semiconductor nanorods and tetrapods.[35-39] Such hybrid structures allow for the coupling of optical and electronic properties of metals and semiconductors. Electronic interaction between metal and semiconductor may result in the change of plasmon resonance of the metal or change in the photoluminescence of the semiconductor.[40] In addition, these hybrids can be self-assembled by selectively functionalizing metal sites.[35] Although deposition of metals on semiconductor nanorods and tetrapods is previously reported,[35-39] there are no examples for the preparation of ultra long metal-semiconductor hybrid nanowires. If created, these structures may find applications in solar energy storage[23] and photocatalysis.[41] Additionally, CdS nanowires can be used as a platform to organize small gold nanoparticles into one dimensional arrays which measure several microns in length.

In this chapter, we describe an efficient synthetic route for the preparation of ultra long cadmium sulfide (CdS) nanowires. These nanowires are coated with a hydrophobic ligand trioctylphosphine oxide (TOPO) and they are soluble in organic solvents like toluene and chloroform. In addition, we also developed a method for the synthesis of hybrid gold on CdS nanowires by uniform deposition of small gold nanoparticles on top of pre-synthesized nanowires. This deposition of gold does not depend on the aspect ratio of CdS structures as we were able to achieve uniform deposition on CdS nanorods with different aspect ratios.

6.2 Results and Discussion

6.2.1 Synthesis of CdS nanowires

Solvothermal synthesis of anisotropic CdS nanorods is generally carried out by reacting stoichiometric amount of sulfur with cadmium-octadecylphosphonic acid (Cd-ODPA) complex prepared by heating a mixture of cadmium oxide, ODPA, and triocylphosphonine oxide (TOPO).[5] The width of nanorods produced by this method is ~5 nm while their length is around 100 nm. Controlling the width around 5 nm is critically important for getting efficient quantum confinement effect.[2,11] Quantum confinement effect (QCE) leads to the blue shift of the absorption peak. Due to QCE, CdS nanostructures having width below 5 nm are greenish-yellow in color as opposed to the bright yellow color of their bulk analogue. However, it is also important to control the length of these nanostructures for certain optical and electronic applications. For that purpose, it is desirable to produce extremely high aspect ratio CdS nanostructures i.e. CdS nanowires. Continuous growth of CdS nanorods by adding additional amount of sulfur precursor in the growth solution often results in the formation of thick and

branched structures. Our systematic investigation showed that when the growth solution was kept without stirring after the introduction of sulfur precursor, ultra long CdS nanowires are produced instead of short rods (Figure 6.1). Rapid addition of sulfur-trioctylphosphine complex into Cd-ODPA complex generates millions of small CdS particles (nucleation sites) which are subsequently converted to CdS nanowires via continuous one dimensional growth. Remarkably, the width of the nanowires remains constant at 5 nm, whereas their length increases several times. These nanowires measure several microns in length with an aspect ratio of ca. 200. In stark contrast, when the exact same growth solution is stirred, only CdS nanorods having aspect ratio ca. 30 are produced (Figure 6.1D). TEM images of CdS nanowires also show that they have strong propensity to form bundles which is a common phenomenon for any high aspect ratio structures.

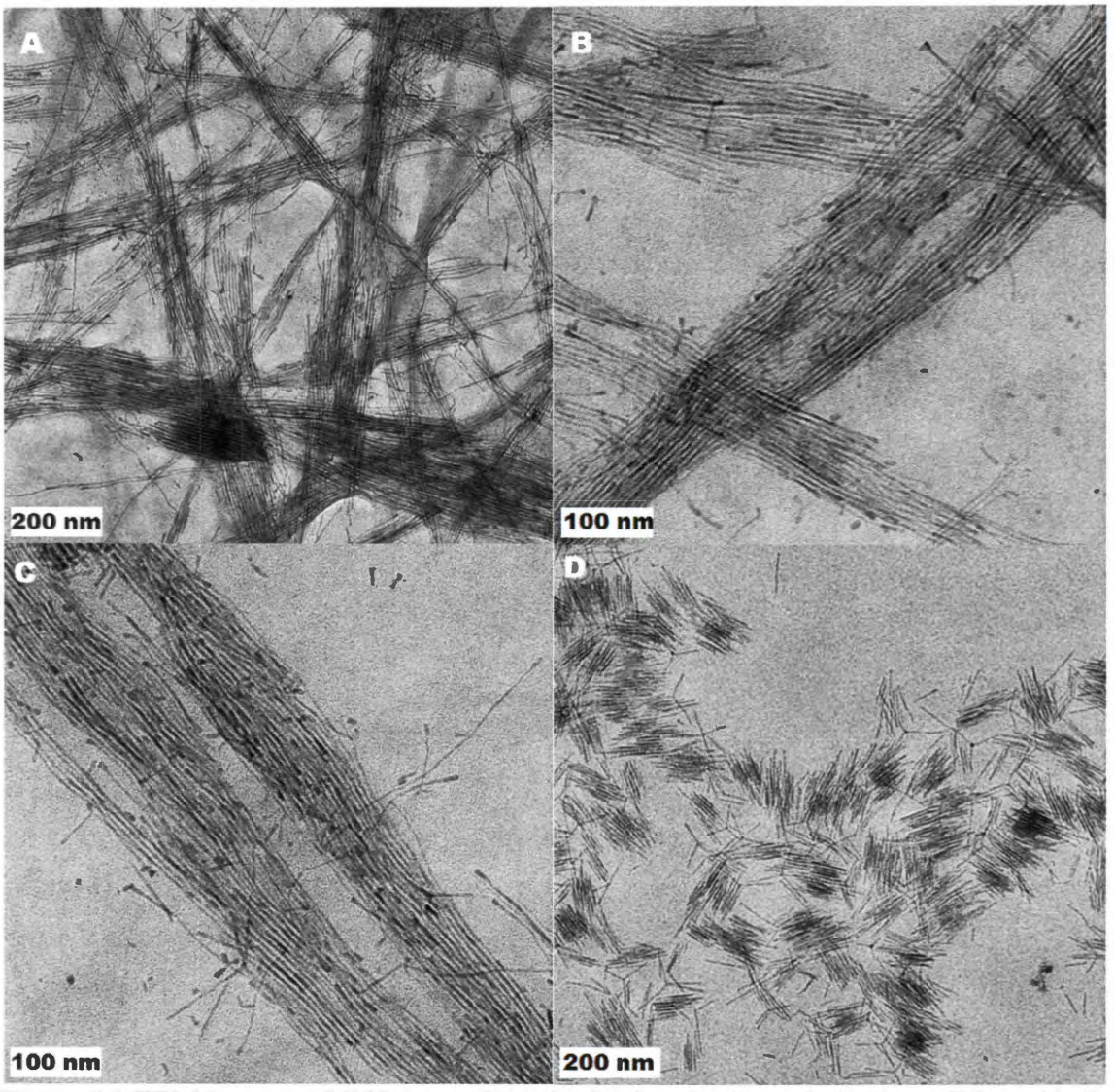

Figure 6.1 TEM images of CdS nanowires obtained under "no stirring" conditions (A, B, and C). CdS nanorods (D) are formed when the same growth solution is vigorously stirred.

In order to prove that the formation of high aspect ratio structures can be induced without stirring the reaction mixture, we explored another synthetic route developed by Korgel and co-workers.[7] In this synthesis, monodisperse CdS nanorods having aspect ratio ca. 15 are produced using tetradecylphosphonic acid (TDPA) instead of ODPA (Figure 6.2A). However, when we performed the same reaction under "no stirring" conditions, high aspect ratio CdS nanowires were formed (Figure 6.2B). These structures

were not well-defined and they contained multiple branches. Nonetheless, this experiment clearly proved that high aspect ratio structures can be prepared without stirring the reaction mixture during the growth.

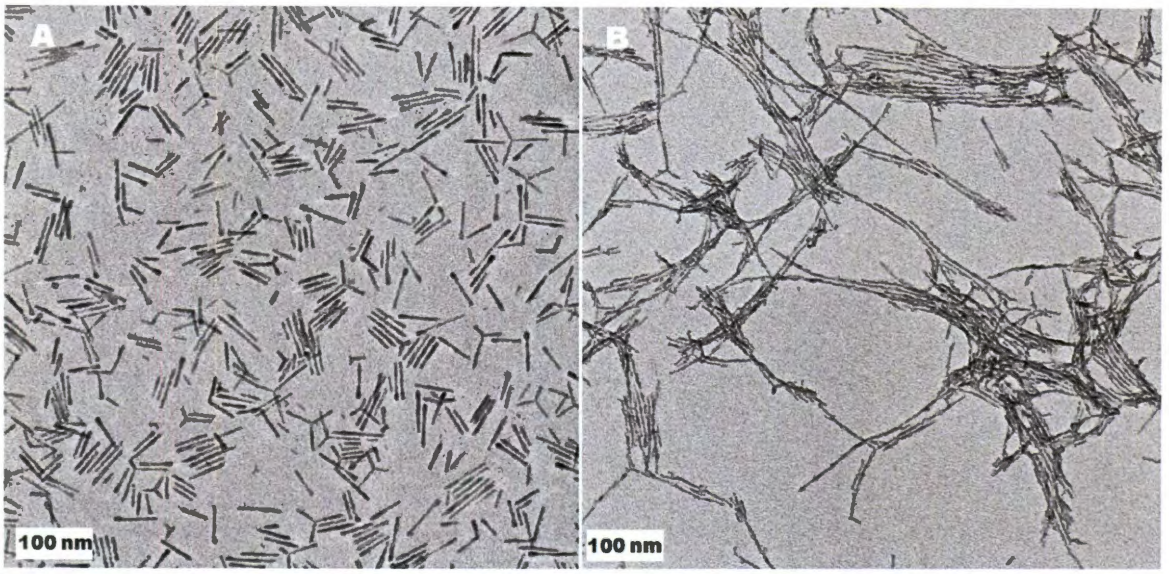

Figure 6.2 CdS nanostructures produced with stirring (A) and without stirring (B) of the growth solution.

We hypothesize that the formation of nanowires and nanorods is governed by the number of nucleation sites formed during the initial stage. The nucleation sites are small spherical CdS particles with well defined crystal facets. Under "no-stirring" conditions, the rate of diffusion of sulfur-trioctylphosphine (S-TOP) complex is low because of the high viscosity of the reaction mixture. For that reason, fewer nucleation sites were converted to CdS nanowires by continuous anisotropic growth. On the other hand, under "stirring" condition, S-TOP solution was instantly mixed with the reaction mixture and made all the nucleation sites readily available for the growth and subsequent conversion to relatively short nanorods (Figure 6.3). In addition, alkylphosphonic acids might play critical role in the formation of nanowires. It is a well-known fact that the anisotropic growth of semiconductor nanostructures is governed by the preferential attachment of

alkylphosphonic acid to certain crystal facets.[42] The ratio between linear and branched structures depends on the chain length of the alkylphosphonic acid. When the synthesis is carried out in the presence of a short phosphonic acid, a higher amount of branched structures is produced.[43] This explains the formation of branched CdS nanostructures when TDPA is used instead of ODPA.

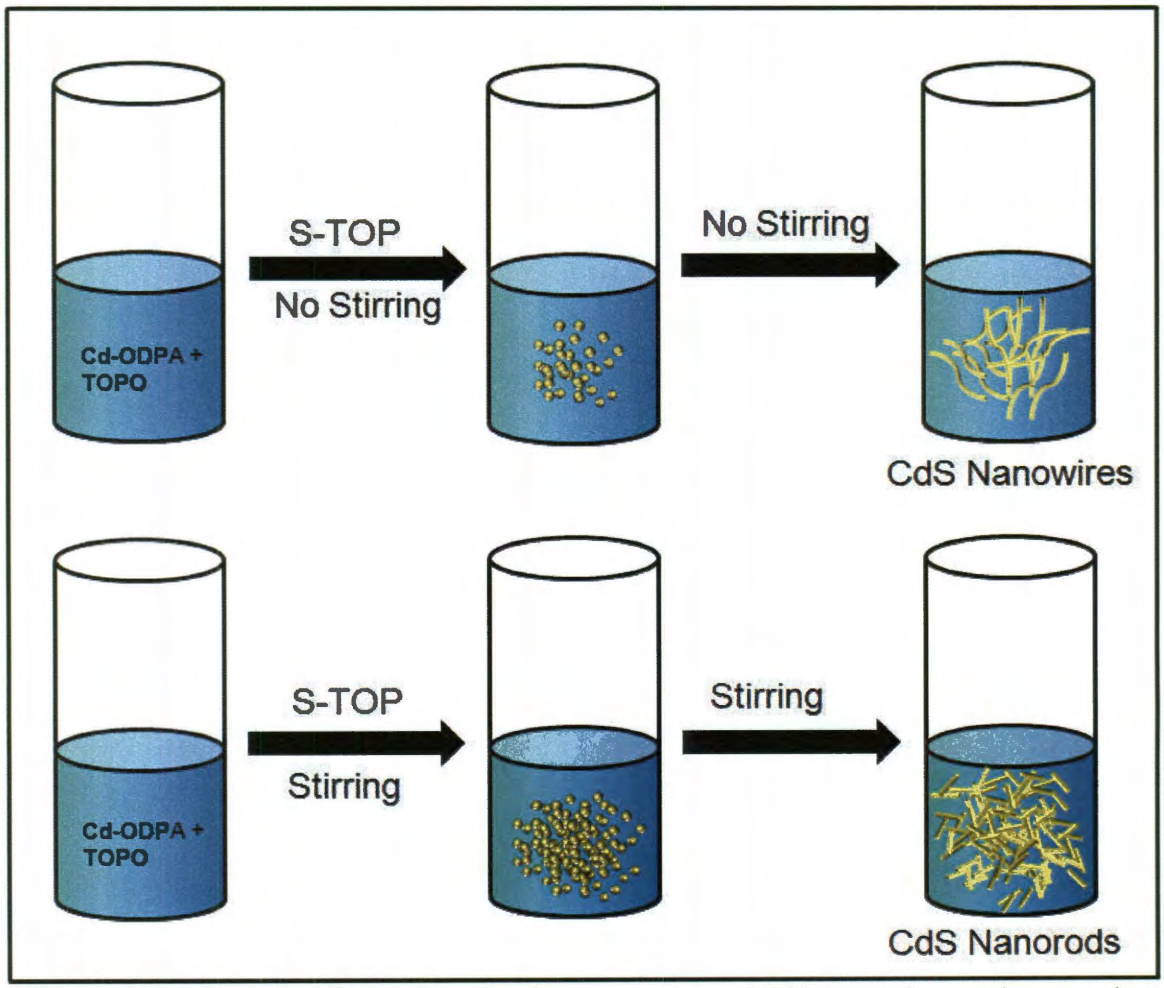

Figure 6.3 Schematic illustrations for the preparation of CdS nanowires and nanorods

6.2.2 Optical properties of CdS nanowires

We also measured basic optical properties of CdS nanowires in order to confirm their structural monodispersity. The absorption peak at 450 nm corresponds to the excitonic transition and the value is consistent with the previous reports (Figure 6.4A).[36]

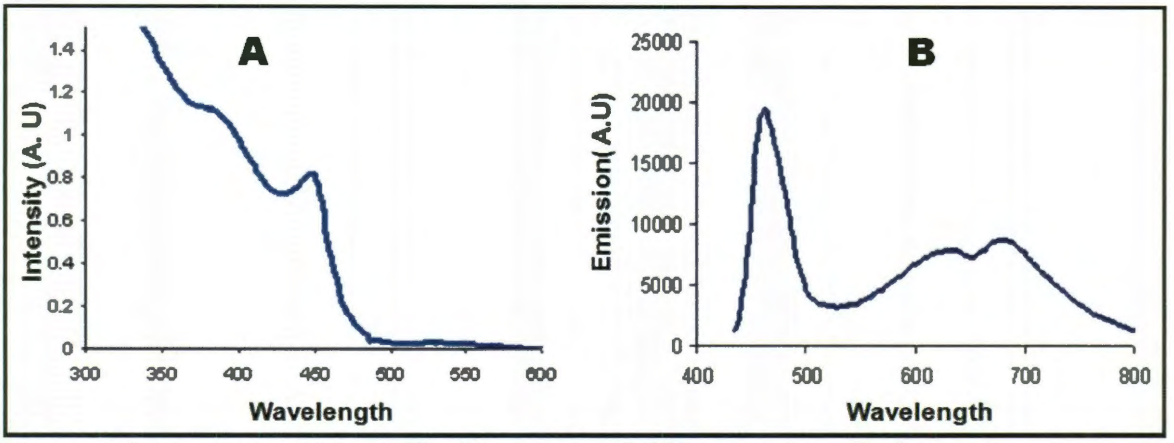

Figure 6.4 Absorption (A) and PL (B) spectra of CdS nanowires. Both spectra were recorded from the toluene solution of the nanowires.

The photoluminescence (PL) spectrum shows a sharp band-edge emission peak at 463 nm (Figure 6.4 B). The sharpness of the band-edge peak indicates that the width of the nanowires is tightly controlled during their anisotropic growth. The lower energy peaks (630 nm and 690 nm) indicate the formation of trap states that are generated because of the structural defects in the nanostructures. However, we did not find any significant difference in the absorbance and PL of CdS nanorods and nanowires. This is expected as the optical properties of anisotropic semiconductors are known to depend only on the width of the nanostructures. Both PL and absorbance data suggests that the diameter of CdS NWs is between 4.6 nm and 5.3 nm, which is consistent with microscopy imaging.

6.2.3 Synthesis of hybrid CdS-Au nanowires

Hybrid CdS-Au nanostructures are generally prepared by the reduction of gold ions by dodecylamine (DDA) on top of the pre-synthesized CdS nanostructures in the presence of surfactant didecyldimethylammoinium bromide (DDAB). Dodecylamine not only acts as a reducing agent, but also promotes controlled deposition of gold by creating multiple defect sites on CdS nanocrystals via chemical etching.[35,36] There are several reports in the literature describing the preparation of hybrid CdS-Au nanorods.[35, 36] However, there are no reports on selective deposition of gold on top of long CdS nanowires which is due to the difficulties associated with the preparation of monodisperse CdS nanowires. We observed that controlled deposition of metallic gold can be obtained by treating CdS nanowires with $AuCl_3$ in the presence of DDA and CTAB (Figure 6.5). The size of the gold particles depends highly on the reaction time. Small gold nanoparticles (~ 3 nm) are formed during the initial stage of the reaction. When the reaction mixture is stirred for 24 hours, these small gold nanoparticles undergo Oswald ripening to form larger particles. Formation of larger particles can also be visually observed as the color of nanostructures solution gradually changes from brown to red. As smaller nanoparticles are suitable for catalysis, it is important to maintain particle size below 3 nm for studying catalytic activity of such hybrid materials. We found that when minimal amount of DDA is used for the reaction, the formation of larger particles is significantly reduced. Deposition of metallic gold can also be monitored by measuring PL intensity. Metal deposition results in the rapid quenching of PL of CdS nanowires. We were also able to demonstrate that the deposition of metallic gold does not depend on the aspect ratio of the nanostructures (Figure 6.6 and Figure 6.7).

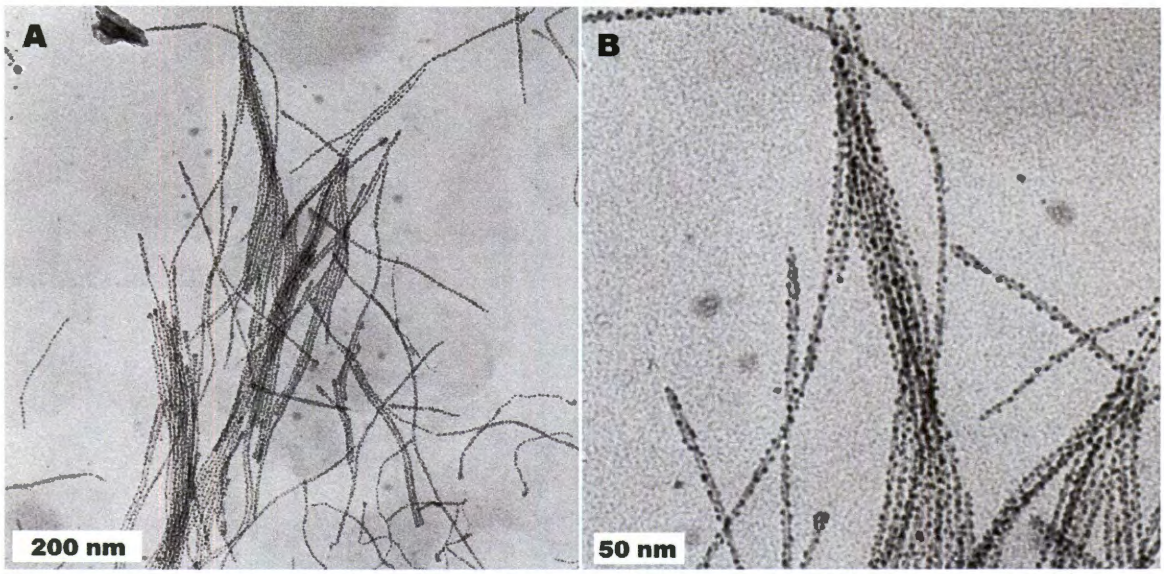

Figure 6.5 Low magnification (A) and high magnification (B) TEM images of CdS-Au nanowires obtained by reducing the concentration of DDA

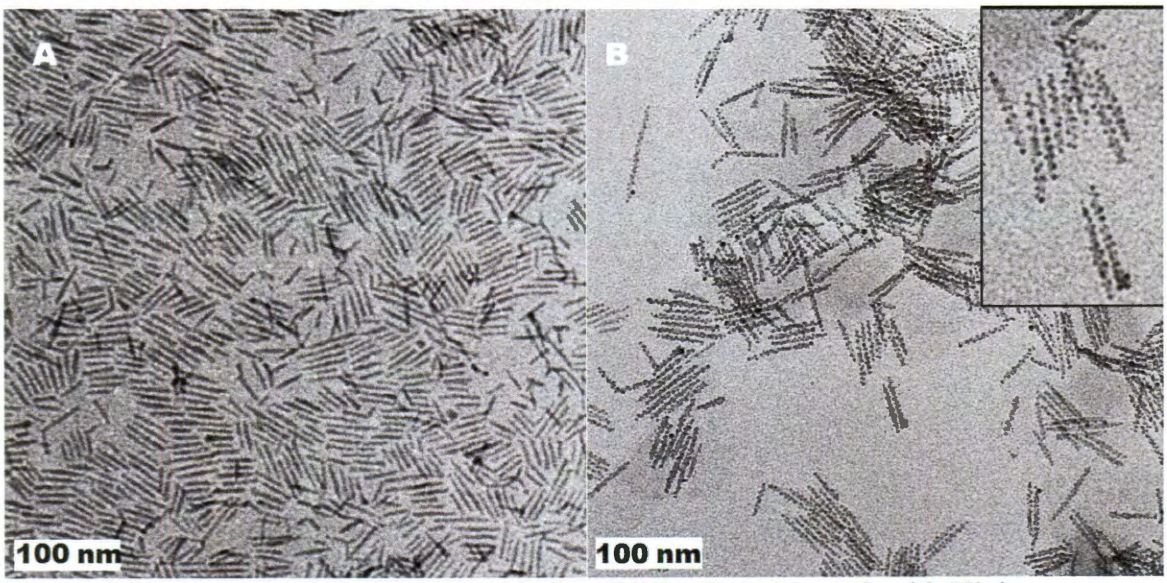

Figure 6.6 CdS nanorods before (A) and after (B) the deposition of gold. High magnification image is shown in the inset.

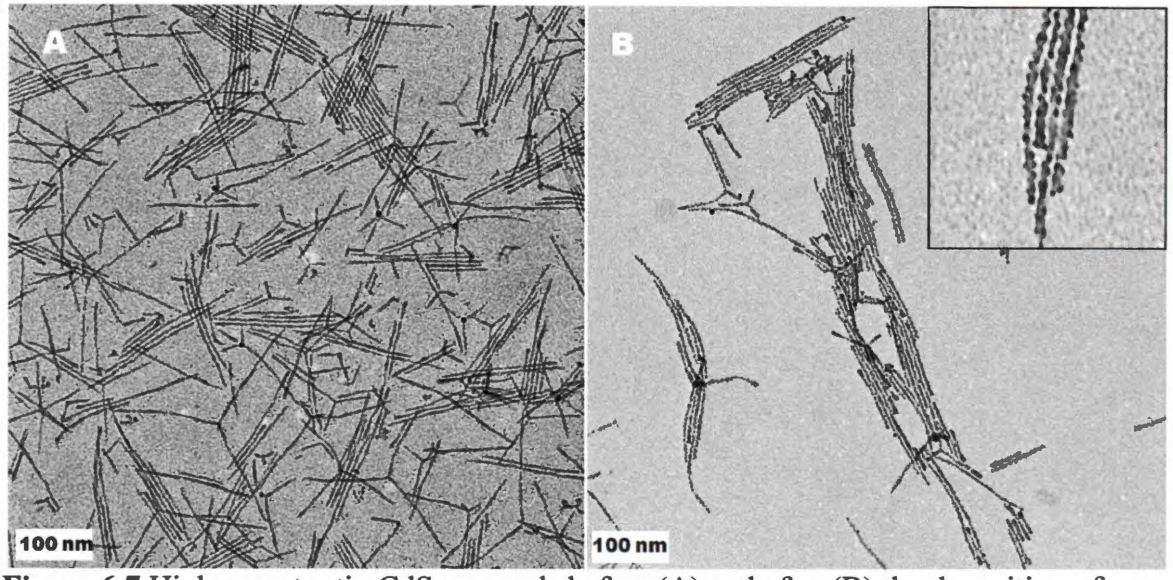

Figure 6.7 High aspect ratio CdS nanorods before (A) and after (B) the deposition of gold. High magnification image is shown in the inset.

We performed high resolution TEM imaging to determine the crystal structure of the hybrid Au-CdS nanorods. HRTEM images clearly show well-defined lattice fringes of CdS nanowires (Figure 6.8). The measured interplanar distance is 3.6 Å which is consistent with d_{002} spacing for hexagonal wurtzite structure of cadmium sulfide (Figures 6.8C and 6.8D).[44] This is an important observation as it proves that wurtzite structure is preserved during the one-dimensional growth of nanowires. In addition, we were also able to confirm the FCC crystal structure of the deposited gold particles by measuring the distance between lattice fringes (d_{111} is 2.5 Å). HRTEM images proved that the average diameter of gold particles is below 3 nm which is critically important for their application in catalysis.

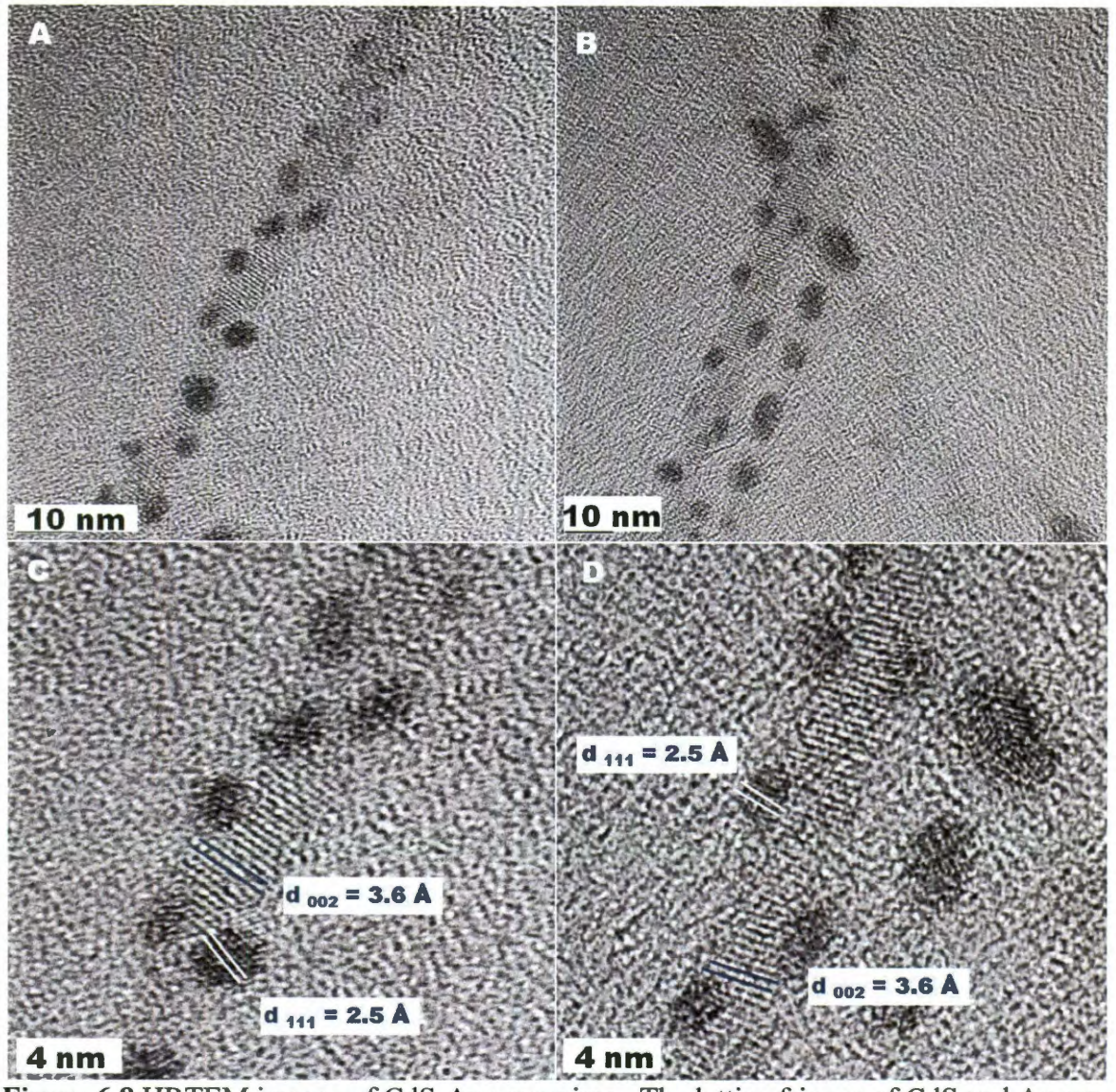

Figure 6.8 HRTEM images of CdS-Au nanowires. The lattice fringes of CdS and Au are shown in Figure 6.6C and 6.6D.

The mechanism of gold deposition on CdS nanowires is similar to that observed on CdS nanorods.[36] CdS nanowires have wurtzite crystal structure which is not centrosymetric. One side of the nanowires is terminated with sulfur atoms, whereas the other side is cadmium-terminated. Additionally, in the presence of atmospheric oxygen, DDA and CTAB cause rapid etching of cadmium ions from the crystal facets of the NWs and sulfur is exposed in the etched region. Gold ions present in the growth solution are

strongly attracted towards the sulfur-rich sites because of the covalent nature of gold-sulfur bond. That results in the selective deposition and growth of gold in the sulfur rich sites.

6.3 Conclusion

In summary, ultra long CdS nanowires were prepared by carrying out their growth under "no stirring" conditions. These nanowires preserved their crystal structure during one dimensional growth. Hybrid CdS-Au nanostructures were also produced by controlled deposition of metallic gold on pre-synthesized CdS nanowires and nanorods. These hybrid materials may have useful application in photocatalysis and solar cells.

6.4 Experimental Section

Trioctylphosphine oxide (TOPO), cadmium oxide, sulfur, trioctylphosphine (TOP), gold chloride ($AuCl_3$), cetyltrimethylammonium bromide (CTAB), didoceyldimethylammonium bromide (DDAB), and dodecylamine (DDA) were purchased from Aldrich Chemical Co. Tetradeylphosphonic acid (TDPA) and octadecylphosphonic acid (ODPA) were purchased from Alfa-Aesar. Unless otherwise stated, all chemicals were used without any further purification. ^{1}HNMR spectra were recorded from CD_2Cl_2 or $CDCl_3$ solutions on Bruker 400 MHz spectrometer. TEM imaging was done using JEOL 1230 high contrast microscope operating at 100 KV accelerating voltage. High resolution TEM imaging was performed using JEOL 2100 field emission gun transmission electron microscope. TEM samples were prepared by dipping a carbon-coated copper grid into the toluene or chloroform solution of nanoparticles.

6.4.1 Synthesis of CdS nanowires

In a three-neck flask, 205 mg of CdO was mixed with 2.73 g of TOPO and 1.1 g of ODPA. Separately, a sulfur solution was prepared by dissolving 48 mg of sulfur in 600 μL of degassed TOP. The mixture in the three- neck flask was heated to 100 °C to melt the solids and subsequently degassed for 45 min. Under vigorous stirring, the mixture was rapidly heated to 310 °C to form Cd-ODPA complex as indicated by the color change from dark red to clear and colorless. The temperature was lowered to 300 °C and S-TOP solution was rapidly injected in the reaction mixture. The stirring was stopped and the solution was kept undisturbed at 300 °C for 30 min to complete the growth of CdS nanowires. Once the growth was complete, the reaction mixture was dissolved in 6 mL of toluene and nanowires were precipitated by adding excess methanol. The precipitate was washed several times with acetone and methanol. The final product was dissolved in toluene and characterized by TEM.

6.4.2 Synthesis of short CdS nanorods (60 x 5 nm)

CdS nanorods having aspect ratio ca. 15 were prepared by procedure described elsewhere.[7] In a three-neck flask 230 mg of CdO was mixed with 7 g of TOPO and 830 mg of TDPA. Separately, a sulfur solution was prepared by dissolving 180 mg of sulfur in 20 mL of degassed TOP. The reaction mixture in the three-neck flask was degassed at 100 °C for 1 hour before heating it to 340 °C to form Cd-TDPA complex. The formation of Cd-TDPA complex can be visually checked as the dark red solution became clear and colorless. The reaction mixture was cooled to 300 °C and 6 mL of TOP solution was introduced under vigorous stirring. After stirring at 300 °C for 1 hour the solution became greenish yellow in color. Remaining 14 mL of S-TOP solution was then introduced at a

very slow rate (10 μL per 5 sec). Once the addition was complete, the reaction mixture was cooled to room temperature and the nanorods were precipitated by adding excess acetone to the reaction mixture. The precipitate was washed several times with acetone/methanol mixture to remove excess TOPO, TDPA, and TOP and finally CdS nanorods were kept as a stock solution in chloroform.

6.4.3 Synthesis of high aspect ratio CdS nanorods (200 x 5 nm)

High aspect ratio CdS nanorods were prepared by the literature procedure.[36] In a three-flask, 46 mg of CdO was mixed with 166 mg of TDPA and 1.4 g of TOPO. The mixture was degassed at 100°C for 1 hour and subsequently heated to 340 °C to produce Cd-TDPA complex. The reaction mixture was cooled to 300 °C and 3.2 mL of S-TOP solution (36 mg of elemental sulfur in 3.2 mL TOP) was introduced at a very slow rate (10 μL per 5 sec). After the addition was complete, the nanorods were purified by precipitating them with excess methanol.

6.4.4 Synthesis of CdS-Au hybrid nanostructures

The gold growth solution was prepared by dissolving 7 mg of $AuCl_3$, 48 mg CTAB, and 43 mg of DDA in 10 mL 4:1 mixture of toluene and chloroform. Resulting dark brown solution was sonicated for 30 sec before adding it to the toluene solution of CdS nanostructures (10 mg in 15 mL of toluene). The solution became brown in color after 3 h indicating the formation of small gold nanoparticles. The CdS-Au hybrid structures were purified by multiple precipitations with excess methanol.

References

(1) Banin, U.; Millo, O. *Ann. Rev. Phys. Chem.* **2003**, *54*, 465.

(2) Peng, Z. A.; Peng, X. *J. Am. Chem. Soc.* **2001**, *123*, 183.

(3) Talapin, D. V.; Shevchenko, E. V.; Murray, C. B.; Kornowski, A.; Forster, S.; Weller, H. *J. Am. Chem. Soc.* **2004**, *126*, 12984.

(4) Li, L.-S.; Walda, J.; Manna, L.; Alivisatos, A. P. *Nano Lett.* **2002**, *2*, 557−560.

(5) Yan, K. M.; Mastroianni, A.; Stancil, K. A.; Liu, H.; Alivisatos, A. P. *Nano Lett.* **2006**, *6*, 1479.

(6) Kim, F.; Kwan, S.; Akana, J.; Yang, P. *J. Am. Chem. Soc.* **2001**, *123*, 4360.

(7) Ghezelbash, A.; Koo, B.; Korgel, B. A. *Nano Lett.* **2006**, *6*, 1832.

(8) Jun, Y, -W.; Choi, J. –S.; Cheon, J. *Angew. Chem. Int. Ed.* **2006**, *45*, 3414.

(9) Koh, W.–K.; Bartnik, A. C.; Wise, F. W.; Murray, C. B. *J. Am. Chem. Soc.* **2010**, *132*, 3909.

(10) Chun, J.; Lee, J. *Eur. J. Inorg. Chem.* **2010**, 4251.

(11) Peng, X. G.; Manna, L.; Yang, W. D.; Wickham, J.; Scher, E.; Kadavanich, A.; Alivisatos, A. P. *Nature* **2000**, *404,* 59.

(12) Huang, X. H.; Neretina, S.; El-Sayed, M. A. *Adv. Mater.* **2009**, *21*, 4880.

(13) Jana, N. R.; Gearheart, L.; Murphy, C. J. *Adv. Mater.* **2001**, *13*, 1389.

(14) Lu, X.; Yavuz, M. S.; Tuan, H.-Y.; Korgel, B. A.; Xia, Y. N. *J. Am. Chem. Soc.* **2008**, *130*, 8900.

(15) Pazos-Perez, N.; Baranov, D.; Irsen, S.; Hilgendorff, M.; Liz-Marzan, L. M.; Giersig, M. *Langmuir* **2008**, *24*, 9855.

(16) Ditlbacher, H.; Hohenau, A.; Wagner, D.; Kreibig, U.; Rogers, M.; Hofer, F.; Aussenegg, F. R.; Krenn, J. R. *Phys. Rev. Lett.* **2005**, *95*, 257403.

(17) Bruchez, M.; Moronne, M.; Gin, P.; Weiss, S.; Alivisatos, A. P. *Science* **1998**, *281,* 2013.

(18) Wu, X.; Liu, H.; Liu, J.; Haley, K. N.; Treadaway, J. A.; Larson, J. P.; Ge, N.; Peale, F.; Bruchez, M. *Nat. Biotech.* **2003**, *21*, 41.

(19) Wang, H. F.; Huff, T. B.; Zweifel, D.A.; He, W.; Low, P. S; Wei, A.; Cheng, J. X. *Proc. Natl. Acad. Sci. USA* **2005**, *102*, 15752.

(20) Mitchell, G. P.; Mirkin, C. A.; Letsinger, R. L. *J. Am. Chem. Soc.* **1999**, *121*, 8122.

(21) Yong, K.-T.; Roy, I.; Pudavar, H. E.; Bergey, E. J.; Tramposch, K. M.; Swihart, M. T.; Prasad, P. N. *Adv.Mater.* **2008**, *20*, 1412.

(22) Durr, N. J.; Larson, T.; Smith, D. K.; Korgel, B. A.; Sokolov, K.; Ben-Yakar, A. *Nano Lett.* **2007**, *7*, 941.

(23) Huynh, W. U.; Dittmer, J. J.; Alivisatos, A. P. *Science* **2002**, *295*, 2425.

(24) Schierhorn, M.; Boettcher, S. W.; Peet, J. H.; Matioli, E.; Bazan, G. C.; Stucky, G. D.; Moskovits, M. *ACS Nano* **2010**, *4*, 6132.

(25) Kim, C.-H.; Cha, S.-H.; Kim, S. C.; Song, M.; Lee, J.; Shin, W. S.; Moon, S.-J.; Bahng, J. H.; Kotov, N. A.; Jin, S.-H. *ACS Nano* **2011**, *5*, 3319.

(26) Kang, Y.; Park, N.–G.; Kim, D. *Appl. Phys. Lett.* **2005**, *86*, 1883319.

(27) Mokari, T. *Nano Rev.* **2011**, *3*, 5983.

(28) Costi, R.; Saunders, A. E.; Banin, U. *Angew. Chem. Int. Ed.* **2010**, *49*, 4878.

(29) Dabbousi, B. O.; Rodriguez-Viejo, J.; Mikulec, F. V.; Heine, J. R.; Mattoussi, H.; Ober, R.; Jensen, K. F.; Bawendi, M. G. *J. Phys Chem B* **1997**, *101*, 9463.

(30) Peng, X.; Schlamp, M. C.; Kadavanich, A. V.; Alivisatos, A. P. *J. Am. Chem. Soc.* **1997**, *119*, 7019.

(31) Mokari, T.; Banin, U. *Chem. Mater* **2003**, *15*, 3955.

(32) Sitt, A.; Sala, F. D.; Menagen, G.; Banin, U. *Nano Lett.* **2009**, *9*, 3470.

(33) Xiang, Y.; Wu, X.; Liu, D.; Jiang, X.; Chu, W.; Li, Z.; Ma, Y.; Zhou, W.; Xie, S. *Nano Lett.* **2006**, *6*, 2290.

(34) Khanal, B. P.; Zubarev, E. R. . *Angew. Chem. Int. Ed.* **2009**, *48*, 6888.

(35) Mokari, T.; Rothenberg, E.; Popov, I.; Costi, R.; Banin, U. *Science* **2004**, *304*, 1787.

(36) Saunders, A. E.; Popov, I.; Banin, U. *J. Phys Chem B* **2006**, *110*, 25421.

(37) Carbone, L.; Jakab, A.; Khalavka, Y.; Sönnichsen, C. *Nano Lett.* **2009**, *9*, 3710.

(38) Cozzoli, P. D.; Curri, M. L.; Giannini, C.; Agostiano, A. *Small* **2006**, *2*, 413.

(39) Pacholski, C.; Kornowski, A.; Weller, H. *Angew. Chem. Int. Ed.* **2004**, *43*, 4774.

(40) Wood, A.; Giersig, M.; Mulvaney, P. *J. Phys Chem B* **2001**, *105*, 8810.

(41) Subramanian, V.; Wolf, E. E.; Kamat, P. V. *J. Am. Chem. Soc.* **2004**, *126*, 4943.

(42) Wolcott, A.; Fitzmorris, R. C.; Muzaffery, O.; Zhang, J. Z. *Chem. Mater.* **2010**, *22*, 2814.

(43) Wang, W.; Banerjee, S.; Jia, S.; Steigerwald, M. L.; Herman, I. P. *Chem. Mater.* **2007**, *19*, 2573.

(44) Acharya, S.; Patla, I.; Kost, J.; Efrima, S.; Golan, Y. *J. Am. Chem. Soc.* **2006**, *128*, 9294.

Chapter VII

Research Summary

In this thesis, various methods for surface modification of gold nanostructures were discussed. We have mainly concentrated our study on spherical gold nanoparticles and anisotropic gold nanorods. Functionalization with small organic ligands allows for the characterization of organic-inorganic hybrid materials by conventional analytical techniques such as NMR and TGA. Rational surface modifications also help to stabilize gold nanostructures in different solvents. We have also explored self-assembly of gold nanostructures in detail. Evaporative self-assembly was implemented to prepare near macroscopic colloidal single crystals of gold nanorods. Furthermore, we have shown a complimentary use of "top-down" and "bottom-up" strategies to control the shape and size of self-assembled structures.

Near monodisperse plasmonic gold nanoparticles were functionalized with functional organic ligand (SOPB) that structurally resembles liquid crystal 5CB. Functionalized hybrid structure was characterized by a combination of NMR, TGA, and TEM. In stark contrast to akanethiolated gold particles, SOPB functionalized gold nanoparticles show increased solubility in bulk liquid crystal matrix owing to the structural similarity between SOPB and 5CB. Optical studies of gold nanoparticles in bulk liquid crystal prove that nanoparticles are completely homogenized in the media without any agglomeration. This is an important step toward the preparation of plasmonic nanoparticles-liquid crystal composite materials which may find applications in new generation LC displays and color filters.

To continue our study about the surface modifications of gold nanostructures, we investigated covalent surface functionalization of gold nanorods with a thiolated analogue of CTAB (TCTAB). Covalent gold-sulfur bond indefinitely stabilized these nanorods in pure water in the absence of free CTAB. Functionalized nanorods were characterized by analytical techniques and exact grafting density of the ligand was precisely determined. Additionally, TCTAB-coated rods showed high cellular uptake while maintain low cytotoxicity. These finding are very important for targeted drug delivery, and photothermal cancer therapy using gold nanorods.

After surface modification, we focused on the self-assembly of these nanostructures into well defined colloidal crystals. Alkanethiolated monodisperse gold nanoparticles undergo crystallization to form well defined three dimensional superlattices that are analogous to atomic FCC crystals. Additionally, anisotropic gold nanorods were self-assembled via solvent evaporation to prepare colloidal crystals that measure more than 100 microns in length. Orientation of nanorods in the colloidal crystal was found to depend greatly on the hydrophobicity of the underlying substrate and vertically standing superllatices of gold nanorods were prepared by carrying out the crystallization on top of a photoresist-coated substrate. Our systematic investigation also proved that the assembly of gold nanorods is driven by their co-crystallization with free CTAB molecules present in solution.

Controlled assembly of nanorods is often required for the preparation of periodic arrays composed of anisotropic building blocks. Combining the optical lithography with self assembly, periodic arrays of gold nanorods were prepared. Controlled assembly was governed by the hydrophilic interactions, de-wetting, and electrostatic forces.

Additionally, highly conductive two dimensional periodic networks of gold nanowires were prepared by template assisted evaporative self assembly. These macroscopic structures can find many practical applications, which include optical filters, electronic devices, and transparent conductive surfaces.

Furthermore, we explored the chemical synthesis of hybrid metal-semiconductor nanostructures. Solvothermal synthesis of ultra long CdS nanowires was carried out by the addition of stoichiometric amount of sulfur precursor to Cd-phosphonic acid complex under "no-stirring" conditions. HRTEM images showed that nanowires preserve their wurtzite crystal structure during the one-dimensional growth. Controlled deposition of gold nanoparticles on pre-synthesized nanowires resulted in the formation of hybrid gold-CdS nanowires which may find applications in photocatalysis and solar cells.